The Pennsylvania State University

The Graduate School

College of Engineering

REDUCED ORDER MODELING, STATISTICAL ANALYSIS AND SYSTEM IDENTIFICATION FOR A BLADED ROTOR WITH GEOMETRIC MISTUNING

A Dissertation in

Mechanical Engineering

by

Vinod Vishwakarma

Submitted in Partial Fulfillment

of the Requirements

for the Degree of

Doctor of Philosophy

December 2014

The dissertation of Vinod Vishwakarma was reviewed and approved* by the following:

Alok Sinha
Professor of Mechanical Engineering
Dissertation Advisor, Chair of Committee

Christopher Rahn
Professor of Mechanical Engineering

Hosam Fathy
Assistant Professor of Mechanical Engineering

George A. Lesieutre
Professor of Aerospace Engineering
Department Head of Aerospace Engineering

Vishal Monga
Monkowski Assistant Professor of Electrical Engineering

Karen Thole
Professor of Mechanical Engineering
Department Head of Mechanical and Nuclear Engineering

*Signatures are on file in the Graduate School.

Abstract

Modified Modal Domain Analysis (MMDA) is a novel method for the development of a reduced-order model (ROM) of a bladed rotor. This method utilizes proper orthogonal decomposition (POD) of Coordinate Measurement Machine (CMM) data of blades' geometries and sector analyses using ANSYS. For the first time ROM of a geometrically mistuned industrial scale rotor (Transonic rotor) with large size of Finite Element (FE) model is generated using MMDA. Two methods for estimating mass and stiffness mistuning matrices are used a) exact computation from sector FE analysis, b) estimates based on POD mistuning parameters. Modal characteristics such as mistuned natural frequencies, mode shapes and forced harmonic response are obtained from ROM for various cases, and results are compared with full rotor ANSYS analysis and other ROM methods such as Subset of Nominal Modes (SNM) and Fundamental Model of Mistuning (FMM). Accuracy of MMDA ROM is demonstrated with variations in number of POD features and geometric mistuning parameters. It is shown for the aforementioned case b) that the high accuracy of ROM studied in previous work with Academic rotor does not directly translate to the Transonic rotor. Reasons for such mismatch in results are investigated and attributed to higher mistuning in Transonic rotor. Alternate solutions such as estimation of sensitivities via least squares, and interpolation of mass and stiffness matrices on manifolds are developed, and their results are discussed.

Statistics such as mean and standard deviations of forced harmonic response peak amplitude are obtained from random permutations, and are shown to have similar results as those of Monte Carlo simulations. These statistics are obtained and compared for 3 degree of freedom (DOF) lumped parameter model (LPM) of rotor, Academic rotor and Transonic rotor.

A state – estimator based on MMDA ROM and Kalman filter is also developed for offline or online estimation of harmonic forcing function from measurements of forced response. Forcing function is estimated for synchronous excitation of 3DOF rotor model, *Academic* rotor and Transonic rotor from measurement of response at few nodes. For asynchronous excitation forcing function is estimated only for 3DOF rotor model and Academic rotor from measurement of response. The impact of number of measurement locations and accuracy of ROM on the estimation of forcing function is discussed.

Table of Contents

List of Figures viii

List of Tables x

List of Symbols xi

Acknowledgments xiv

Chapter 1
Introduction 1
1.1 Literature review . . . 3
1.2 Advances in mistuning studies . . . 7
1.3 Mistuning and forcing function identification . . . 10
1.4 Summary of research . . . 11

Chapter 2
Application of MMDA on Transonic rotor 13
2.1 Transonic rotor . . . 14
2.2 Academic Rotor . . . 14
2.3 MMDA methodology . . . 16
2.3.1 Basis Matrix . . . 19
2.4 Results . . . 24
2.4.1 MMDA accuracy measure . . . 24
2.4.2 SNM and FMM comparison . . . 30
2.4.3 Forced harmonic response . . . 31
2.5 Summary . . . 34

Chapter 3
MMDA with Approximate Deviations in Mass and Stiffness Matrices via Taylor Series 35
3.1 Taylor series approximation of deviations in matrices . . . 35
3.1.1 First and second order partial derivatives . . . 36

3.1.2 Results . . . 37
3.1.3 Limitations . . . 38
3.2 Linear Least Squares Approximation . . . 41
3.3 Interpolation on Manifold . . . 43
3.3.1 *Academic* Rotor . . . 46
3.3.2 Transonic like rotor . . . 47
3.4 Summary . . . 48

Chapter 4
Forced Response Statistics **50**
4.1 Random Permutations . . . 51
4.2 Forced response statistics : 3DOF model . . . 54
4.3 Forced response statistics : *Academic* rotor . . . 58
4.4 Forced response statistics : Transonic rotor . . . 62
4.5 Computation Time . . . 64
4.6 Summary . . . 64

Chapter 5
Forcing Function Estimation **66**
5.1 Dynamic Model . . . 67
5.2 Forcing estimation . . . 68
5.2.1 3DOF bladed rotor model . . . 71
5.2.2 *Academic* Rotor . . . 75
5.2.3 Transonic Rotor . . . 77
5.3 Summary . . . 80

Chapter 6
Conclusion and Future Research **82**

Appendix A
Modified Modal Domain Analysis (MMDA) **87**
A.1 Computation of M_r and K_r via sector analysis . . . 89
A.1.1 Reduced order tuned matrices . . . 89
A.1.2 Reduced order mistuned matrices . . . 92

Appendix B
Modified Modal Domain Analysis with Approximate Deviations in Mass and Stiffness Matrices **94**
B.1 Mass and Stiffness Matrices Mistuning Approximation by Taylor Series expansion . . . 94

B.1.1 Calculation of First and Second order partial derivative terms 95
B.1.2 Reduced order mistuning matrices 97

Appendix C
Frequency Mistuning Approaches **100**
C.1 Subset of Nominal Modes 100
C.2 Fundamental Mistuning Model 102

Appendix D
Karhunen-Loève expansion **104**

Bibliography **105**

List of Figures

1.1 Simple lumped parameter model 3

2.1 ANSYS FE mesh model of Transonic like rotor and *Academic* rotor . 15
2.2 Transonic rotor nodal diameter map and singular values 23
2.3 Transonic rotor frequency deviations comparison between ANSYS and MMDA for 17 POD, and 5 and 10 families of modes 25
2.4 Transonic rotor frequency deviations comparison between ANSYS and MMDA for various POD numbers 27
2.5 Transonic rotor MAC comparison between ANSYS and MMDA for 17 POD, and 5 and 10 families of modes in the basis 28
2.6 Transonic rotor MAC comparison between ANSYS and MMDA for 5 families of modes and various POD features in the basis 29
2.6 Transonic rotor MAC comparison between ANSYS and MMDA for 5 families of modes and various POD features in the basis 30
2.7 Transonic rotor frequency deviations comparison for ANSYS, SNM and FMM for first and second family of modes 31
2.8 Transonic rotor MAC values for first and second families of modes of SNM and FMM 32
2.9 Transonic rotor forced response comparison for MMDA, SNM and ANSYS results 33

3.1 Transonic rotor MAC values for mode shapes from ANSYS and MMDA with Taylor series approximation of deviation matrices 37
3.2 MAC comparison between ANSYS and MMDA for Artificial rotor for various reduced perturbation (γ) 39
3.3 Frequency deviations comparison between ANSYS and MMDA for Artificial rotor for various reduced perturbation (γ) 40
3.4 MAC values for MMDA with sensitivities obtained by linear least squares method from Transonic like training rotor and tested on test rotor 43

3.5 *Academic* rotor MAC values for MMDA with interpolation on manifold of sector mass and stiffness matrices using POD mistuning parameters for a training rotor and a test rotor 46
3.6 *Academic* test rotor frequency deviation for MMDA with interpolation on manifold of sector mass and stiffness matrices 46

4.1 Concept of distribution due to random permutations 51
4.2 Example of random permutations distribution with θ from standard normal 53
4.3 3DOF sector model 54
4.4 NPMA comparison between random permutations and Monte Carlo for uniform distribution of stiffness for 3DOF model 56
4.5 NPMA comparison between random permutations and Monte Carlo for Gaussian distribution of stiffness for 3DOF model 57
4.6 Finite element mesh model of *Academic* rotor blades and POD features 58
4.7 NPMA comparison between random permutations and Monte Carlo for uniform distribution of ξ for *Academic* rotor 60
4.8 NPMA comparison between random permutations and Monte Carlo for Gaussian distribution of ξ for *Academic* rotor 61
4.9 NPMA comparison for various cases of Transonic rotor 63

5.1 Nodal diameter map for 3DOF rotor model 72
5.2 3DOF rotor model force estimation for tip excitation and displacement observed at tip 72
5.3 3DOF rotor model force estimation for synchronous excitation 73
5.4 3DOF rotor model force estimation for asynchronous excitation . . . 74
5.5 *Academic* rotor force estimation for synchronous excitation 76
5.6 *Academic* rotor force estimation for asynchronous excitation 77
5.7 Transonic rotor force estimation for synchronous excitation 78
5.7 Transonic rotor force estimation for asynchronous excitation 79

C.1 Young's Modulus modification for SNM 101

List of Tables

2.1 Academic rotor and Transonic rotor FEM properties comparison . . . 16

4.1 Parameter values for 3DOF simple rotor model 54
4.2 Time (in seconds) comparison for one sample of random permutations and Monte Carlo for forced response for various cases 64

List of Symbols

C	Damping matrix of the mistuned system
C_p	Observation matrix
C_r	Reduced order damping matrix
C_t	Damping matrix of the tuned system
$\mathbf{f}(t)$	Forcing vector
$\mathbf{f}_0$	Forcing vector amplitude
$\mathbf{f}_k(t)$	Forcing vector for sector # k
$\mathbf{h}(t)$	Measurement vector
M	Mass matrix of the mistuned system
M_r	Reduced order mass matrix
M_t	Mass matrix of the tuned system
$M_{t\rho}^c$	Cyclic mass matrix for the tuned system for ρ^{th} interblade phase angle
N_a	Number of POD features available in given set of blades
N_b	Number of sectors/blades in the rotor
N_d	Length of displacement vector $\mathbf{x}$
N_f	Number of family of modes in the bases $\mathbf{\Phi}$
N_p	Number of POD features in the bases $\mathbf{\Phi}$
N_s	Number of sectors available for analysis
K	Stiffness matrix of the mistuned system
K_r	Reduced order stiffness matrix
K_t	Stiffness matrix of the tuned system
p	p^{th} engine order excitation
t	Time
$\mathbf{u}_p$	p^{th} POD feature vector
v_{sp}	Coefficient of mistuning parameter p^{th} POD feature and sector # s
$\mathbf{w}$	Spatial nodal co-ordinate vector
$\overline{\mathbf{w}}$	Spatial mean nodal co-ordinate vector
$\mathbf{x}$	Nodal DOF displacement vector
$\mathbf{x}_0$	Nodal DOF displacement vector amplitude
$\mathbf{x}_{0t}$	Nodal DOF displacement vector amplitude for tuned rotor

$\mathbf{y}$	Reduced order model co-ordinate vector
$\mathbf{z}$	Modal co-ordinate vector
$\mathbf{z}_0$	Modal co-ordinate vector amplitude
α	Mass proportionality constant for damping
β	Stiffness proportionality constant for damping
γ	Perturbation reduction factor
δM_s	Deviation in mass matrix for sector # s
δK_s	Deviation in stiffness matrix for sector # s
$\delta \mathbf{w}_k$	Spatial deviation in nodal co-ordinate vector for sector # k
$\boldsymbol{\eta}$	Rotation frequency of the rotor
ι	Complex number $\sqrt{-1}$
$\xi_{s,p}$	Random variable for coefficient of mistuning parameter of p^{th} POD feature and sector # s
σ_p	p^{th} POD feature singular value
ω_f	Angular frequency of excitation
$\boldsymbol{\Phi}$	Reduced order model basis matrix
$\boldsymbol{\Phi}^H$	Complex conjugate transpose of $\boldsymbol{\Phi}$
$\boldsymbol{\Phi}^T$	Transpose of $\boldsymbol{\Phi}$
Φ_0	Set of tuned modes of the system with blades having the average geometry
Φ_i	Set of tuned modes of the system with blades having geometries perturbed along i^{th} POD feature
$\phi_{l,s,p}$	Mode shapes for l^{th} POD feature, sector number # s and p^{th} nodal diameter
Ψ	Set of modes obtained for reduced order model
Ω	Angular rotation frequency of the rotor
CMM	Co-ordinate measurement machine
CMS	Component mode synthesis
DOF	Degree of freedom
EO	Engine order
FEM	Finite element method
FMM	Fundamental mistuning model
IBR	Integrally bladed rotor
LPM	Lumped parameter model
LS	Least squares
MAC	Modal assurance criterion
MMDA	Modified modal domain analysis
NMA	Normalized maximum amplitude
NPMA	Normalized peak maximum amplitude
POD	Proper orthogonal decomposition
ROM	Reduced order model
SMART	Secondary modal analysis reduction technique

SNM	Subset of nominal modes
SPD	Symmetric positive definite

Acknowledgments

Foremost, I would like to express my sincere gratitude to my Ph. D. supervisor Dr. Alok Sinha for the continuous and untiring support of my Ph. D. study and research, for his patience, motivation, enthusiasm, and immense knowledge. His guidance helped me in all the time of research and writing of this thesis. I could not have imagined having a better advisor and mentor for my Ph. D. study. Besides my advisor, I would like to thank the members of my Ph. D. committee Dr. Hosam Fathy, Dr. Chris Rahn, Dr. George Lesieutre and Dr. Vishal Monga for their feedbacks on my thesis and their guidance in course work.

I would also like to thank the Department of Mechanical and Nuclear Engineering, the College of Engineering at The Pennsylvania State University, and GUIde4 consortium for the financial support which made this work possible and without which I may not have begun in the first place. I would also like to extend my thanks to Research Computing and Cyberinfrastructure at The Pennsylvania State University for their computational resources.

I am grateful to my roommates and friends, Devesh and Debasish for helping me get through the difficult times, for all the emotional support, and caring they had provided.

Chapter 1
Introduction

The structural part of turbomachines such as turbines and compressors are described as bladed disks. They are cyclic structures with repetition of sectors and blades in the substructure. In general, a bladed disk has identical substructures and it is also called cyclically symmetric bladed disk. Even after time intensive process of designing of a bladed disk; manufacturing process limitations, material properties tolerance, damage and wear in operation contribute to variations in geometry and material properties of bladed disk. These variations are termed as *Mistuning*. Mistuning changes natural frequencies and mode shapes of bladed disk from those of designed bladed disk. It can cause phenomena such as mode splitting and mode localization, affecting forced response behavior which can be detrimental to the bladed disk assembly. The dynamic characteristics of cyclically symmetric as well as mistuned bladed disks have been studied widely. In many cases mistuning has been reported to increase stress levels in blades significantly [1, 2].

Mistuning phenomenon has negative influence on bladed disk's forced response and high-cycle fatigue (HCF) life. Of particular interest are turbomachines that operate at very high speeds, such as turbine in jet engines. At such high speeds the importance of vibration characteristics of these bladed rotors can not be undermined. Non-uniform pressure distribution, caused by fluid flow, on the surface of bladed disk assembly can force the bladed rotor to vibrate at their natural frequencies. At high speeds these vibrations can cause high cycle fatigue quickly, which can lead to premature failure of the turbomachines' components, consequently durability and reliability of the turbomachines are affected. Since randomness in processes such as

manufacturing and wear affects these mistunings, thus the statistics of forced response are desirable in assessing the life of bladed disk assembly.

Estimation of natural frequencies, mode shapes and forced response for cyclically symmetric bladed disk is very fast using "Cyclic Symmetry Analysis" [3]. Each sector with a blade of such a bladed disk is identical and called *nominal sector* with *nominal blade* respectively. With each sector being identical, using properties of cyclic symmetry the eigenvalue analyses of only one sector (primary sector) suffice to obtain natural frequencies and mode shapes of full bladed disk. The mode shapes of other sectors are obtained by multiplying mode shapes of primary sector by terms from Fourier matrix. Forced response can also be obtained using only the primary sector [3].

In mistuned bladed disk this cyclic symmetry is lost, hence cyclic symmetric properties do not hold. Analysis of full mistuned bladed disk will be required to obtain natural frequencies, mode shapes and forced response.

The structural dynamic characteristics of a bladed disk assembly not only include the natural frequencies of vibration of the assembly, but also its mode shapes and damping. These characteristics are required for forced response and resonant vibrations estimation. Thus, the estimation of natural frequencies and forced response of a bladed rotor is of significance. A simple estimation of forced response and resonant vibrations can be done by lumped parameter models (LPMs) such as using mass, spring and damper as depicted in Figure 1.1, as used in [2, 4, 5]. These estimations are usually approximate. An accurate estimate for a given bladed rotor is usually obtained by Finite Element Methods (FEM) using a commercial package, such as ANSYS, ABACUS, NASTRAN etc.

With the theory of cyclic symmetry analysis for nominal sectors, the computation time to obtain vibration characteristics for cyclically symmetric structure by FEM packages is drastically reduced as compared to that of a full structure FEM analysis. But as mentioned before, due to mistuning this cyclic symmetry is lost and hence full

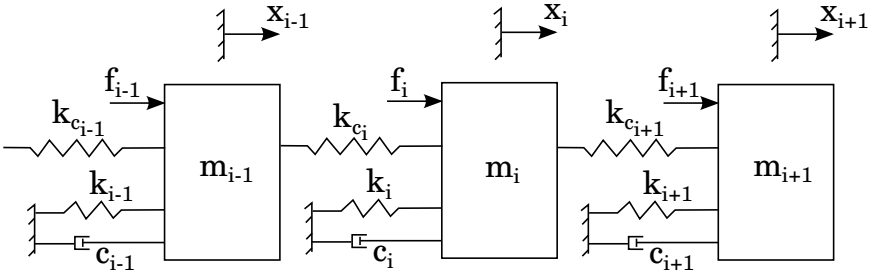

Figure 1.1: Simple lumped parameter model

(360°) structure FEM analysis is required. The order of the full FEM model of these turbomachines is very large compared to that of the nominal sector. Though these FEM packages are certainly accurate, they require a lot of computational power and time, and thus assessing statistics of forced response becomes a formidable task.

Resonance in the bladed disk assembly during operation can occur due to various aerodynamic excitations, such as flow defects, unsteady wakes, potential pressure disturbances and flow distortion etc. These uncontrollable factors affect the forcing on each blade of the bladed disk assembly during operation and may cause resonance. Estimation of these forcing during resonance can provide valuable inputs for future designs. Measuring these forcing on the blades in real time is a difficult task, a method to estimate such harmonic forcing from blade's response measurements, while the bladed disk is in operation, is desirable. These measurements of blade's deflection and stresses are usually made online and non–intrusively for health monitoring of the structure e.g. Agilis [1] Non–Intrusive Stress Measurement System (NSMS) blade tip–timing system.

1.1. Literature review

Blade mistuning has been extensively researched since mid 20^{th} century and a lot of results have helped in improving the design of turbomachines. In 1957, Tobias

[1] Agilis Engineering, Inc. is an engineering company with focus on engineering design, development and turbine engine analysis

and Arnold [6], showed analytically and experimentally that mistuning in disks causes splitting of modes of the tuned disk (disk with nominal geometry). In a special case it was shown that the controlled mistuning can reduce the amplitude of forced response compared to that of tuned disk due to aerodynamic damping and mode splitting .

In 1966, Whitehead [7] work shed light on the underlying physics of vibration induced by wakes. Under special circumstances the amplitude of forced response is shown to increase by a maximum factor of $\frac{1}{2}(1 + \sqrt{N})$, where N is the number of sectors in the bladed rotor.

In 1969, Ewins [1] in his pioneering work used an analytical model of coupled lumped masses to understand the effects of mistuning, this lumped parameter model represented various magnitude of frequency mistunings. He also showed that the forced response for certain arrangements of mistuned blades can cause upto 20% increase in stress level in blades as compared to that of the tuned system. This was also verified experimentally with a five-bladed disk. Dye and Henry [5] used a lumped parameter model to study inter–coupling between blades mounted on a flexible disk. Ewins [8] used a complete bladed disk, and made a theoretical and experimental investigation on the effect of coupling and found that the complete bladed disk has more natural frequencies as compared to those of cantilevered blades.

In 1975, Bayoumy and Srinivasan [2] included aerodynamic damping as well as mechanical damping in their model to study the influence of mistuning in vibratory stress levels. An important observation was made that the maximum stress level may not be in the worst mistuned sector.

Though intentional mistuning has been used to reduce the risk of flutter instability [9, 10], even small mistuning can cause phenomena such as mode separation, mode localization etc, which in turn can change forced response by a significant factor at the operating point.

The study of the effects of mistuning on forced response in a deterministic framework is certainly advantageous, but due to changes in these mistuning over the life of

the bladed rotor makes the study of statistics of forced response a priority. With the limited availability of computing in early years, these statistics were obtained through Monte Carlo simulations of simple lumped parameter models (LPMs).

Research efforts in 1980s and 90s were concentrated on methods to obtain these statistics. Earliest attempt in this direction made by Sogliero and Srinivasan [11] in 1980 aimed at obtaining expected time to fatigue failure of a bladed disk by simulations of various mistuned bladed disk assembly to obtain such statistics.

Huang [12] used a closed ring model to obtain analytical solutions for statistics of mistuned natural frequencies, mode shapes, free and forced response by treating mistuning in structural parameters as random processes.

Griffin and Hoosac [13] used computer simulations to analyze the statistical distribution of forced responses due to mistuning. This model had three lumped masses representing the sector, blade of each sector was connected to their respective disk by springs and adjacent disks were also interconnected by springs.

These statistical analysis were computationally expensive. Therefore, researchers started developing various analytical methods for predicting the distribution of the mistuned forced response without using Monte Carlo simulations. In 1986, Sinha [4] developed an analytical method to obtain probability density functions of blade's amplitude for blades with Gaussian mistuning by combining first order perturbation methods with statistical theory. Later, Sinha and Chen [14] extended the method to non–Gaussian distribution of mistuning.

In 1988, Wei and Pierre [15] used a simplified single degree of freedom per blade model of rotor and suggested that for system with small mistuning to coupling ratio, the mistuned system behaves like perturbation of tuned system, while with large mistuning to coupling ratio (*i.e.* weak coupling) makes mistuned system to behave like perturbation of decoupled mistuned system. Furthermore Wei and Pierre [16] determined that the localization in forced and free response of the system depends on mistuning to coupling ratio, and for free response the degree of localization increases

as mistuning to coupling ratio increases but this phenomenon is not necessarily true for forced response.

Wei and Pierre [17] also compared Monte Carlo simulations with analytical first–order statistical perturbation method. It was found that sensitivity of statistics to mistuning is dependent on relative magnitude of coupling, mistuning and damping.

Lin and Mignolet [18] used damping variation analysis to study the forced response. Their results showed that the damping mistuning can also lead to a scatter of blade amplitudes comparable to that of stiffness mistuning.

Although these analytical techniques were applied to lumped parameter models, the insights gained from such simple models can be applied to more general finite element models. These techniques also included nonlinearities caused by the presence of frictional dampers [19, 20].

Since these LPMs themselves are not very accurate, thus these inaccuracies creep in the statistics and therefore use of these statistical methods in industrial application is limited. With recent advances in computing power the utility of FEM packages has greatly increased, thus the use of full rotor FEM models and cyclically symmetric models for forced response analysis is achievable. Even with this increase in computing power, Monte Carlo simulations of full rotor model to generate statistics of forced response is a formidable task. Therefore, reduction techniques are used to generate a Reduced Order Model (ROM) by choosing a suitable basis for order reduction, then these ROMs can be used to perform Monte Carlo simulations to obtain results with sufficient accuracy.

A considerable effort has been directed towards enriching the knowledge of the vibration characteristics of mistuned bladed disks, and developing new perspectives and formulations to study the mistuning problem. Several comprehensive surveys, such as [1, 7, 21] summarize the existing mistuning literature. In 1997, Srinivasan [22] published an in–depth study of the literature on mistuning in bladed disk, their causes and characteristics. The article dealt with mistuning modeling, effects of damping and

coupling on forced response, flutter and resonance conditions etc. Slater et. al. [23] published a survey on study of forced response of bladed disk assemblies.

1.2. Advances in mistuning studies

Use of Finite Element Modeling techniques as a numerical tool for modal analysis and forced response analysis is extensive. These models utilize linear algebra tools to solve eigenvalue problem for natural frequencies and mode shapes of a mistuned system. Using these mode shapes as bases in modal superposition technique forced response is estimated quickly. Computation time for estimation of mode shapes for an industrial scale bladed disk is extremely large, thus use of Monte Carlo simulations for statistics of forced response estimation is infeasible.

Reduced Order Model (ROM) techniques focus on reducing the order of the model to a manageable size, such that the accuracy of results with the ROM is not compromised. An early and efficient approach for reduced order modeling came with the idea proposed by Craig and Bampton [24] in 1968. The method is termed as Component Mode Synthesis (CMS). The idea was to divide the original structure into smaller substructures or components, for which nominal modes are computed independently and can be more computationally inexpensive. Then the assembled system is represented by a truncated set of component modes through necessary compatibility constraints. Seshu [25] and Craig [26] have published excellent surveys on CMS techniques.

In 1994, Ottarsson et. al. [27] introduced a modified CMS technique for mistuned bladed disks. The idea was proposed that the motion of individual mistuned blade can be approximated by linear combinations of subsets of normal modes of vibration of cantilevered blade and disk–induced motion. Mistuning in the model is introduced via blade modal stiffness as the parameter, which is essentially a frequency mistuning approach. There, the use of Monte Carlo simulations for forced response statistics is suggested. Kruse et. al. [28] validated the technique extensively using a FEM of

an industrial rotor and obtained forced response. This technique has been used in industries.

In 1997, Yang and Griffin [29] developed a reduced order modeling method based on the idea of decomposition of bladed disk into substructures and the response is represented in terms of degree of freedom associated with their interface. They also compared their results with FEM analysis and observed that this reduced order modeling method was not capable of estimating forced response for the case where modes of two different families were in close frequency and excited simultaneously.

In 2001, Yang and Griffin [30] improved on their previous method and developed Subset of Nominal Modes (SNM) ROM which is based on the finite element model of sectors. This method is also a frequency mistuning approach. In this method the Young's modulus of a nominal blade clamped at the base of each sector is modified such that its frequency is same as that of mistuned blade. The accuracy of the results from this method increases as the number of nominal modes in the ROM increases. For this method also they have suggested to use Monte Carlo simulations for estimation of forced response statistics.

In 2001, Bladh et. al. [31, 32] improved on CMS technique by doing further modal analysis of ROM obtained by Craig–Bampton approach. This secondary ROM is obtained based on only those modes which comes in the frequency range of the desired family of modes. They called this method Secondary Modal Analysis Reduction Technique (SMART). Comparisons of free and forced response are made between SMART and other CMS techniques.

In 2002, Feiner and Griffin [33] extended the concept in SNM to ROM for a single family of modes called Fundamental Model of Mistuning (FMM). For reduced order modeling FMM uses only a single family of modes, where vibration energy is dominant in the blade as compared to the disk. The tuned frequencies in that particular family is approximated by its average frequency. After some algebra, the order of the ROM becomes equal to the number of sectors in the rotor. This method is useful for first

few isolated families of modes, which have strain energy primarily in the blades.

In 2007, Lim et. al. [34] developed a general ROM for mistuned bladed disk that is applicable for both small and large mistuning. The method uses tuned modes and virtual blade mistuned components in component mode synthesis technique for ROM. With so many modes as bases, several mistuned natural frequencies can be captured. However, the ROM order is large.

In 2009, Amsallem et. al. [35] developed a method for approximation of system matrices on manifold based on mistuning parameters to generate ROMs quickly. The mass and stiffness matrices are symmetric positive definite (SPD), their method ensures that these approximated matrices also have this property. They have shown validity of this method using FEM models of systems such as aircraft wing.

Although a large body of literature [30, 31, 33, 34, 36, 37, 38, 39] exists, only recently a reduced order model [40, 41, 42, 43, 44], Modified Modal Domain Analysis (MMDA) has been developed, which can accurately predict mode shapes, natural frequencies and forced response of a bladed rotor with geometric mistuning. In this method Co-ordinates Measurement Machine (CMM) data gives proper orthogonal decomposition (POD) features. The basis vectors for reduced order model are composed of modes of nominal tuned sector and the sectors perturbed by these POD features. Since this method requires only the sector analyses data for mistuned sectors, thus the ROM method is computationally faster than full rotor FEM model. This approach has been validated for an *Academic* rotor where geometric mistuning was of the class of uniform thickness change and linear variations in thickness by Sinha [40], and Sinha and Bhartiya [44]. The size of the finite element model for *Academic* rotor was relatively low as compared to an industrial scale rotor FE model.

An extension of MMDA is also developed in Bhartiya and Sinha [42] and Bhartiya [45], where mistuned sector's mass and stiffness matrices deviations are approximated using 2^{nd} order Taylor series. Then these approximated deviations in mass and stiffness matrices are used to obtain ROM. It has been shown that this kind of

approximation is quite fast and results are also satisfactory for geometric mistuning in the *Academic* rotor.

1.3. Mistuning and forcing function identification

Geometric mistuning can be directly measured using CMM or optical techniques, but during the operation of turbine it is difficult to measure geometric mistuning in such a way. This is again difficult for integrally bladed rotors (IBR) because the total assembly need to be taken out for measurements. So far mistuning has been associated with certain properties such as mistuned frequencies, damping etc, which are then used to obtain forced response for mistuned system.

In 1999, Mignolet et. al. [46, 47] have developed two distinct approaches from the measurements of the blade alone lowest natural frequencies - random modal stiffnesses (RMS) and the maximum likelihood (ML) strategy - for estimation of dynamic properties of the bladed disk to be used in accurate prediction of the forced response.

In 2001, Bladh et. al. [32] have used a CMS based reduced order model method to develop the mistuning identification algorithm. After a secondary modal analysis, the mistuning in the isolated blade modal stiffness is obtained using a sample of experimental system response.

In 2004, Lim et. al. [48] have developed a new identification method, in which both free and forced response data can be used to gather blade mistuning data.

Feiner and Griffin [49, 50] have developed mistuning identification algorithm based on FMM, called *FMM ID*, by inversion of FMM method. The method relies on the measurements of the vibratory response of the system as a whole. They have also extended the method to identification of damping variation [51]. Hattori [52] have successfully applied mistuning identification based on FMM on radial inflow turbines.

In 2012, Bhartiya and Sinha [53] used Taylor series approximations of deviation in sector mass and stiffness matrices, to invert the MMDA process using iterative least

squares method and obtain geometric mistuning parameters.

Among all of these reduced order modeling methods, MMDA developed by Sinha [40] has been satisfactory in accurately estimating forced response. Also, the approximation of deviations in mass and stiffness matrices based on Taylor series expansion suggests an opportunity to study the statistics of forced response quickly. But, first all of these methods have to be validated on an industrial scale bladed rotor. Since the order of FEM model for industrial scale bladed rotor is much large than that of *Academic* rotor, some challenges and solutions to generate ROM using this method are discussed in following chapters.

Usual health monitoring of bladed disk is done by measurements of forced response behavior. This is usually done by measuring vibratory blade surface strain or by employing tip-timing techniques [54]. Both approaches aim to quantify vibratory stresses. While the cause of these forcing can be unsteady flow variations, pressure fluctuations etc, measurement of such a forcing function is difficult in operation.

Early work on measurement of steady and unsteady blade surface pressure is discussed in [55, 56]. Liu et. al. [57] used pressure sensitive fluorescent paints in combination with temperature sensitive fluorescent paints to measure pressure distribution in Transonic rotor blades. Miller et. al. [58, 59] were able to obtain unsteady pressure measurement in a short-duration test facility. Lately Kammerer and Abhari [60] had proposed an experimental approach to measure unsteady pressure distribution on rotating impeller blades by installing various pressure sensors and strategic perturbation in fluid flow.

1.4. Summary of research

Based on the review of the existing research it is understood that the FE analysis of a full rotor is able to get accurate estimates of natural frequencies and mode shapes. These methods are time consuming and computationally intensive, thus a

reduced order method with a higher degree of accuracy is helpful. Among various ROM methods, MMDA has been shown to give the best results for estimates of mistuned natural frequencies and mode shapes. Thus, it is a suitable candidate to obtain modal characteristics, statistics of forced response and other analyses. In previous studies, MMDA had been tested only on the *Academic* rotor, but the order of the FEM model was smaller than that of full scale industrial rotor. Also, the nature of geometric mistuning in *Academic* rotor were simple and known a priori. Hence MMDA has to be verified first for a full scale industrial rotor. With all these information in mind, following issues are dealt in this dissertation:

1. Analysis of MMDA method for a full scale industrial rotor with exact deviations in mass and stiffness matrices obtained from sector analyses (this is faster compared to full scale FEM analyses).

2. Analysis of MMDA method for a full scale industrial rotor with approximations in deviations in mass and stiffness matrices obtained from methods such as Taylor series expansion etc. Study their limitations and suggest solutions.

3. Develop method based on MMDA to obtain statistics of forced response of full scale industrial rotor and compare with those obtained by Monte Carlo simulations.

4. Develop a method based on MMDA to estimate harmonic forcing function offline or online from measurement of forced response of few nodes.

Chapter 2

Application of MMDA on Transonic rotor

Modern design trend is to have integrally bladed rotors or blisks where blades and disk are constructed from a single metal piece unlike previous design where blades were mounted on disk. The profile of each blade is generated by a milling machine [61]. This process leads to geometric mistuning which represents variations in blades' geometries resulting in simultaneous and dependent variations in the mass and stiffness matrices. The variations in these geometries are measured by co–ordinate measurement machine [62] or optical method [63]. This new design feature leads to a higher aerodynamic efficiency and reduced maintenance costs because of a large reduction in the number of engine parts. On the other hand, damping in an IBR is extremely low because there is no friction at blade and disk joints. For a lower damping, it is well know that the amplification of blade vibrations due to geometric mistuning can be even higher. Hence, it is necessary to have an accurate reduced order modeling technique to study vibration characteristics, forced response and their statistics at resonance.

In this chapter mistuned natural frequencies, mode shapes and forced response of an industrial scale rotor are computed using Modified Modal Domain Analysis (MMDA). Further, accuracy of MMDA in estimation of these characteristics is compared with other frequency mistuning approaches based reduced order methods like SNM and FMM.

2.1. Transonic rotor

The industrial rotor used for this research is the first stage rotor of a research Transonic Compressor [64] which is an 18 airfoil integrally bladed rotor. Geometry of each blade is measured by co–ordinate measurement machine (CMM). Figure 2.1 shows Finite Element (FE) model of a similar rotor used in Bladh [31].

The finite element representation of the full (360°) rotor consists of 166068 nodes and 181800 elements. All elements of the model are linear hexahedral elements except for a small hex-tet transition layer at the disk rim to transition the mesh from the disk to airfoil geometries. The hexahedral elements use reduced integration with hourglass control so the analysis will not suffer from volumetric locking. Three hex elements are used through the thickness of the airfoil to further improve the model's ability to accurately capture the bending response.

Typical Ti 6-4 material properties are used with 17.5 Mpsi Young's Modulus, 0.168 lbm/in^3 density, and 0.3 Poisson's ratio. The model is constrained in all directions at the aft side of the flange located at the disk bore. Special care was used to maintain consistent element topology for each sector so that numerical variations were not introduced from the sector discretization approach. A single sector of the disk and airfoil fillet was created, meshed, and then copied and rotated to build the 360° disk. The geometries of the as–measured airfoils (CMM data) were provided as consistent sets of coordinates defined as cross sections and used to generate the surface and volume definition of each blade. With mesh seeding to define element numbers, hex meshing and the copied disk sector, each sector was topologically consistent.

2.2. Academic Rotor

MMDA had been tested successfully on an *Academic* Rotor in Bhartiya [45]. The *Academic* rotor has approximately same diameter as the Transonic rotor. It has simpler model and sparser node density than the Transonic rotor.

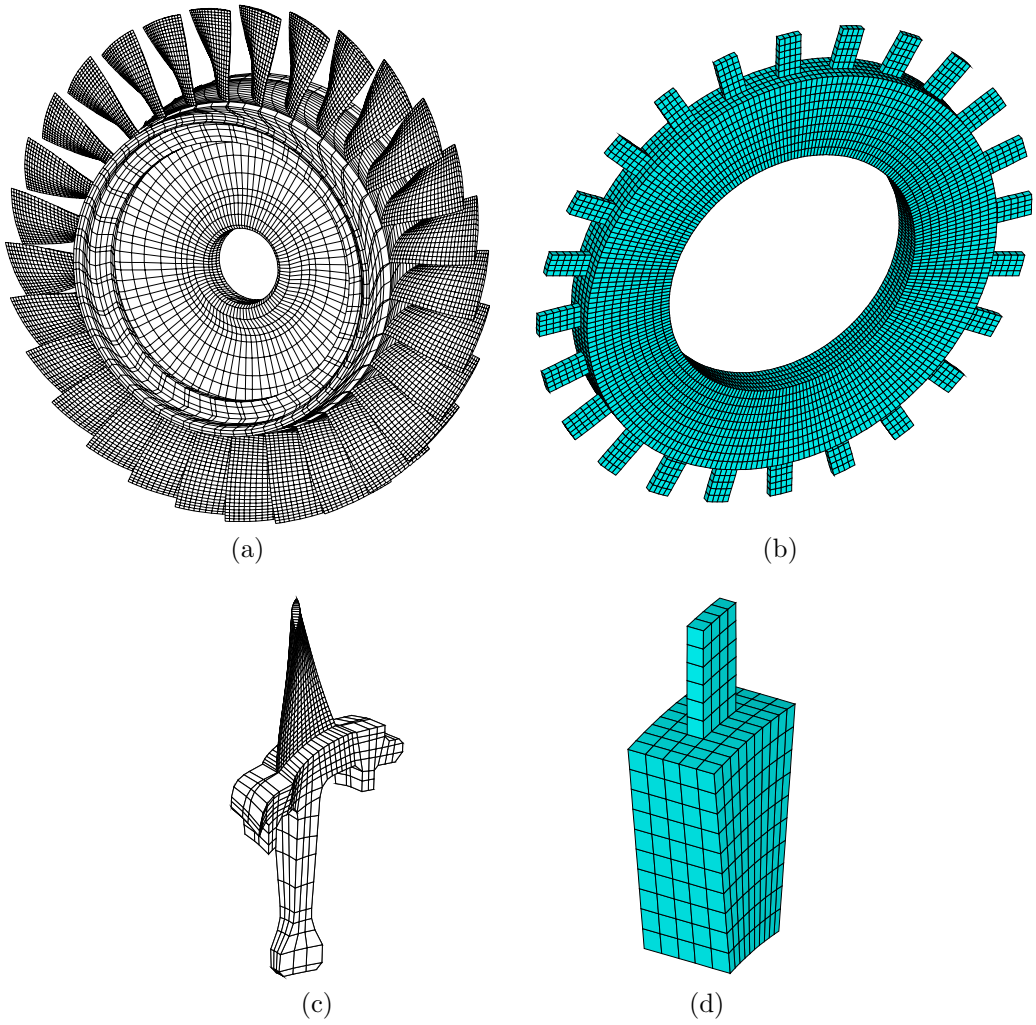

Figure 2.1: ANSYS FEM model of a) Transonic like full rotor, b) *Academic* full rotor, c) Transonic like sector and d) *Academic* sector

The FE model of the *Academic* rotor is created in ANSYS v12.1. The nominal blade is designed as a rectangular block and no interior nodes. The nominal full rotor disk is a cylindrical block. All elements in the mesh are `SOLID45` elements (8 node brick volume element). The full rotor disk is created by cyclic volume sweep of a sector model. All degrees of freedom (DOFs) of the nodes at the disk bore are constrained.

The FE model order of the *Academic* rotor is smaller than that of the Transonic rotor, hence it has worked as a good test case. With good results from MMDA for

Table 2.1: Academic rotor and Transonic rotor FEM properties comparison

	Academic rotor	Transonic rotor
ANSYS FEM properties		
Nodes/sector	786	9409
Unconstrained DOF/sector	1980	27372
Elements/sector	524	9194
Full rotor FEM model order	47520	492696
Material properties		
Young's Modulus (Mpsi)	30	17.5
Density (lbm/in^3)	0.27	0.168
Poisson's ratio	0.3	0.3

the *Academic* rotor, the next step is to test it on FEM model of the Transonic rotor. Comparison of few FEM parameters between *Academic* and Transonic rotor is given in Table 2.1.

2.3. MMDA methodology

Details of the MMDA method for *Academic* rotor is described in Bhartiya [45]. Here, MMDA method is described for Transonic like rotors. The differential equation of motion of the nodal co–ordinates (degree of freedom, DOF) of the mistuned bladed disk assembly can be written as,

$$M\ddot{\mathbf{x}} + C\dot{\mathbf{x}} + K\mathbf{x} = \mathbf{f}(t) \tag{2.1}$$

where M, K, C and $\mathbf{f}(t)$ are mass, stiffness, damping matrices, and forcing vector respectively, and $\mathbf{x}$ is the nodal DOF displacement vector. Let the dimension of vector $\mathbf{x}$ be N_d. Further, mass and stiffness mistuning are represented as,

$$M = M_t + \delta M \tag{2.2}$$

$$K = K_t + \delta K \tag{2.3}$$

where M_t and K_t are mass and stiffness matrices of the cyclically symmetric rotor with each sector being the average sector respectively. Matrices δM and δK are deviations in mass and stiffness matrices due to geometric mistuning. Note that, δM and δK are block diagonal matrices as given in the equation (A.22).

The reduced order model for the mistuned rotor is obtained by choosing a basis for transformation of $\mathbf{x}$ as,

$$\mathbf{x}(t) = \mathbf{\Phi}\mathbf{y}(t) \tag{2.4}$$

where

$$\mathbf{\Phi} = \begin{bmatrix} \Phi_0 & \Phi_1 & \Phi_2 & \dots & \Phi_{N_p} \end{bmatrix} \tag{2.5}$$

Φ_0 : set of tuned modes of the system with blades having the average geometry.

Φ_i : set of tuned modes of the system with blades having geometries perturbed along i^{th} POD feature, $i = 1, 2, \dots, N_p$

N_p : Number of POD features

For each set of tuned modes, Φ_i, the number of modes is $N_b N_f$ where N_b and N_f are number of blades in the rotor and number of families of modes chosen. Hence, the dimension of the matrix $\mathbf{\Phi}$ is $N_d \times N_r$ where $N_r = N_b N_f \, (N_p + 1)$. It is clear that the dimension of vector $\mathbf{y}$ be N_r.

Substituting equation (2.4) in (2.1) and pre–multiplying the equation by $\mathbf{\Phi}^H$, the reduced-order-model equation of motion can be written as,

$$M_r \ddot{\mathbf{y}} + C_r \dot{\mathbf{y}} + K_r \mathbf{y} = \mathbf{\Phi}^H \mathbf{f}(t) \tag{2.6}$$

where

$$M_r = \mathbf{\Phi}^H M_t \mathbf{\Phi} + \mathbf{\Phi}^H \delta M \mathbf{\Phi} \tag{2.7}$$

$$K_r = \mathbf{\Phi}^H K_t \mathbf{\Phi} + \mathbf{\Phi}^H \delta K \mathbf{\Phi} \tag{2.8}$$

$$C_r = \mathbf{\Phi}^H C \mathbf{\Phi} \tag{2.9}$$

The dimension of the reduced order model, equation (2.6) is N_r and $\mathbf{\Phi}^H$ is the complex conjugate transpose of the matrix $\mathbf{\Phi}$. Natural frequencies (ω_k) and mode shapes (ψ_k) are obtained by solving the following eigenvalue/eigenvector problem,

$$K_r \Psi = M_r \Psi \Lambda_r \tag{2.10}$$

$$\Lambda_r = \text{diag}\begin{pmatrix} \omega_1^2 & \omega_2^2 & \dots & \omega_{N_r}^2 \end{pmatrix} \tag{2.11}$$

$$\Psi = \begin{bmatrix} \psi_1 & \psi_2 & \dots & \psi_{N_r} \end{bmatrix} \tag{2.12}$$

Proportional damping is assumed for forced harmonic response *i.e.*

$$C = \alpha M + \beta K, \quad \text{thus,} \quad C_r = \alpha M_r + \beta K_r \tag{2.13}$$

where α and β are proportionality constants for damping. The forced harmonic response can be obtained using mode superposition technique,

$$\mathbf{y}(t) = \Psi \mathbf{z}(t) \tag{2.14}$$

Substituting equation (2.14) in (2.6) and pre-multiplying the result by Ψ^H the equation becomes,

$$\ddot{\mathbf{z}} + (\alpha I_{N_r} + \beta \Lambda_r)\, \dot{\mathbf{z}} + \Lambda_r \mathbf{z} = \Psi^H \mathbf{\Phi}^H \mathbf{f}(t) \tag{2.15}$$

For the p^{th} engine order excitation, the forcing function is given by,

$$\mathbf{f}(t) = \mathbf{f}_0 e^{\iota \omega_f t} \tag{2.16}$$

$$\mathbf{f}_0 = \begin{bmatrix} \mathbf{f}_1 & \mathbf{f}_1 e^{\iota\rho} & \mathbf{f}_1 e^{\iota 2\rho} & \dots & \mathbf{f}_1 e^{\iota(N_b-1)\rho} \end{bmatrix}^T \tag{2.17}$$

where,

$$\rho = \frac{2\pi p}{N_b} \tag{2.18}$$

$\mathbf{f}_1$ is the complex force row vector with phase information for each DOF acting on sector # 1 and ω_f is the forcing frequency. The steady state forced response is given by

$$\mathbf{z}(t) = \mathbf{z}_0 e^{\iota\omega_f t} \tag{2.19}$$

Substituting equation (2.19) in (2.15), equations become decoupled,

$$\left[-\omega_f^2 I_{N_r} + \iota\omega_f \left(\alpha I_{N_r} + \beta\Lambda_r\right) + \Lambda_r\right] \mathbf{z}_0 = \mathbf{g} \tag{2.20}$$

$$\mathbf{g} = \Psi^H \mathbf{\Phi}^H \mathbf{f}_0 \tag{2.21}$$

Thus, the k^{th} term of $\mathbf{z}_0$ is easily obtained as,

$$z_{0k} = \frac{g_k}{\omega_k^2 - \omega_f^2 + \iota\omega_f \left(\alpha + \beta\omega_k^2\right)} \tag{2.22}$$

Hence, the complex valued steady-state forced response amplitude vector for physical co-ordinates is obtained by the transformation

$$\mathbf{x}_0 = \mathbf{\Phi}\Psi\mathbf{z}_0 \tag{2.23}$$

2.3.1. Basis matrix $\mathbf{\Phi}$

Obtain POD features for Transonic rotor

Proper orthogonal decomposition (POD) features from the Transonic rotor are extracted by using the method developed by Sinha et. al. [62] and described here.

Let the ANSYS model of the average/mean sector blade has a total of n nodes. Spatial co-ordinates of k^{th} node of sector # j is given by $\begin{bmatrix} p_{x_j}^{(k)} & p_{y_j}^{(k)} & p_{z_j}^{(k)} \end{bmatrix}$. Then, for each of the n nodes, these co-ordinates are arranged as a one-dimensional column

vector $\mathbf{w}$ of length $3n$. For each sector # j we can write,

$$\mathbf{w}_j = \begin{bmatrix} p_{x_j}^{(1)} & p_{y_j}^{(1)} & p_{z_j}^{(1)} & p_{x_j}^{(2)} & \dots & p_{y_j}^{(n)} & p_{z_j}^{(n)} \end{bmatrix}^T \tag{2.24}$$

The average blade geometry due to available N_s sectors is obtained as

$$\overline{\mathbf{w}} = \frac{1}{N_s} \sum_{j=1}^{N_s} \mathbf{w}_j \tag{2.25}$$

For each blade, deviations in nodal coordinates from their mean values are obtained as

$$\delta\mathbf{w}_j = \mathbf{w}_j - \overline{\mathbf{w}} \tag{2.26}$$

Arranging these nodal coordinate deviations vectors as columns, the following nodal deviation matrix is formed,

$$\delta W = \begin{bmatrix} \delta\mathbf{w}_1 & \delta\mathbf{w}_2 & \dots & \delta\mathbf{w}_{N_s} \end{bmatrix} \tag{2.27}$$

POD vectors for the mistuned rotor are obtained from the singular value decomposition (SVD) of δW

$$\delta W = U\Sigma V^T \tag{2.28}$$

where

$$U = \begin{bmatrix} \mathbf{u}_1 & \mathbf{u}_2 & \dots & \mathbf{u}_{N_a} \end{bmatrix} \tag{2.29}$$

$$\Sigma = \text{diag}\begin{bmatrix} \sigma_1 & \sigma_2 & \dots & \sigma_{N_a} \end{bmatrix},\ \sigma_i > 0 \tag{2.30}$$

$$V = \begin{bmatrix} \mathbf{v}_1 & \mathbf{v}_2 & \dots & \mathbf{v}_{N_a} \end{bmatrix} \tag{2.31}$$

where N_a is the number of available POD features in the rotor, the dimensions of U, Σ and V are $3n \times N_a$, $N_a \times N_a$ and $N_s \times N_a$ respectively. These matrices are composed of orthonormal sets of vectors. Vectors $\mathbf{u}_i$ are described as POD features,

singular values σ_i are weights of the these POD features and v_{ji} are coefficient of POD mistuning parameter for i^{th} POD feature and j^{th} blade. Thus the perturbation in blade # j can be written again as,

$$\delta \mathbf{w}_j = \sum_{i=1}^{N_a} \mathbf{u}_i \sigma_i v_{ji} \tag{2.32}$$

More precisely, the contribution of i^{th} POD feature to deviation in j^{th} blade's nodal coordinates is given by $\mathbf{u}_i \sigma_i v_{ji}$, where v_{ji} is the j^{th} element of vector $\mathbf{v}_i$. Singular values for Transonic rotor are shown in Figure 2.2b.

The singular values for POD features are also related to Karhunen-Loève (KL) expansion, Sinha [62]. The KL expansion up to N_p significant eigenvalues is given by

$$\delta \mathbf{w}_j = \sum_{i=1}^{N_p} \xi_{j,i} \sqrt{\lambda_i} \mathbf{u}_i \tag{2.33}$$

where, $\xi_{j,i}$ is an instance of random variable ξ_i. These random variables are uncorrelated with zero mean and unit variance.

$$E(\xi_i) = 0 \quad \text{and} \quad E(\xi_i \xi_k) = \delta_{ik}$$

where, δ_{ik} is the Kronecker-delta function and λ_i is the eigenvalue corresponding to i^{th} POD feature. The singular value is related to corresponding eigenvalue by,

$$\lambda_i = \frac{\sigma_i^2}{N_s} \tag{2.34}$$

Details of MMDA method with ANSYS sector analysis for faster and efficient computation are given in the Appendix A. Following steps are necessary to generate pre–processing data from ANSYS to be used with MMDA for the Transonic rotor.

1. Generate POD features for Transonic rotor using singular value decomposition (SVD) as described in section 2.3.1.

2. For each POD feature, create cyclically tuned symmetric rotor with the blades having geometry perturbed along the POD feature and obtain mode shapes for all harmonic indices and required families of modes for each such bladed rotor.

3. For average rotor (cyclically tuned, blades have mean geometry) obtain

   (a) Mode shapes for all harmonic indices (nodal diameters) and required families of modes.

   (b) Cyclic mass and stiffness matrices for all nodal diameters.

4. For each sector of the mistuned rotor, obtain cyclic mass and stiffness matrices for 0^{th} nodal diameter to compute mistuning in the respective sector's tuned matrices.

Mode shapes due to a POD feature

The average sector has the blade geometry given by $\overline{\mathbf{w}}$. The mode shapes due to i^{th} POD feature are obtained as follows,

1. The mode shapes Φ_0 are obtained by cyclic symmetry analysis of the average sector for all the harmonic indices and families of modes.

2. Add the perturbation to blades of an average sector due to i^{th} POD feature with an average contribution $v_{ji} = 0.5$, *i.e.*

$$\mathbf{w}_i = \overline{\mathbf{w}} + \mathbf{u}_i \sigma_i 0.5 \tag{2.35}$$

3. The mode shapes Φ_i are obtained by cyclic symmetry analysis of this perturbed sector for all the harmonic indices and families of modes.

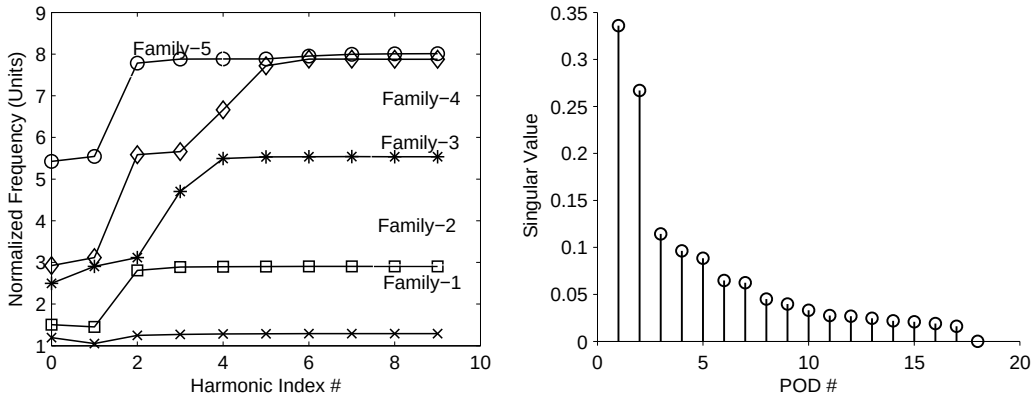

(a) (b)

Figure 2.2: Transonic rotor, a) nodal diameter map for cyclically tuned average rotor; b) singular values for the mistuned Transonic rotor

The mistuned mass and stiffness matrices are block diagonal matrices *i.e.*

$$\delta M = \begin{bmatrix} \delta M_1 & 0 & \cdots & 0 \\ 0 & \delta M_2 & \cdots & 0 \\ \vdots & \vdots & \ddots & \vdots \\ 0 & 0 & \cdots & \delta M_{N_s} \end{bmatrix} \tag{2.36}$$

δK also has a similar structure. δM_j and δK_j are deviations in mass and stiffness matrices of sector # j due to geometric mistuning. For faster computation, mass and stiffness matrices are obtained from cyclic symmetry analysis for each mistuned sector for 0 degree interblade phase angle. $\delta M_j = M^c_{j0} - M^c_{t0}$, where M^c_{j0} and M^c_{t0} are sector mass matrices obtained for 0 degree interblade phase angle from cyclic symmetry analysis of mistuned sector # j and sector with "average" blade geometry, respectively. Similarly δK_j is obtained without any approximations.

Figure 2.2a shows nodal diameter map of the tuned rotor with each blade having the average geometry described by equation (2.25). The first family of modes represents first bending modes, second family of modes contains predominantly first torsion modes, third family of modes is predominantly second bending modes *i.e.*

blades have one antinode in the middle of the blade, fourth family of modes is found to have a mix of second bending modes and torsion modes. Figure 2.2b shows singular values for the available mistuned Transonic rotor with respect to POD feature index, using all the sectors to obtain POD features.

2.4. Results

Following are the parameters for reduced order modeling with MMDA for Transonic rotor

1. Number of sectors available in the Transonic rotor $N_b = 18$.
2. Number of sectors used to obtain POD features $N_s = 18$.
3. Number of POD features obtained from SVD analysis $N_a = 17$.
4. Number of family of modes in the basis of each POD $N_f = 5$.

Thus, the maximum order of ROM can be $N_r = N_b N_f (N_a + 1) = 1620$, which is much smaller than the order of full rotor FEM model as given in Table 2.1. Various results like natural frequencies, mode shapes, forced response etc. are obtained from MMDA and compared with results from other methods.

2.4.1. MMDA accuracy measure

Following two results obtained from MMDA ROM for mistuned Transonic rotor using equation (2.10) are compared with those from full (360°) analysis of the bladed rotor via ANSYS,

1. *Frequency deviation* : It is the difference between natural frequencies of mistuned rotor and tuned average rotor for any given mode shape # j. The frequency deviation is a good metric to show the mistuning in the natural frequency

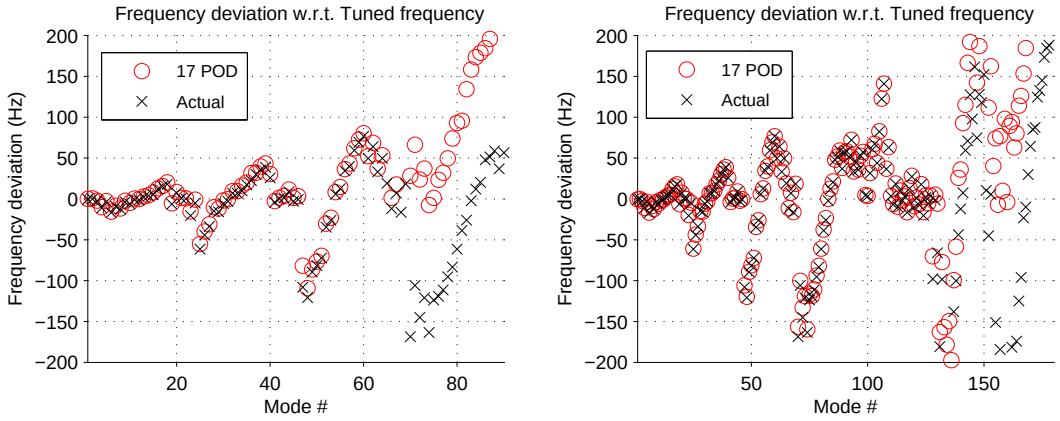

Figure 2.3: Transonic rotor frequency deviations comparison between ANSYS and MMDA for $N_p = 17$ POD a) $N_f = 5$ families of modes; b) $N_f = 10$ families of modes

of a particular mode number with respect to average rotor natural frequency. It is better at representing the frequency deviation as compared to percentage of tuned average rotor natural frequency, because in practice the tuned average rotor natural frequency is a large number, thus even a significant value of frequency deviation will be represented by a small percentage which can be misleading.

2. *MAC* : Modal Assurance Criterion (MAC) [65] of mode shape # j is given by,

$$\text{MAC} = \frac{|\phi_{j,\text{MMDA}}^T \cdot \phi_{j,\text{ANSYS}}|}{\|\phi_{j,\text{MMDA}}\| \cdot \|\phi_{j,\text{ANSYS}}\|} \tag{2.37}$$

where $\phi_{j,\text{MMDA}}, \phi_{j,\text{ANSYS}}$ are j^{th} mode shape obtained from MMDA and ANSYS analyses also called "Actual mode", respectively. $\|\cdot\|$ is the ℓ^2 norm and $|\cdot|$ is the absolute value. A MAC $= 1$ indicates perfect agreement between mode shapes.

In Figure 2.3, the frequency deviations obtained from MMDA method with different number of families of modes in the basis of ROM, and ANSYS full rotor analysis are compared. Figures 2.3a and 2.3b correspond to 5 families of modes and 10 families of modes taken with 17 POD features in the basis $\mathbf{\Phi}$ respectively. Thus, there

are total 90 modes and 180 modes respectively, which are estimated via MMDA and compared with mode shapes from ANSYS. The frequency deviations for both the cases are in agreement for a range of lower mode number/index (mode # 1 – 63) and as the mode number increases the difference in the deviations increases as seen in Figure 2.3a. A possible reason for this difference in frequency deviation for higher mode numbers is due to interaction of modes of these families with other families of modes not included in the basis, *e.g.* refer nodal diameter map, Figure 2.2a, 6^{th} and 7^{th} family of modes can interact with the modes in 4^{th} and 5^{th} family but they are not used in the basis.

Also, it has been found that if these higher families of modes are also included in the MMDA, the agreement in frequency deviation for these modes improves, and again as expected the results do not match for much higher mode numbers. From Figure 2.3b, as number of families of modes in the basis is increased to $N_f = 10$ the frequency deviations for modes which were not in agreement previously (mode # 64 – 130) improved, but for much higher mode number (mode # 131 – 180) results do not match.

In Figure 2.4, the frequency deviations results comparison between ANSYS and MMDA with various POD features and 5 families of modes in the basis are shown. Results suggest that as the number of POD features increases in MMDA, lower index modes have agreement in frequency deviation. Results are shown only up to those mode numbers (mode# 63) for which mode shapes could be predicted with good accuracy via MMDA.

In Figure 2.5, MAC values are shown for mode shapes obtained from ANSYS and MMDA with 5 and 10 families of modes, and 17 POD features in the basis. As with frequency deviations results, here also the higher index mode shapes (mode # 64 – 90) obtained from ANSYS and MMDA do not match, but a good agreement is seen for lower index mode shapes (mode # 1 – 63) with MAC values close to 1, shown in Figure 2.5a. As the number of families of modes in the basis increased to 10, the MAC

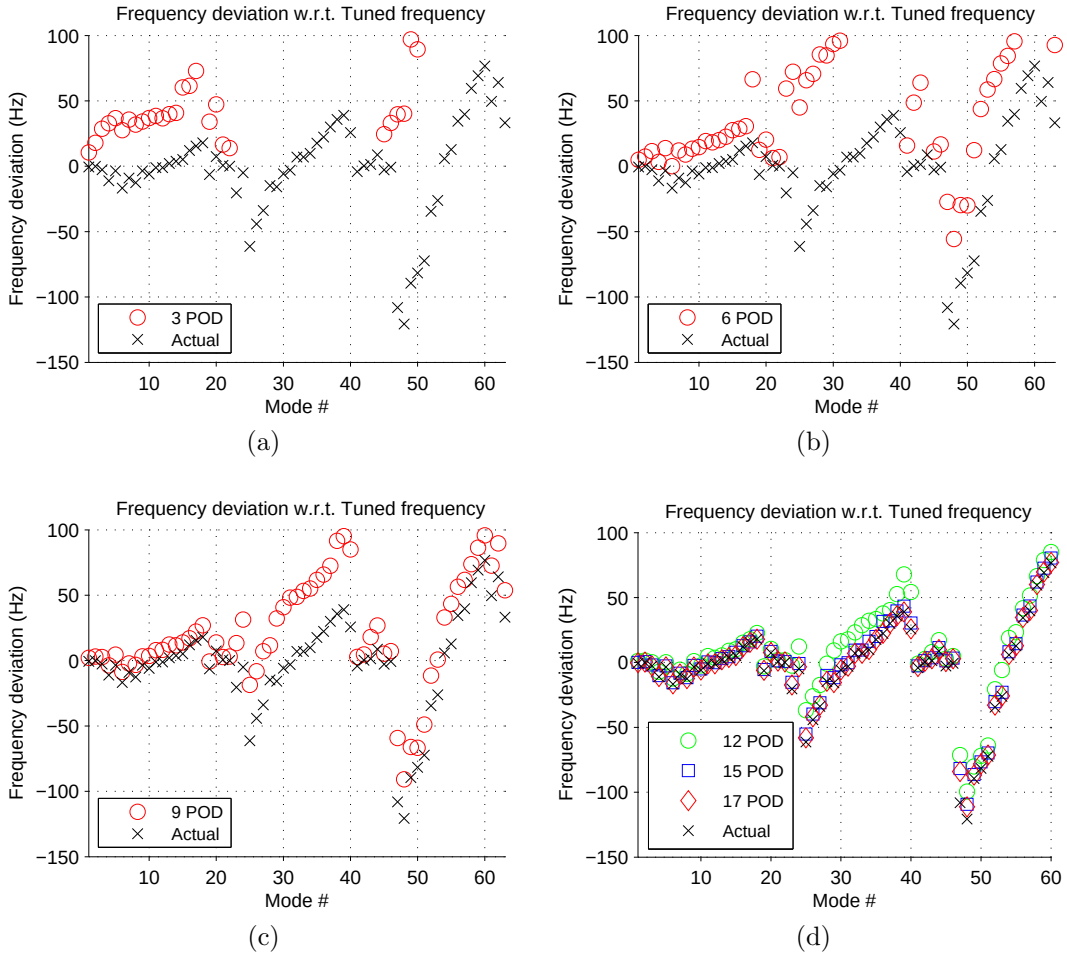

Figure 2.4: Transonic rotor frequency deviations comparison between ANSYS and MMDA for $N_f = 5$ and a) $N_p = 3$; b) $N_p = 6$; c) $N_p = 9$ d) $N_p = 12, 15$ and 17 POD in the basis

value for previously unmatched mode shapes (mode # 64 – 130) improves, but again other higher mode shapes (mode # 131 – 180) do not match, shown in Figure 2.5b.

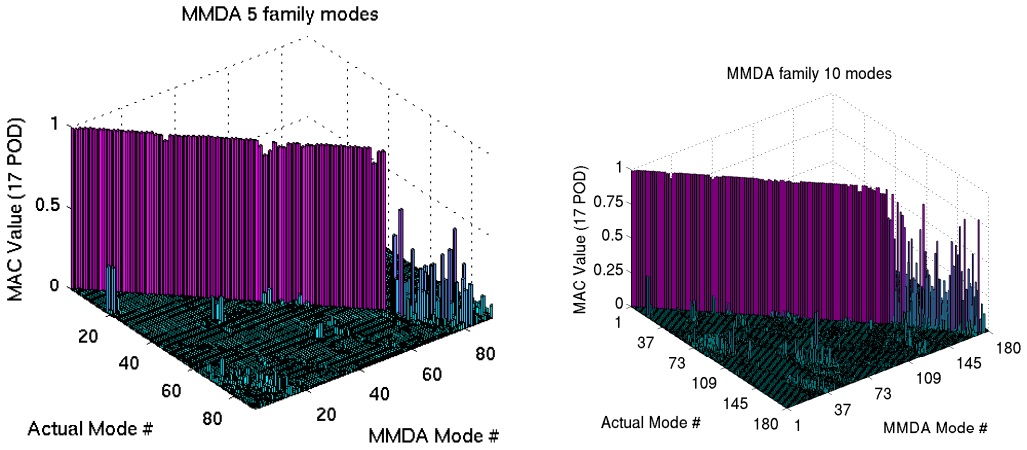

(a) (b)

Figure 2.5: Transonic rotor MAC comparison between ANSYS and MMDA for 17 PODs and a) $N_f = 5$ families of modes ; b) $N_f = 10$ families of modes in the basis

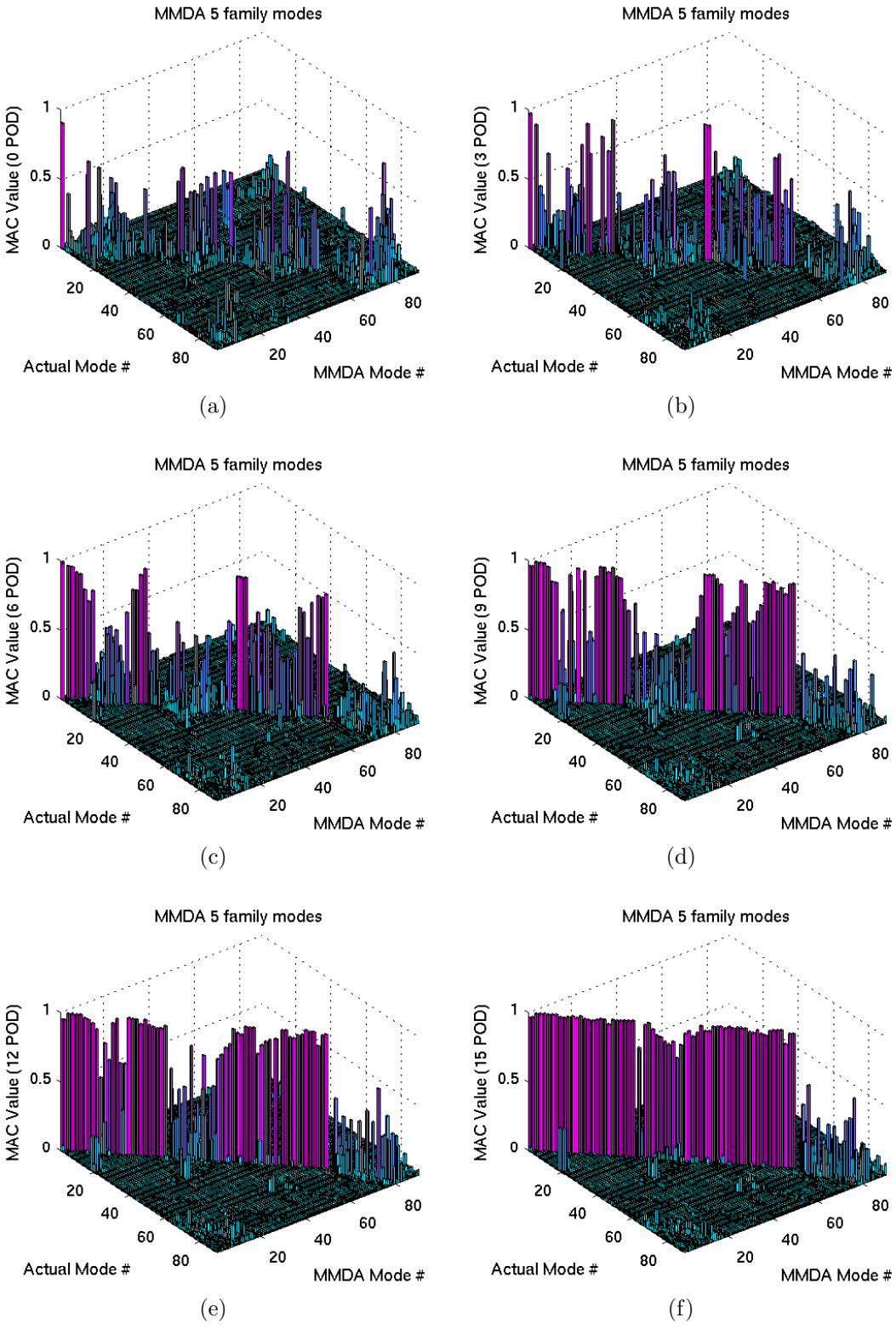

Figure 2.6: Transonic rotor MAC comparison between ANSYS and MMDA for $N_f = 5$ and a) $N_p = 0$; b) $N_p = 3$; c) $N_p = 6$; d) $N_p = 9$; e) $N_p = 12$; f) $N_p = 15$; g) $N_p = 17$ POD in the basis

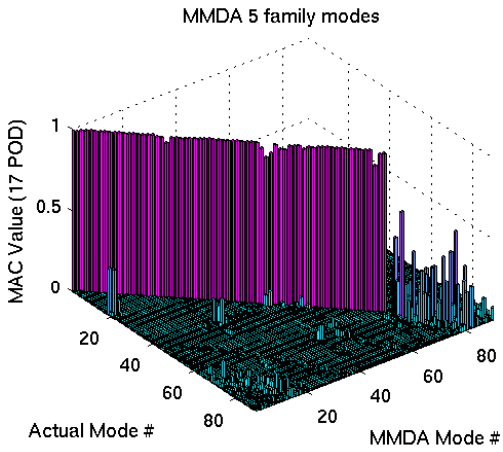

(g)

Figure 2.6: Transonic rotor MAC comparison between ANSYS and MMDA for $N_f = 5$ and a) $N_p = 0$; b) $N_p = 3$; c) $N_p = 6$; d) $N_p = 9$; e) $N_p = 12$; f) $N_p = 15$; g) $N_p = 17$ POD in the basis

In Figure 2.6, a comparative study of mode shapes from ANSYS and MMDA using MAC values with 5 families of modes and various number of POD features in the basis are shown. It is found that as the number of POD features in the basis increases the MAC values for mode shapes improve, suggesting that the mode shapes obtained from MMDA are similar to those obtained from ANSYS full rotor analysis. The results also indicates that the lower families of mode shapes for Transonic rotor can be estimated via MMDA with 12–15 POD features in the basis, instead of having all the 17 POD features. It also suggests that the POD features with lower singular values (higher POD index) have significant effect in estimation of mode shapes and frequency deviations via MMDA.

2.4.2. SNM and FMM comparison

Subset of Nominal Modes (SNM) and Fundamental Mistuning Model (FMM) are frequency mistuning based reduced order model methods developed by Yang and Griffin [30], and Feiner and Griffin [33] respectively, and are described in the Appendix C. These ROM methods have lower order than MMDA due to smaller size

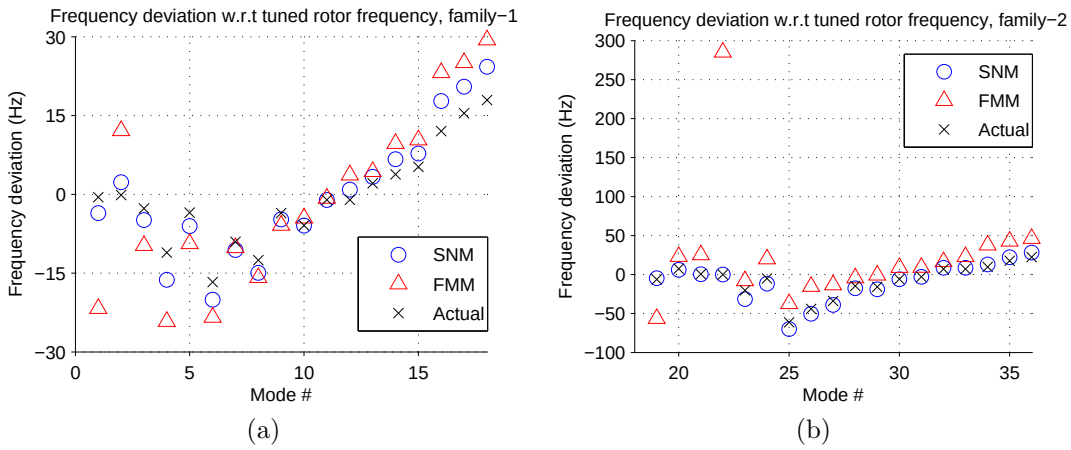

Figure 2.7: Transonic rotor frequency deviations comparison for ANSYS, SNM and FMM for a) first family of modes; b) second family of modes

of the basis. These methods are targeted for a single isolated family of modes which do not have mode interaction with other families of modes.

In Figures 2.7 and 2.8, frequency deviations and MAC values for the first and second families of modes from ANSYS, SNM (90 modes) and FMM (18 modes) are compared. Mistuned natural frequencies and mode shapes from FMM deviate from their true values (ANSYS result) by large amounts. Even though SNM results are better, there are significant errors in mode shapes and natural frequencies. The errors in the first family of modes due to FMM and SNM are notable as the first family is an isolated family of mode which was assumed for the development of both SNM and FMM. Surprisingly, mistuned frequencies and mode shapes for non-isolated second family SNM are more accurate, Figure 2.8. The impact of these errors on the forced harmonic response will be presented next.

2.4.3. Forced harmonic response

Forced harmonic response of the Transonic rotor based on the mode shapes obtained from MMDA and SNM are compared with that of obtained from full rotor ANSYS mode shapes. It is assumed that $\alpha = 0$ in equation (2.20) and β is chosen

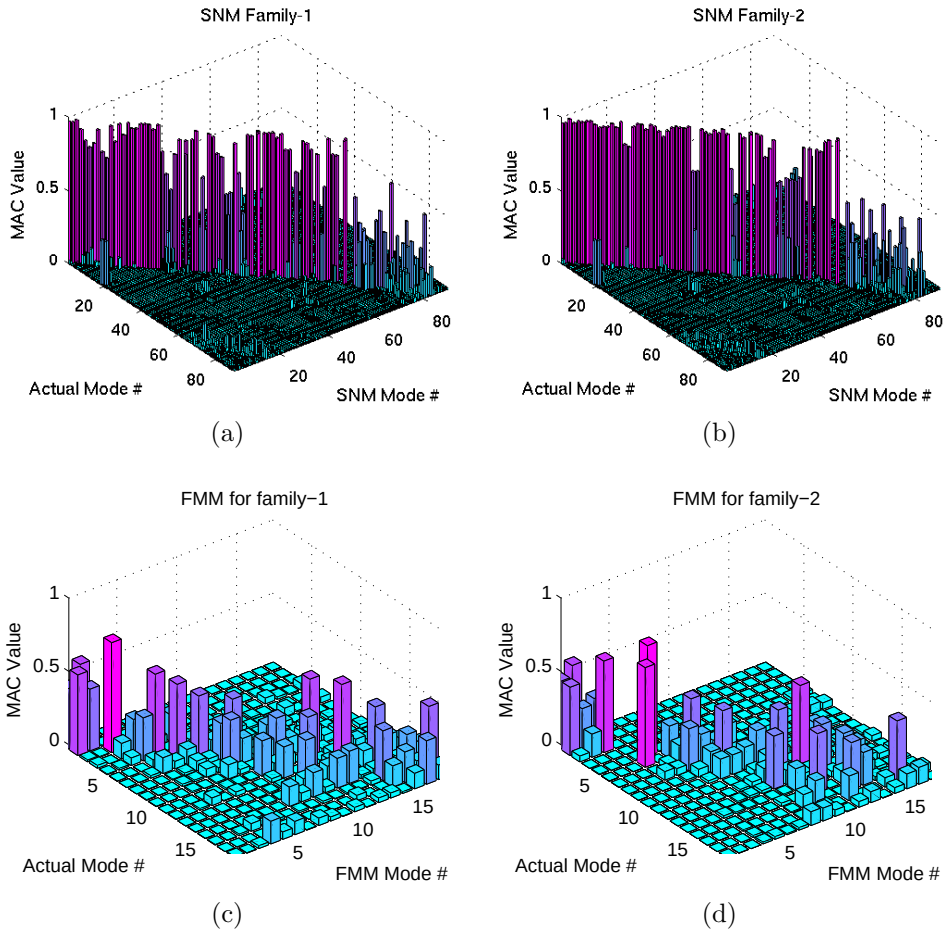

Figure 2.8: Transonic rotor MAC values for first and second families of modes of SNM (a) first families of modes and (b) second families of modes; FMM (c) first families of modes and (d) second families of modes

such that the modal damping ratio in the excited mode is 0.001. It is again observed that the forced harmonic response of the Transonic rotor based on the MMDA converges to that based on ANSYS as the number of POD features increase in the construction of basis $\mathbf{\Phi}$, equation (2.5).

In Figure 2.9, the forced harmonic response results for MMDA and SNM are compared with those obtained on the basis of ANSYS mistuned modes for first and second family of modes with 2^{nd} engine order (E.O.) excitation, Figures 2.9a and 2.9b respectively. Many excitation frequencies are chosen within $\pm 3\%$ of the first and

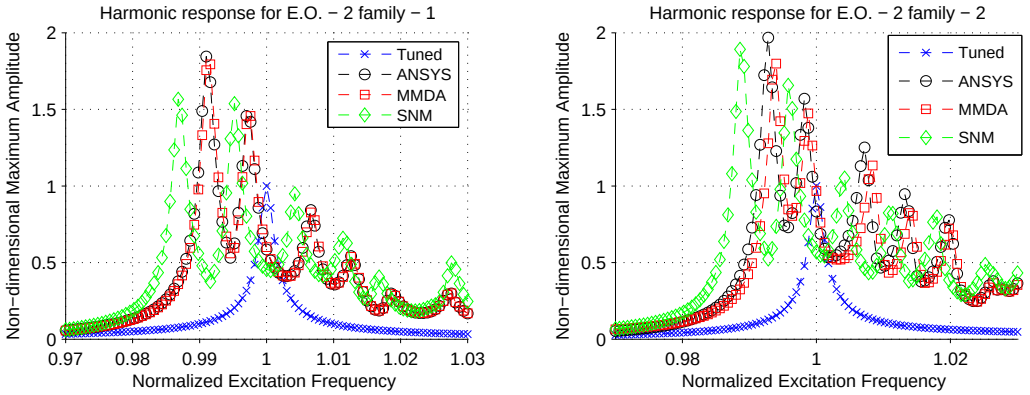

(a) (b)

Figure 2.9: Transonic rotor forced response comparison for MMDA (17 POD), SNM and ANSYS results for engine order excitation 2 and a) 1st family b) 2nd family

second family natural frequencies corresponding to the 2nd nodal diameter of the tuned average rotor. Note that the non-dimensional maximum amplitudes (NMA) in Figure 2.9 are computed at each frequency as follows,

$$\text{NMA} = \frac{\|\mathbf{x}_0\|_\infty}{\max\limits_{\omega_f} \|\mathbf{x}_{0t}\|_\infty} \tag{2.38}$$

where $\mathbf{x}_0$ and $\mathbf{x}_{0t}$ are steady state forced response amplitude vectors for mistuned and average rotors, respectively. Since mode shapes obtained from MMDA are similar to those obtained from ANSYS analysis, as a result forced harmonic response from MMDA is much closer to that obtained based on ANSYS mode shapes. Hence the forced response estimation can be obtained quickly and accurately for excitation of certain families of modes shapes from MMDA ROM.

So far, the mistuned mass and stiffness matrices (δM and δK) have been computed using sector analysis of mistuned sectors from ANSYS. In the next chapter, these mistuned matrices are approximated using Taylor series expansion of POD mistuning parameters.

2.5. Summary

In previous studies MMDA ROM method had been used only with *Academic* rotor. Now, it has been applied to a full scale industrial rotor and its results are comparable to that of ANSYS full scale rotor FEM analysis. Vibrational characteristics such as mode shapes, natural frequencies and forced response are computed and compared. Results from this chapter are summarized below.

1. With exact estimation of δM and δK from ANSYS analysis, the results from MMDA are much closer to ANSYS as compared to other reduced order model methods.

2. MMDA has emerged as a strong contender for reduced order modeling with accurate estimation of mistuned natural frequencies, mode shapes and forced response.

3. Results from MMDA improves as the number of POD features in the basis increase and even though higher index of POD features have lower contribution in blades' geometry perturbation, due to smaller singular values, they are much needed for accurate estimation of mistuned rotor frequencies and mode shapes.

4. As the number of families of modes in the basis increases, more mistuned modes' natural frequency and mode shape can be estimated accurately via MMDA.

5. Frequency mistuning approaches such as SNM and FMM did not give accurate results for mode shapes, frequency deviations and forced response, hence not suitable for reduced order modeling of Transonic rotor.

Chapter 3
MMDA with Approximate Deviations in Mass and Stiffness Matrices via Taylor Series

Previous studies on *Academic* rotor have shown that the approximate deviations in mass and stiffness matrices based on the Taylor series expansion are quite useful for MMDA ROM [42]. These approximate deviation matrices can be obtained much quickly as compared to generating the required matrices from ANSYS sector analysis, this method is also useful in Monte Carlo simulation and study of the statistics of forced harmonic response etc. Another advantage of these approximate deviation matrices is that based on the forced response one can get the mistuning parameters in each sector by simple inversion based on least squares [42, 45], thus assisting in health monitoring of individual blades based on mistuning parameters. Based on these advantages of this method the study to test this idea on a full scale industrial rotoris an attractive avenue. The large number of DOFs in Finite Element (FE) model poses a lot of questions on viability of this method on an industrial rotor. In this chapter the results for MMDA ROM of Transonic rotor with approximate deviations in mass and stiffness matrices generated by different methods are shown, also limitations of these methods are discussed.

3.1. Taylor series approximation of deviations in matrices

The details of computing approximate deviations in matrices from partial derivatives (sensitivities) are given in the Appendix B and Bhartiya [45]. Here, only final results of this theory are given. The approximate deviation (perturbation) in the mass

matrix is obtained by expanding the mass matrix about the nominal mass matrix, *i.e.* average sector mass matrix, via Taylor series and is given by

$$\delta M_s = \sum_{p=1}^{N_p} \frac{\partial \delta M}{\partial \xi_p} \xi_{s,p} + \sum_{p=1}^{N_p} \sum_{q=1}^{N_p} \frac{\partial^2 \delta M}{\partial \xi_p \partial \xi_q} \frac{\xi_{s,p} \xi_{s,q}}{2} + \Theta\left(\partial \xi^3\right) \tag{3.1}$$

where δM_s is the approximate deviation in the mass matrix for sector # s, $\dfrac{\partial \delta M}{\partial \xi_p}$ & $\dfrac{\partial^2 \delta M}{\partial \xi_p \partial \xi_q}$ are components of first order and second order deviation terms respectively in the Taylor series expansion of deviation in the mass matrix. These terms are collectively called "sensitivities". These sensitivities are computed using central difference method and explained in the Appendix B. $\xi_{s,p}$ is the mistuning parameter associated with POD feature # p for sector # s as described in KL expansion given in equation (2.33).

The reduced order mass matrix M_r is then obtained by using equation (B.17). Similarly reduced order stiffness K_r is also obtained. The computation time required for these operations is much smaller as compared to that with exact deviations in mass and stiffness matrices obtained from sector analysis from ANSYS as done in Chapter 2.

3.1.1. First and second order partial derivatives

The sensitivities are computed using central difference approach as explained in the Appendix B. For Transonic rotor a total of $N_a = 17$ first order and $\binom{N_a+1}{2} = \binom{17+1}{2} = 153$ second order terms for δM_s are needed to be computed. For this, all $\xi_{s,p} = \pm 0.5$, a constant value depending on the required matrix, are chosen for the ease of computation. Many artificial blades are created with their geometries perturbed by these $\xi_{s,p}$ as required by the method. Respective mass and stiffness matrices for these artificial sectors are obtained using ANSYS sector analysis for 0° interblade phase angle. Thus, obtained sensitivities from these matrices are stored to be used

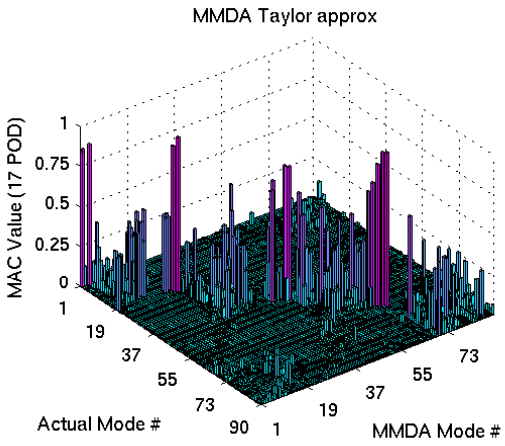

Figure 3.1: Transonic rotor MAC comparison between ANSYS and MMDA with Taylor series approximation of deviation matrices, $N_p = 17$ POD and $N_f = 5$ families of modes in the basis

later for approximating perturbations for new set of POD mistuning parameters.

The mistuning parameters $\xi_{s,p}$ for the Transonic rotor are obtained using SVD equation (2.28). The approximate deviations in mass and stiffness matrices are obtained for each sector using equation (B.17) by simple matrix addition of sensitivities and scalar multiplication of Discrete Fourier transform of $\xi_{s,p}$.

3.1.2. Results

These approximated deviations in mass and stiffness matrices are then used in MMDA algorithm; mode shapes and natural frequencies are obtained from ROM. The MAC values for mode shapes obtained from ANSYS and MMDA with all the $N_p = 17$ POD and $N_f = 5$ families of modes for each POD in the basis matrix are shown in Figure 3.1. Since MAC values are not close to the value 1, the mode shapes from MMDA with approximate deviations in matrices computed using Taylor series are not same as those obtained from ANSYS full rotor analysis. Also the frequency deviations comparison will not be accurate, hence not shown in this dissertation. This result is surprising, since this method has worked for *Academic* rotor in previous studies, but results from this method for Transonic rotor with higher FEM model

order and larger number of POD features are not accurate.

In following sections some analyses and comparison of this result and alternative approaches to approximate deviations in mass and stiffness matrices are discussed.

3.1.3. Limitations

From MAC value comparison, it is evident that MMDA with Taylor series approximation for deviations in mass and stiffness matrices needs further investigation, whereas this method has worked for *Academic* rotor case. Few possible reasons can be attributed to such results,

1. Mistuning in the Transonic rotor is too high to approximate δM and δK with only first and second order terms.

2. "Sensitivities" obtained using central difference approach are not accurate.

3. More higher order terms are needed to arrive at accurate approximations of δM and δK. For up to 3^{rd} order terms, this would require additional $\binom{N_a+2}{3} = \binom{17+2}{3} = 969$ sensitivities, which is again a time consuming task.

After further investigation it is observed that the largest singular value of Transonic rotor is much higher than that of the *Academic* rotor. To test the idea of the effect of large singular values on the industrial scale rotors, new artificial Transonic like rotors are created by using the same POD features, coefficient of mistuning parameters of Transonic rotor, and only varying their singular values. Thus reducing all singular values for nodal deviation matrix, equation (2.28), by a factor γ a new set of blades is obtained, whose perturbation is reduced by the factor γ as compared to the original Transonic rotor, *i.e.*

$$\delta W_{\text{Artificial Rotor}} = \frac{1}{\gamma}\delta W_{\text{Transonic}} \tag{3.2}$$

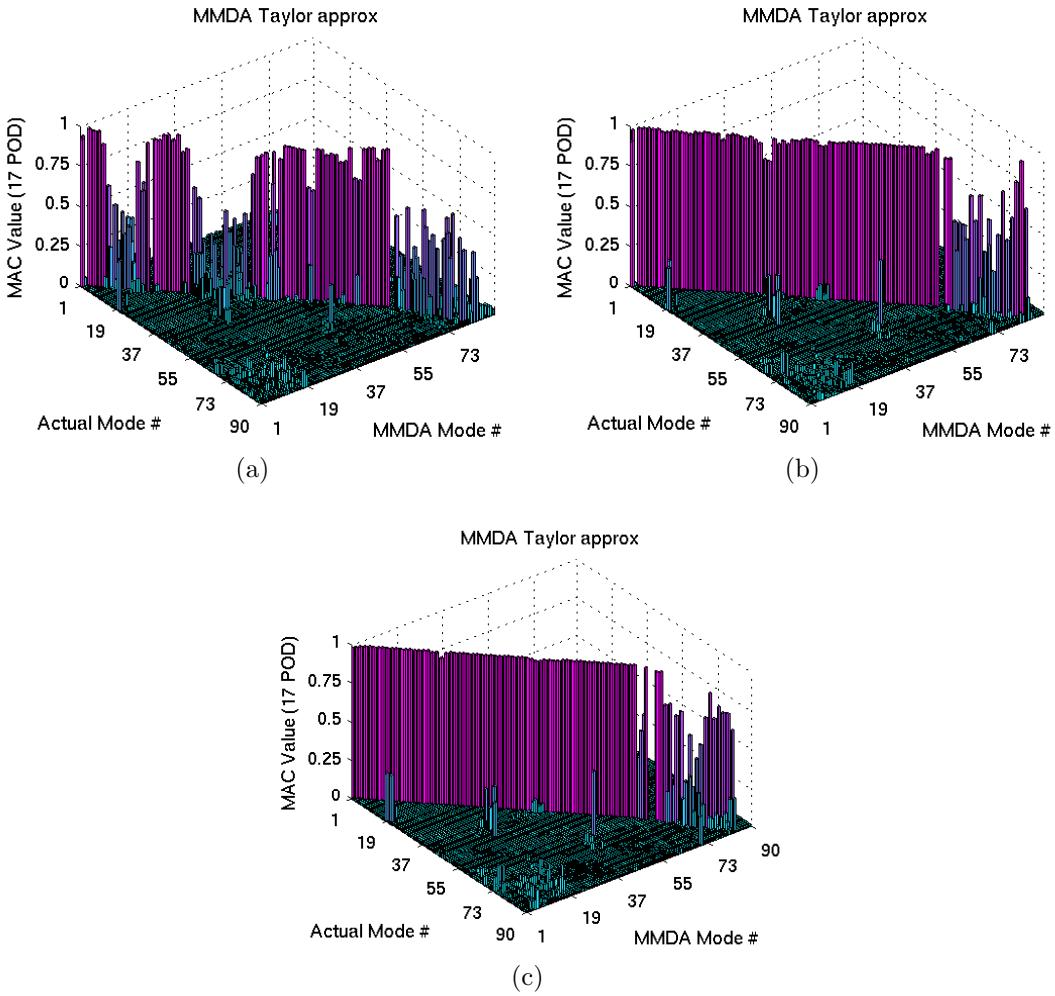

Figure 3.2: MAC comparison between ANSYS and MMDA for Artificial rotor for perturbation reduced by a) $\gamma = 2$ b) $\gamma = 5$ and c) $\gamma = 10$

Since singular values are reduced (it can also be viewed as reduction in POD mistuning parameter $\xi_{s,p}$ values), the effect of higher order partial derivative terms should be minimized.

In Figure 3.2, MAC values for mode shapes from ANSYS full rotor and MMDA with Taylor series expansion are shown for the "Artificial Rotor" with various values of γ. For each value of the factor γ a new rotor is created and its sensitivities are computed with changed singular values. Then the mode shapes of this new rotor are obtained from ANSYS full rotor analysis and compared with those obtained from

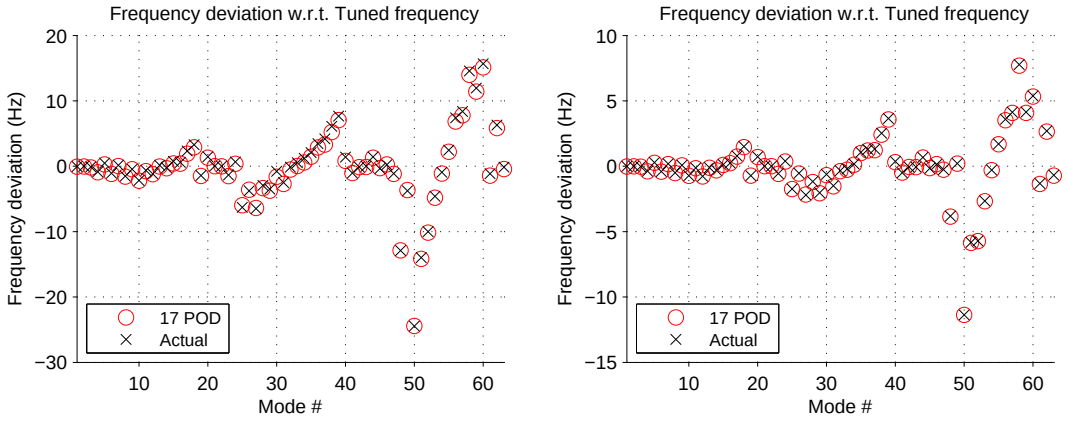

Figure 3.3: Frequency deviations comparison between ANSYS and MMDA for Artificial Rotor for perturbation reduced by a) $\gamma = 5$ b) $\gamma = 10$

MMDA with perturbations from sensitivities via Taylor series.

As γ increases mistuning in the blades decreases, thus approximate deviations in matrices from Taylor series approximation are almost equal to the exact deviations. The results also suggest that as γ increases, agreement in MAC values improves.

In Figure 3.3, frequency deviations comparison for two rotor with $\gamma = 5$ and 10 are shown. Here also, as expected with increase in γ, frequency deviations for ANSYS full rotor analysis match with those from MMDA with Taylor series approximations of deviation matrices. The nature of results is almost similar to those for MMDA with exact mass and stiffness matrix deviations in Chapter 2. Higher index modes results do not match for the similar reasons.

These results for artificial rotors having smaller geometric mistuning show that their corresponding sensitivities give accurate estimation of deviations in mass and stiffness matrices. But as observed from MAC results where mode shapes for artificial rotor having higher mistuning, $\gamma = 2$, are inaccurate, the sensitivities do not yield accurate estimation of deviations in mass and stiffness matrices.

From this study, it is thus concluded that using "sensitivities" obtained from central difference for rotors with high mistuning is not valid for Taylor series approx-

imation of mass and stiffness matrices for MMDA ROM.

3.2. Linear Least Squares Approximation

Previous methods were unable to include the effects of higher order terms in the Taylor series expansion. In this section, a method to obtain the sensitivities in mass and stiffness matrices from linear least square approximation is developed. The least squares method minimizes the error between actual values and approximation, thus the effects of higher order terms should be negligible. The method is described here to compute sensitivities for mass matrices, similar method is used to compute sensitivities for stiffness matrices.

For a known set of deviations in mass matrices and their corresponding POD mistuning parameters, an inverse problem is solved such that the error in the approximation of deviation in mass matrix obtained by these sensitivities (as used in equation (3.1)) will have least Frobenius norm [66] *i.e.*

$$\|\delta M_{\text{LS}}\|_F \leq \|\delta M_{\text{other methods}}\|_F$$

where δM_{LS} and $\delta M_{\text{other methods}}$ are deviation in mass matrices due to least square approximation and any other method, respectively, and

$$\|X\|_F = \sqrt{\sum_i \sum_j |x_{ij}|^2}$$

where, x_{ij} is i$^{\text{th}}$ row and j$^{\text{th}}$ column element of X. The deviation in mass matrix of a sector in terms on unknown sensitivities and corresponding POD features can be expressed as

$$XA = B \tag{3.3}$$

A, B and X are defined as follows. Let the deviation in mass matrix for s^{th}

sector be known, then s^{th} column of A, represented as A_s, contains POD mistuning parameter corresponding to s^{th} sector and A_s is given by

$$A_s^T = \begin{bmatrix} \xi_{s,1} & \xi_{s,2} & \dots & \xi_{s,N_p} & \xi_{s,1}\xi_{s,1} & \xi_{s,1}\xi_{s,2} & \dots & \xi_{s,1}\xi_{s,N_p} & \xi_{s,2}\xi_{s,2} & \xi_{s,2}\xi_{s,3} & \dots & \xi_{s,N_p}\xi_{s,N_p} \end{bmatrix} \tag{3.4}$$

The known deviation of mass matrix for s^{th} sector is stored as a vector in s^{th} column of the matrix B. The total number of columns, N_s, of B is same as that of A.

$$B = \begin{bmatrix} \text{vec}(\delta M_1) & \text{vec}(\delta M_2) & \dots & \text{vec}(\delta M_{N_s}) \end{bmatrix} \tag{3.5}$$

where, vec(M) is the standard vectorization operation on matrices and obtained by stacking columns of M as a vector. The unknown sensitivities in X are expanded as a column vector as well

$$X = \begin{bmatrix} \frac{\partial \text{vec}(\delta M)}{\partial \xi_1} & \frac{\partial \text{vec}(\delta M)}{\partial \xi_2} & \dots & \frac{\partial \text{vec}(\delta M)}{\partial \xi_{N_p}} & \frac{\partial^2 \text{vec}(\delta M)}{\partial \xi_1 \partial \xi_1} & \frac{\partial^2 \text{vec}(\delta M)}{\partial \xi_1 \partial \xi_2} & \dots & \frac{\partial^2 \text{vec}(\delta M)}{\partial \xi_{N_p} \partial \xi_{N_p}} \end{bmatrix} \tag{3.6}$$

The solution to X is obtained by using pseudo inverse [66] of A and given by

$$X = BA^{\dagger} \tag{3.7}$$

Similar solution for sensitivities for deviation in stiffness can be obtained. Sensitivities are obtained from a training rotor for which POD features, mass and stiffness matrices for all the sectors are known. These sensitivities are then used for computing deviations in mass and stiffness matrices for test rotors (only POD features for all the sectors are known) using equation (3.3), where X and A are known but B will be unknown.

Figure 3.4 shows MAC values results for a Transonic like rotor artificially created by selecting POD mistuning parameters from uniform distribution. Two different artificial rotors are created in this manner. One of them is used as a training rotor to

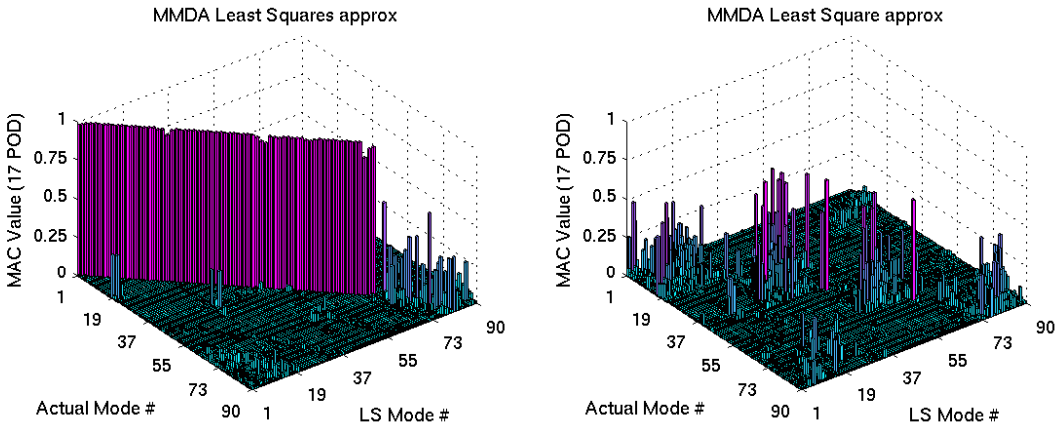

(a) Training Rotor (b) Testing Rotor

Figure 3.4: MAC values for MMDA with sensitivities obtained by linear least squares method from Transonic like training rotor and tested on test rotor

obtain the sensitivities using linear least approximation method discussed above. The other is used as a test rotor, the deviation in mass and stiffness matrices are obtained using its POD mistuning parameters and sensitivities obtained from training rotor.

In other words, a self test of this method is done, where sensitivities generated from training rotor are used to approximate deviations in mass and stiffness matrices of the training rotor itself. The MAC from MMDA ROM are close to 1 as expected, shown in Figure 3.4a. These sensitivities are then used for test rotor. The mode shapes from MMDA do not match with those of ANSYS mode shapes, shown in Figure 3.4b. The results for Transonic like rotor suggest that even though the error in estimation of mass and stiffness matrices may be small for some cases, but it is significant enough to affect the overall system dynamics for various other set of rotors, hence mode shapes do not match for test rotor.

3.3. Interpolation on Manifold

A recent method has been developed for interpolating linear structural dynamics reduced order models on manifolds by Amsallem et. al. [35]. This method maps ROM

data on a manifold to its tangent space, then the interpolation is performed on the mapped data in the tangent space and final result is mapped back to corresponding manifold to obtain interpolated data on the manifold. It is another promising method for interpolation of symmetric positive definite (SPD) matrices on SPD manifolds for approximation of deviations of mass and stiffness matrices.

Mass and Stiffness matrices for sectors and blades are SPD matrices. Previous interpolation techniques used so far did not guarantee this property after the interpolation, but interpolation on the tangent space of SPD matrices and then mapping interpolated matrices back to SPD manifold guarantee that for small perturbations the interpolated SPD matrix is a good approximation. Thus, the efficacy of this method for generating deviations in mass and stiffness matrices for MMDA will be tested.

This interpolation technique has been described in details for SPD manifold in [35]. Following steps are followed to use this method for bladed disks. Here, the steps are outlined only for computation of deviation in mass matrices, deviation in stiffness matrices of blades or sectors also follow same steps. Note that the deviations in mass and stiffness matrices are not SPD.

1. The cyclically tuned mass matrix for 0^{th} harmonic index (M^c_{t0}) of average sector is chosen as the origin. This is a SPD matrix.

2. A set of sectors are chosen from training rotor and their respective cyclically tuned mass matrices for 0^{th} harmonic index are stored. For sector $\#s$ it is represented as ${M^c_{t0}}^{(s)}$. These are also SPD matrices.

3. Mass matrix of each sector of training rotor is mapped to the tangent space of SPD manifold with origin at M^c_{t0}. This mapping is given by

$$\Gamma_s = \text{Log}_{M^c_{t0}}({M^c_{t0}}^{(s)}) = \texttt{logm}\left({M^c_{t0}}^{-1/2} {M^c_{t0}}^{(s)} {M^c_{t0}}^{-1/2}\right) \tag{3.8}$$

   where Γ_s is the mapped data matrix of ${M^c_{t0}}^{(s)}$ on the tangent space of the SPD

manifold. `logm` is matrix logarithm and MATLAB command `logm` is used for this purpose. Note that, though each mass matrix itself is a sparse matrix, but their mapping to the tangent space need not be sparse. This MATLAB command only works for full matrices and not sparse matrices.

4. The interpolation on the tangent space is obtained via second order Taylor series approximation with POD mistuning parameters. Corresponding sensitivities are obtained using training rotor sector's Γ_s and POD mistuning parameters via linear least squares approximation method. The process of obtaining these sensitivities is similar to the process described in the section 3.2.

5. For a sector # s in a test rotor with known POD mistuning parameters, the cyclically tuned interpolated mass matrices are obtained by first computing corresponding interpolation $\Gamma^s_{\text{interpolated}}$ on the tangent space using sensitivities obtained in the above steps and then mapping $\Gamma^s_{\text{interpolated}}$ on the SPD manifold using exponential mapping represented by

$$M^{c\,(s)}_{t0\text{interpolated}} = \text{Exp}_{M^c_{t0}}(\Gamma^s_{\text{interpolated}}) = M^{c\,1/2}_{t0}\texttt{expm}(\Gamma^s_{\text{interpolated}})M^{c\,1/2}_{t0} \tag{3.9}$$

where `expm` is matrix exponential and MATLAB command `expm` is used for this purpose. The resultant matrix is SPD but not necessarily a sparse matrix.

6. Deviation in the interpolated mass matrix is then computed using

$$\delta M^{(s)}_{\text{interpolated}} = M^{c\,(s)}_{t0\text{interpolated}} - M^c_{t0} \tag{3.10}$$

These interpolated deviations in mass and stiffness matrices (non SPD) are then used to obtain MMDA ROM for the test rotor.

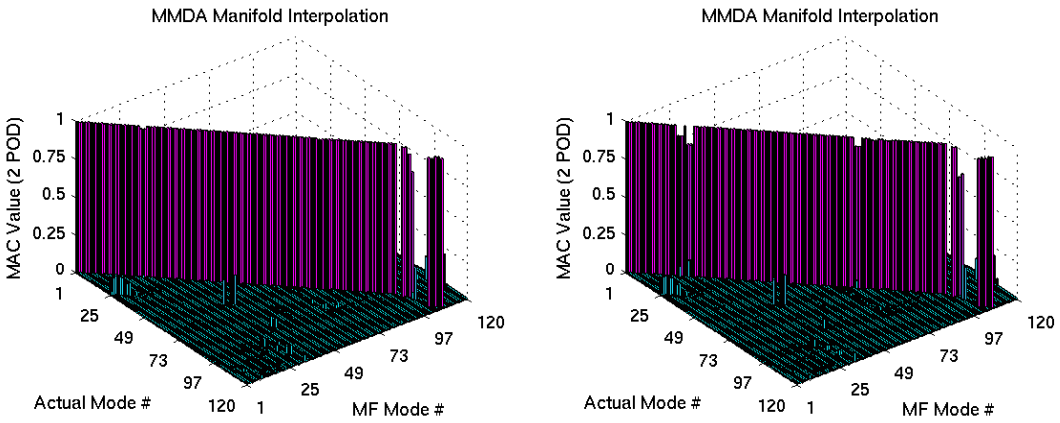

(a) Training Rotor (b) Test Rotor

Figure 3.5: *Academic* rotor MAC values for MMDA with interpolation on manifold of sector mass and stiffness matrices using POD mistuning parameters of a) Training rotor b) Test rotor

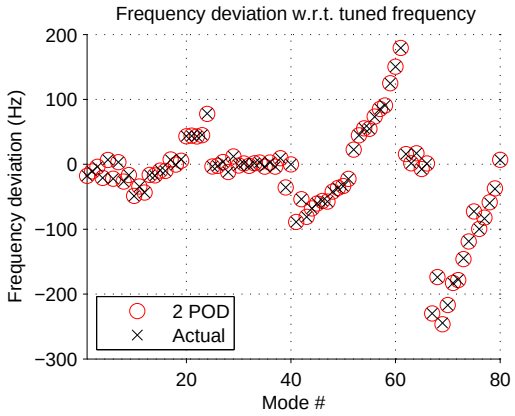

Figure 3.6: *Academic* test rotor frequency deviation for MMDA with interpolation on manifold of sector mass and stiffness matrices

3.3.1. *Academic* Rotor

The method is first tested on a set of *Academic* training and test rotor. The MAC value results for MMDA with deviations in mass and stiffness matrices obtained from interpolation on SPD manifold is shown in Figure 3.5. The sensitivities for interpolation of matrices on tangent space are computed using mass and stiffness matrices of the training rotor. Figure 3.5a shows excellent MAC value match when these sen-

sitivities are used to obtain approximated mass and stiffness matrices for training rotor from its POD mistuning parameters. Figure 3.5b also shows high accuracy for MAC value match when these sensitivities are used to obtain approximated mass and stiffness matrices for test rotor from its POD mistuning parameters. The frequency deviation results shown in Figure 3.6 for test rotor are also similar to those of actual frequency deviations. These results show that this method is able to obtain good approximation of mass and stiffness matrices to model geometric mistuning in *Academic* rotor while guaranteeing SPD properties on approximated matrices. A number of test rotors has been tested and similar good results for MAC and frequency deviations are obtained for them. Thus, this method has potential to be used to generate accurate ROM for Transonic like industrial scale rotors.

3.3.2. Transonic like rotor

This method is now applied to Transonic like rotors. The distribution of actual Transonic rotor's POD mistuning parameters are unknown, hence a new set of training and test rotors are artificially created to validate this idea on an industrial scale size rotor FE model. The POD features of Transonic like rotors are same as those of actual Transonic rotor, only the mistuning parameters are chosen from a distribution. For both training and test rotors, POD mistuning parameters are chosen from a uniform distribution between [-0.5, 0.5] range.

The number of nodes in a sector of Transonic like industrial scale rotor is extremely large as compared to *Academic* rotor. The computation resource required to apply this method to obtain approximate deviations in mass and stiffness matrices of a sector is extremely large and beyond our resource at this stage.

For the Transonic like rotors used in this research, only blades have geometric mistuning and disks are identical. Thus deviations in mass and stiffness matrices corresponding to disk part will be zero matrix for all the sectors. Therefore, to reduce the computational complexity the mass and stiffness matrices (SPD matrices)

of blades are interpolated on manifold. Sensitivities for interpolation on tangent space are obtained from blade's mass and stiffness matrices of sectors of training rotor.

Even for the interpolation of blade's mass and stiffness matrices, the computation resource was insufficient and the sensitivities could not be generated. Further research on reducing computational resource requirement is needed to use this method for approximation of mass and stiffness matrices of Transonic like rotors.

3.4. Summary

The use of approximate deviations in mass and stiffness matrices is an attractive idea. For this purpose various methods have been developed and tested for *Academic* and Transonic rotor. The results for this chapter are summarized below.

1. MMDA with approximate deviations in matrices via Taylor series expansion did not work for Transonic rotor, while it worked for *Academic* rotor case. The method has been investigated and found that this poor result is attributed to the way "sensitivities" are computed using central difference approach.

2. Sensitivities obtained from central difference approach can be used to approximate deviations in mass and stiffness matrices for rotors with small mistuning. As the mistuning increases this approximation is not valid.

3. Sensitivities are computed via linear least squares approximation. The method has resulted in good agreement for MAC for *Academic* rotor and when training Transonic like rotor is used as test rotor, but it performed poorly with a different Transonic like test rotor. It is believed that the approximated deviation in mass and stiffness matrices though may have least square error for some set of rotors but they may not be valid for other set of test rotors. These errors change system dynamics, thus ROM performs poorly.

4. Deviations in mass and stiffness matrices for sectors and blades are obtained via interpolation on SPD manifold. The interpolated mass and stiffness matrices retain their SPD properties. The method has been tested with *Academic* rotor and has been shown to yield very good results as shown in MAC and frequency deviation plots. This method has potential application for Transonic like rotors. The interpolated matrices obtained from this method are not necessarily sparse matrices, thus under computational resource constraints even blades's deviations in mass and stiffness matrices could not be obtained.

Chapter 4
Forced Response Statistics

The mistuning in the blades is a random process. Many factors such as manufacturing process, operating conditions etc. may affect the geometries of blades. The statistical distribution of forced response is highly needed to assess the life of the bladed rotor. It has been widely used in industry and literature [4, 13, 14, 17, 22, 67]. A survey of research on forced response statistics has been presented by Slater [23].

So far, most of the statistics are obtained for LPMs by Monte Carlo simulations or analytical methods. Statistical study using ROM method such as CMS with integrally bladed rotor has been done by Beck [38]. In Monte Carlo simulations forced response is computed via full rotor analysis or some ROM method for various samples of mistuned bladed-disks individually and then statistics such as mean and standard deviation are obtained.

Since MMDA with exact deviations in mass and stiffness matrices has been shown to give accurate estimates of natural frequencies, mode shapes and forced response, it is a good candidate to obtain the statistics of forced response. So far MMDA with approximation of deviations in mass and stiffness matrices with Taylor series has not worked for Transonic rotor, thus it cannot be employed for Monte Carlo simulations.

Even though MMDA with exact deviations in mass and stiffness matrices requires smaller computation time as compared to ANSYS, the time required for Monte Carlo simulations is still significant. In this chapter another method is proposed to compute the statistics by random permutations of blades of a rotor. It is also shown that these statistics are similar to those obtained by Monte Carlo simulations. These ideas are first tested on a simple lumped parameter 3 DOF model, later they are developed

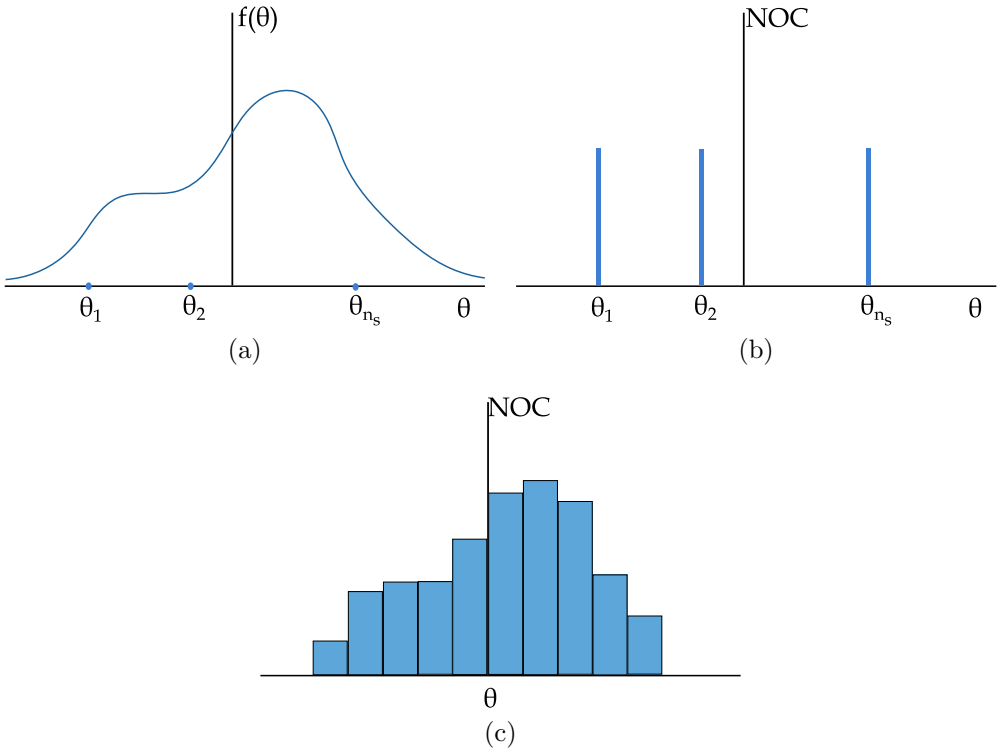

Figure 4.1: Distribution due to random permutations a) Given probability density of θ b) Number of occurrence (NOC) of discrete θ after permutations c) Histogram after random permutations

and verified for *Academic* rotor and Transonic rotor.

4.1. Random Permutations

In MMDA ROM of a new rotor, it is necessary to have same POD features in the basis as those used to construct blades' geometries. These new rotors with same POD features will only differ in the mistuning parameters' values. These random mistuning parameters $\xi_{s,p}$ are usually dependent on process parameters like age of the manufacturing machine, hours of operation etc. If the approximation of deviations in mass and stiffness matrices gives accurate results, the time required to obtain mistuned mode shapes and natural frequencies will be drastically reduced. Furthermore, obtaining forced response and its statistics from simulations of various new rotors will

also be fast.

In the absence of such an working approximation method, another method is suggested based on random permutations of blades from a given set of blades. In this method, deviations in mass and stiffness matrices for each blade are known a priori via ANSYS sector analysis. Thus, MMDA analysis for a rotor constructed from randomly selecting blades from this set is easy and forced response can be obtained quickly. In this chapter it will be shown that the statistics of forced response obtained from rotors with random permutations of blades are almost same as those from conventional Monte Carlo method.

Let the probability density of a random variable θ is given by $f(\theta)$. Let N_s samples be randomly chosen from this distribution, Figure 4.1a. Next, random permutations of these N_s samples are constructed without bias and repetition in a permutation. Each such sample will be a discrete random variable with a uniform distribution for a sufficiently large number of permutations, Figure 4.1b. A histogram made with the number of occurrences in equisized intervals will emulate the original distribution, Figure 4.1c.

For example, consider $f(\theta)$ to be a standard normal distribution with zero mean and unity standard deviation, Figure 4.2a. Let $N_s = 100$ samples be chosen randomly from this distribution, Figure 4.2b. After $10,000$ uniform random permutations (without repetitions) of this set, the histogram of the permutated set is almost similar to standard normal distribution, Figure 4.2c.

The equivalence of the distribution obtained via random permutations with original distribution can be measured using measure such as Kullback–Leibler divergence (KL divergence or relative entropy) [68]. Let the discrete probability distribution due to random permutations and standard Monte Carlo simulations be given by Q and P, respectively. The KL distance expressing the information lost when Q is used to

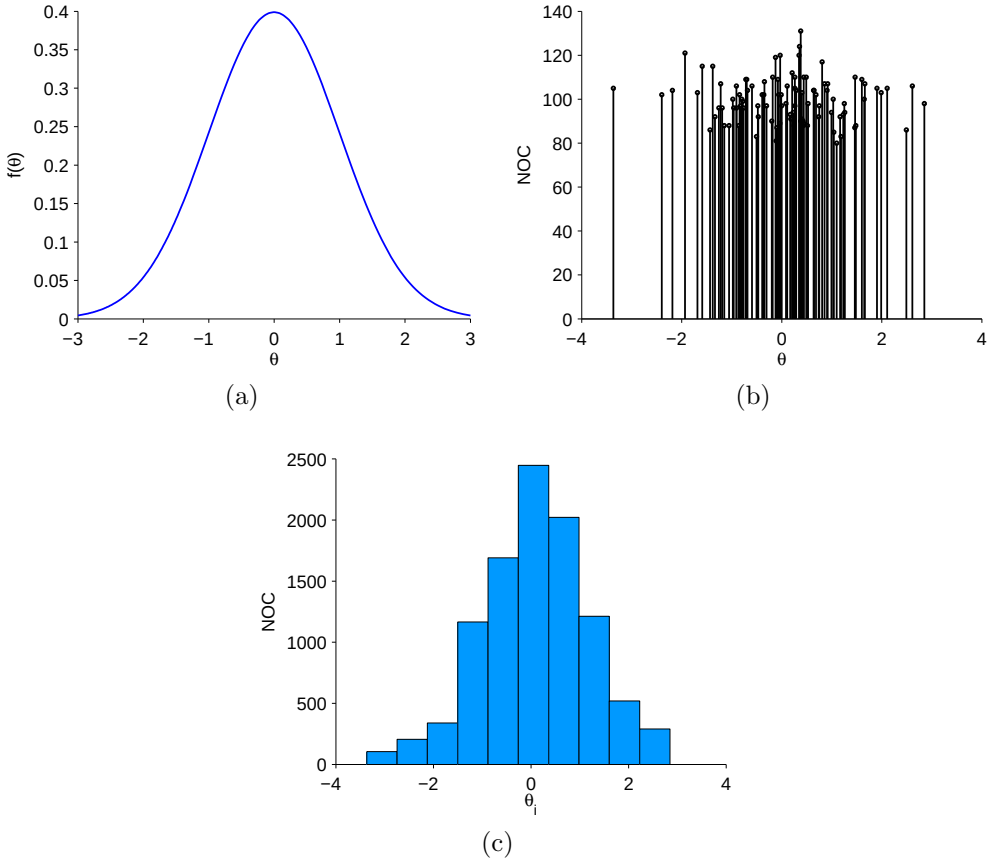

Figure 4.2: Example of random permutations distribution a) $\Theta \sim \mathcal{N}(0,1)$, b) $10,000$ random permutations of θ for $N_s = 100$ samples and , c) Histogram after random permutations

approximate the distribution P is given by,

$$D_{KL}(P||Q) = \sum_i P(i) \ln\left(\frac{P(i)}{Q(i)}\right) \tag{4.1}$$

where, P and Q both sum to 1, and $D_{KL}(P||Q) = 0$ iff $P = Q$. As Q deviates from P the KL distance increases.

In the following work, POD mistuning parameters in the bladed rotor will be considered as random variables for random permutations and Monte Carlo analyses.

Table 4.1: Parameter values for 3DOF simple rotor model

Parameter values for average rotor			
$\overline{m}_1$	0.0114	$\overline{k}_1$	4.3×10^5
$\overline{m}_2$	0.0427	$\overline{k}_2$	1.735×10^7
$\overline{m}_3$	0.0299	$\overline{k}_3$	7.52×10^6
$\overline{c}$	1.3814	$\overline{k}_c$	3.084×10^7

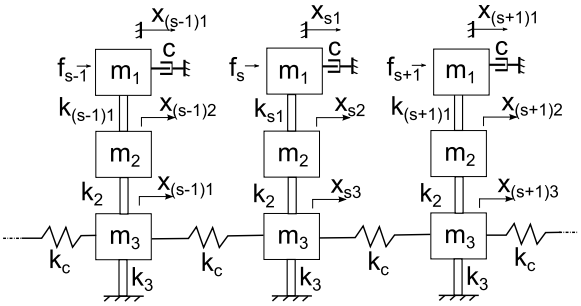

Figure 4.3: 3DOF sector model

4.2. Forced response statistics : 3DOF model

A 3DOF (3 degree of freedom) lumped parameter model of a sector of bladed rotor as described in Griffin and Hoosac [13] is used. The idea being that a sector consists of two major components disk and blade. They can be represented by three masses namely m_1, m_2 and m_3 as shown in Figure 4.3. Disk component of the sector is represented by a single mass m_3, the blade component of the sector is represented by two masses m_1 and m_2, which allow blades to simulate first and second bending modes, connected by linear springs k_1 and k_2. The disk's mass is connected to adjacent sector masses by coupling springs k_c and to the ground by another spring k_3. Mass m_1 is connected to a viscous damping, representing aerodynamic damping in the system. Values of these parameters for tuned average model are given in Table 4.1.

The simplicity of this model is an advantage to test ideas, compare the statistics obtained from random permutations and Monte Carlo simulations.

The 3DOF model is used with $N_b = 24$ number of sectors in the rotor. Only the stiffness, k_{s1}, of spring # 1 of each sector is perturbed, thus $k_{s1} = \overline{k}_1 + \delta k_{s1}$, while all

the other parameters were kept same as the average model. Following test cases are used to compare statistics from random permutations and Monte Carlo.

1. δk_{s1} is chosen randomly from uniform distribution with $\pm 2\%$ of the average stiffness $\overline{k}_1$ (standard deviation = 0.0115).

2. δk_{s1} is chosen randomly from normal distribution with zero mean and 0.0115 standard deviation of the average stiffness $\overline{k}_1$.

In both the cases for random permutations two subcases are compared. First $N_s = 24$ and then $N_s = 48$ samples of δk_{s1} are generated. The stiffnesses of sectors are interchanged according to random permutations, thus creating new set of rotors with each permutation.

For Monte Carlo simulations of both the cases, a new set of stiffness deviations for spring # 1 of each sector is created in each simulation. These stiffness deviations are uncorrelated (theoretically) with any other set.

In each simulation, forced response for the 2^{nd} E.O. excitation for the first family of modes of this simple model is computed by simple inversion of matrices.

$$\mathbf{x}_0 = \left(-\omega_f^2 M + K + \iota\omega_f C\right)^{-1} \mathbf{f}_0 \tag{4.2}$$

where $\iota = \sqrt{-1}$. M, K and C are mass, stiffness and damping matrices, respectively. $\mathbf{f}_0$ and $\mathbf{x}_0$ are amplitudes of force at each node and forced harmonic response of each node respectively. For each simulation normalized peak maximum amplitude (NPMA) of the forced response is computed in a similar way as NMA, equation (2.38).

$$\text{NPMA} = \frac{\max\limits_{\omega_f} \|\mathbf{x}_0\|_\infty}{\max\limits_{\omega_f} \|\mathbf{x}_{0t}\|_\infty} \tag{4.3}$$

where $\mathbf{x}_0$ and $\mathbf{x}_{0t}$ are amplitude vectors for mistuned and tuned cases respectively, described in Chapter 2.

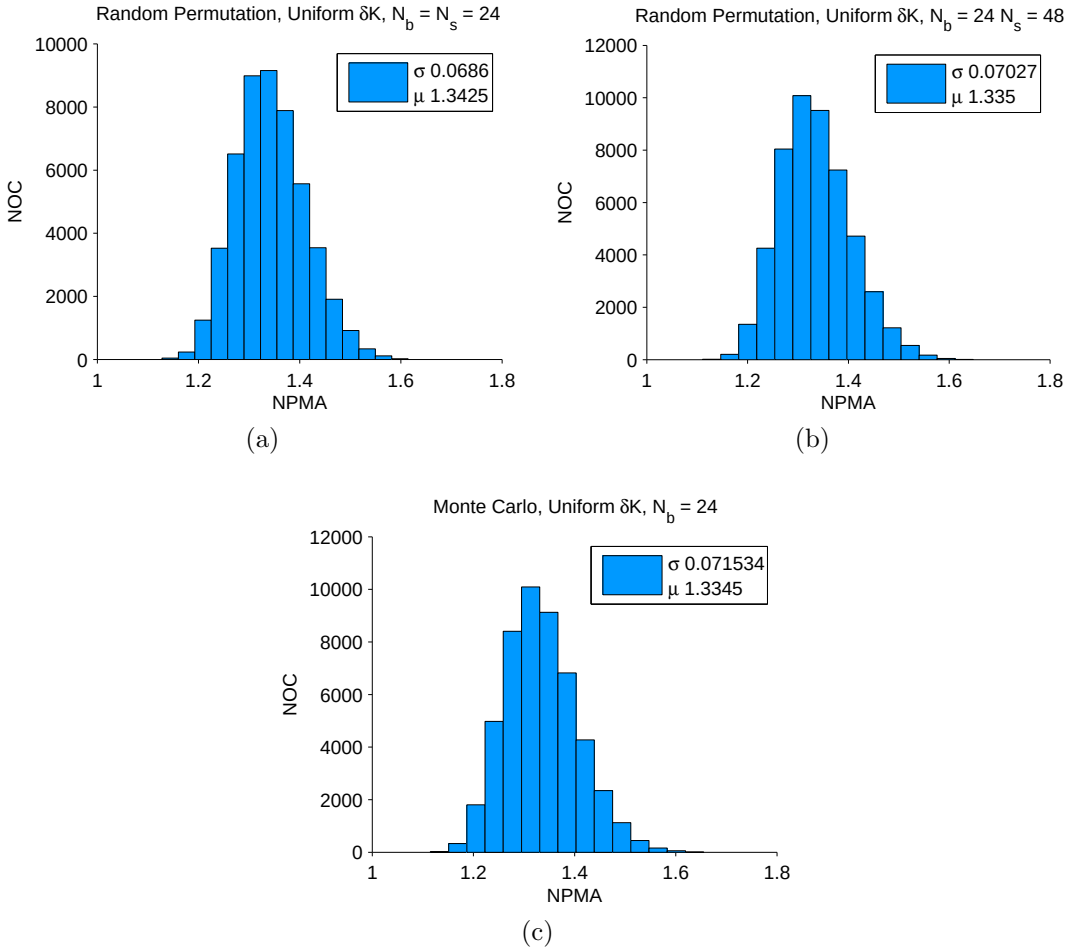

Figure 4.4: NPMA comparison for E.O. 2 and first family of modes excitation for uniform distribution of stiffness for 3DOF model with $50,000$ simulations a) random permutations ($N_s = 24$), b) random permutations ($N_s = 48$), c) Monte Carlo

In Figure 4.4 and 4.5, NPMA from random permutations and Monte Carlo simulations are compared for 50,000 simulations of cases with uniform and Gaussian mistuning in stiffness. Quantitatively, mean and variance obtained for NPMA in random permutations simulation are almost similar to those of Monte Carlo. Also, this result improves as the number of samples (N_s) in the set increases from 24 to 48. Qualitatively, histogram of NPMA for random permutations is similar to that of Monte Carlo simulations. It is to be noted that the statistics of NPMA from Monte Carlo simulations for uniform distribution and Gaussian distribution of stiffness de-

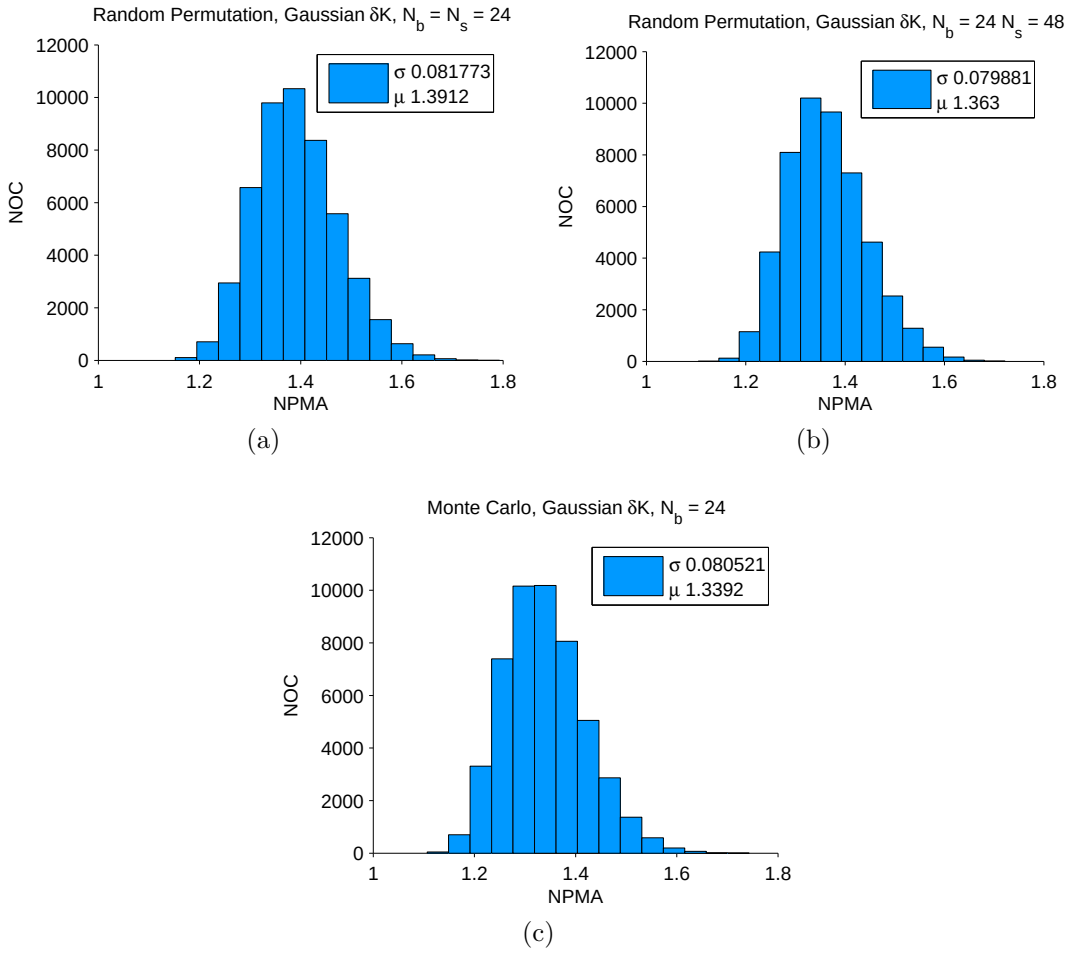

Figure 4.5: NPMA comparison for E.O. 2 and first family of modes excitation for Gaussian distribution of stiffness for 3DOF model with $50,000$ simulations a) random permutations ($N_s = 24$), b) random permutations ($N_s = 48$), c) Monte Carlo

viations are different.

For the case when the mistuning in the stiffness is generated from uniform distribution the KL distance for approximating the distribution obtained from Monte Carlo simulation to those obtained from random permutations with $N_s = 24$ and $N_s = 48$ are 0.0326 and 0.0048, respectively. These distances for the case when the mistuning in the stiffness is taken from Gaussian distribution are 0.0031 and 0.0981, respectively. These low values of KL distance suggest that the distribution of forced response obtained from random permutation are similar to those from Monte Carlo

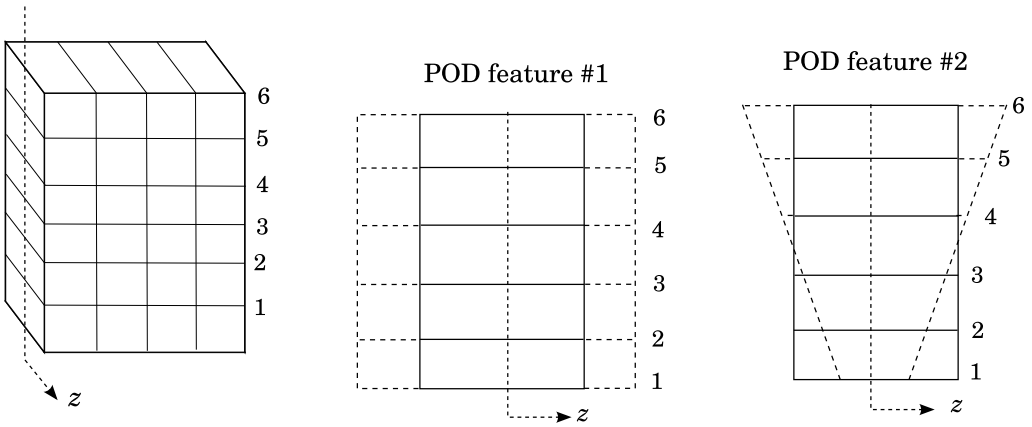

(a) (b) (c)

Figure 4.6: Finite element mesh model of *Academic* rotor a) blades b) POD feature # 1 and c) POD feature # 2

simulations.

4.3. Forced response statistics : *Academic* rotor

As an advanced example, similar idea for random permutations based statistics is applied to the *Academic* rotor of $N_b = 24$ sectors in the rotor. Let a set of sectors/blades be available, then mass and stiffness matrices for this set can be computed and stored a priori. From equation (A.26) computing reduced order matrices is just a matter of scalar multiplication and rearrangement of these matrices. Thus, generating ROM from MMDA is quick for random permutations based simulation cases.

The geometric mistuning in sector # s is represented by blade to blade variations in thicknesses containing two POD features. The geometries of blades are modified linearly by the mistuning parameters and given by

$$\mathbf{u}_0 + \mathbf{u}_1\sigma_1 v_{s1} + \mathbf{u}_2\sigma_2 v_{s2} \quad s = 1, 2, \ldots, N_b \tag{4.4}$$

$$\begin{aligned}
\mathbf{u}_0 &= \begin{bmatrix} 1 & 1 & 1 & 1 & 1 & 1 \end{bmatrix} \\
\mathbf{u}_1 &= \frac{1}{\sqrt{6}}\mathbf{u}_0 \\
\mathbf{u}_2 &= \frac{1}{\sqrt{2.8}} \begin{bmatrix} -1 & -0.6 & -0.2 & 0.2 & 0.6 & 1 \end{bmatrix}
\end{aligned} \tag{4.5}$$

where vector $\mathbf{u}_0$ is the nominal geometry, $\mathbf{u}_1$ and $\mathbf{u}_2$ are POD features used to scale co–ordinates of blades in z–direction [40] given in equation (4.5). Finite element mesh sketches for blades and POD features of *Academic* rotor are given in Figure 4.6. $\sigma_1 v_{s1}$ and $\sigma_2 v_{s2}$ are POD mistuning parameters.

Following cases are used to compare statistics from random permutations and Monte Carlo simulations of the *Academic* rotor,

1. POD mistuning parameters $\sigma_1 v_{s1}$ and $\sigma_2 v_{s2}$ are chosen from uncorrelated uniform distribution in the range $[-0.03, 0.03]$ (standard deviation $= 0.0173$) using MATLAB and then multiplied by $\sqrt{6}$ and $\sqrt{2.8}$ respectively. Thus the POD mistuning parameters are bounded.

2. POD mistuning parameters $\sigma_1 v_{s1}$ and $\sigma_2 v_{s2}$ are chosen from uncorrelated normal distribution with zero mean and 0.0173 standard deviation, and then multiplying by $\sqrt{6}$ and $\sqrt{2.8}$ respectively.

As in 3DOF model, here also in both the cases for random permutations two subcases are compared. First $N_s = 24$ and then $N_s = 48$ artificial mistuned sectors are created. Reduced order deviation matrices are computed only once and their rearrangement is done according to the permutation.

For Monte Carlo simulations of both the cases, a new set of $N_s = 24$ sectors is created in each simulation with mistuning parameters chosen from appropriate distributions for the case.

In Figure 4.7 and 4.8, NPMA from random permutations and Monte Carlo simulations are compared for 1000 simulations of cases with mistuning parameter obtained from uniform and Gaussian distribution. Here, again mean and variance of NPMA

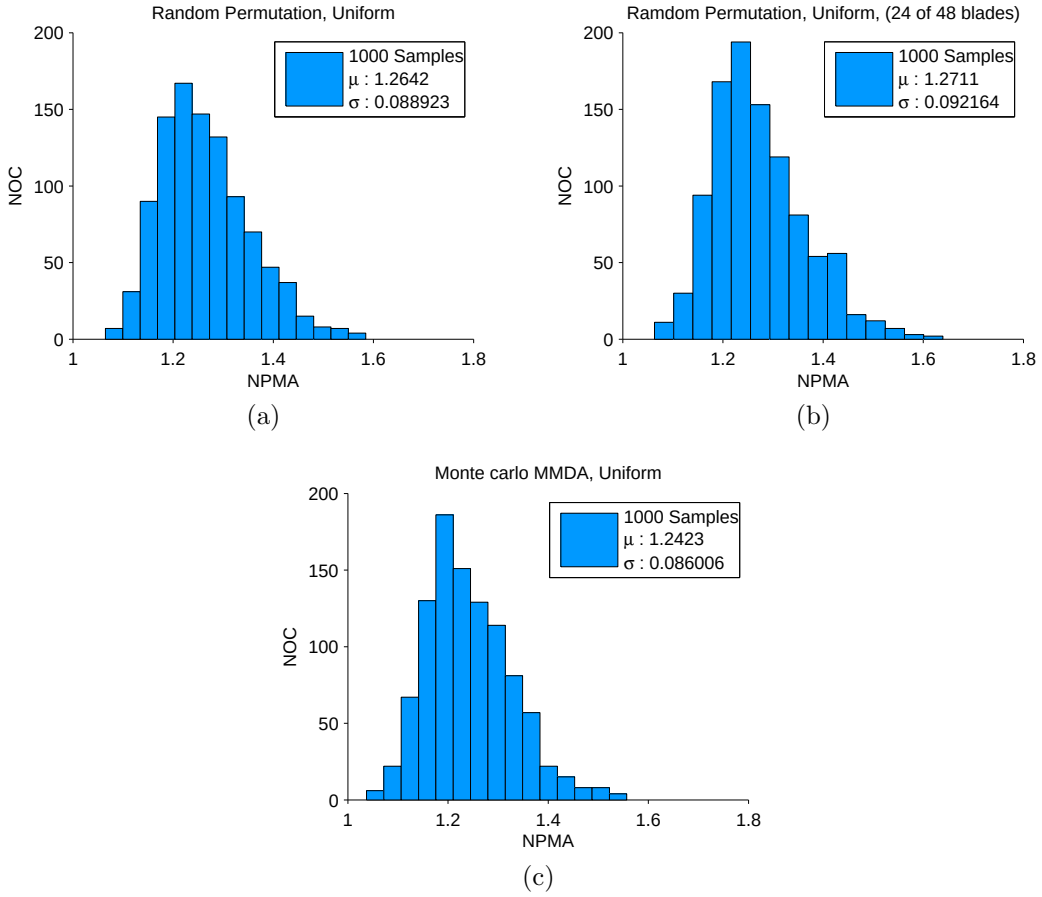

Figure 4.7: NPMA comparison E.O.2 and second family of modes excitation for uniform distribution of ξ for *Academic* rotor with 1000 simulations a) random permutations ($N_s = 24$), b) random permutations ($N_s = 48$), c) Monte Carlo

from random permutations are almost similar to those of Monte Carlo results. Also, qualitatively, the distribution of NPMA from random permutations and Monte Carlo simulations are similar. Results for random permutations approach to those of Monte Carlo simulations as the number of sectors (N_s) in initial set increases. It is to be noted that the statistics of NPMA from Monte Carlo simulations for uniform distribution and Gaussian distribution of POD mistuning parameters are different.

For the case when the POD mistuning parameters are chosen from uniform distribution the KL distance for approximating the distribution obtained from Monte Carlo simulations to those obtained from random permutations with $N_s = 24$ and

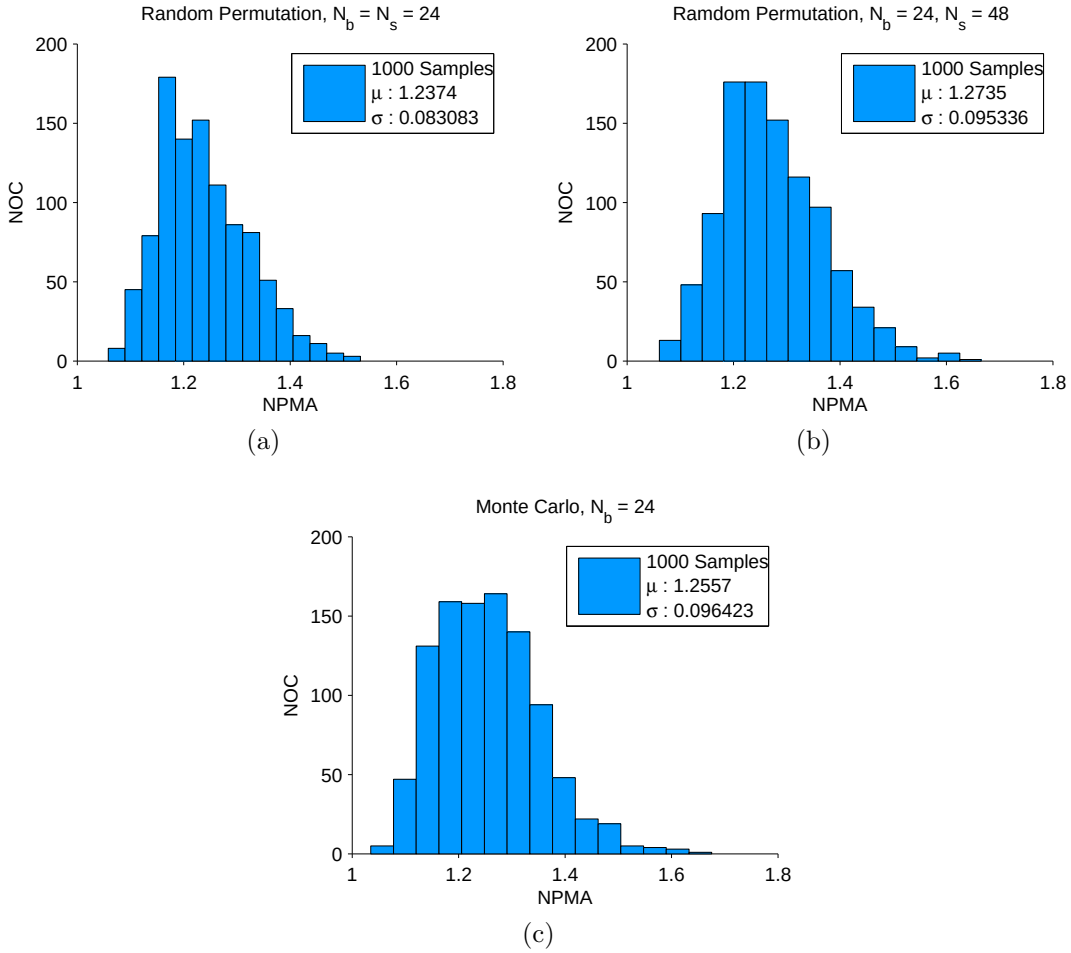

Figure 4.8: NPMA comparison E.O.2 and second family of modes excitation for Gaussian distribution of ξ for *Academic* rotor with 1000 simulations a) random permutations ($N_s = 24$), b) random permutations ($N_s = 48$), c) Monte Carlo

$N_s = 48$ are 0.0144 and 0.029, respectively. These distances for the case when the POD mistuning parameters are taken from Gaussian distribution are 0.0529 and 0.0203, respectively. Again, these low values of KL distance reinforce the conclusion from last case that the distributions of forced response obtained from random permutations are similar to those from Monte Carlo simulations.

With the computation time saving in random permutations as compared to Monte Carlo simulations, the obtained statistics can serve as a reliable metric for design and analysis. The computation time is compared in later section.

4.4. Forced response statistics : Transonic rotor

A similar approach, as in *Academic* rotor, is applied to Transonic rotor ($N_b = 18$ sectors in the rotor) to compute the NPMA statistics. Since the FEM model order for Transonic rotor is large compared to the *Academic* rotor, the Monte Carlo simulation is a formidable task. Though MMDA with random permutations is a quick substitute to compute such statistics, running only a few simulations is computationally feasible. Further there are only 18 blades' CMM data available, therefore only 17 POD features can be extracted and the inherent probability distribution of coefficients of POD mistuning parameter are unknown. Thus new Transonic like rotors are constructed for Monte Carlo simulations. Following cases are considered for comparison of forced response statistics;

1. Random permutations of available blades of original mistuned Transonic rotor.

2. Random permutations of artificially created set of sectors ($N_s = 24$) with coefficients of p^{th} POD mistuning parameters and sector # s, v_{sp} equation (2.32), taken from uncorrelated uniform distribution in $[-0.5, 0.5]$ using MATLAB and then divided by root-sum-square value of all the sectors and p^{th} POD feature.

3. Monte Carlo simulations by creating artificial Transonic like rotors by choosing v_{sp}, equation (2.32), in each simulation from the same uniform distribution as in case 2.

4. Monte Carlo simulations by creating artificial rotors by choosing v_{sp} from Gaussian distribution with zero mean and unit standard deviation then dividing it by root–sum–square value of all the sectors and p^{th} POD feature.

In Figure 4.9, NPMA for all the four cases are compared. 500 simulations are run for each case. Since original mistuned Transonic rotor's POD mistuning parameter distribution is unknown, random permutations are also generated for an artificially

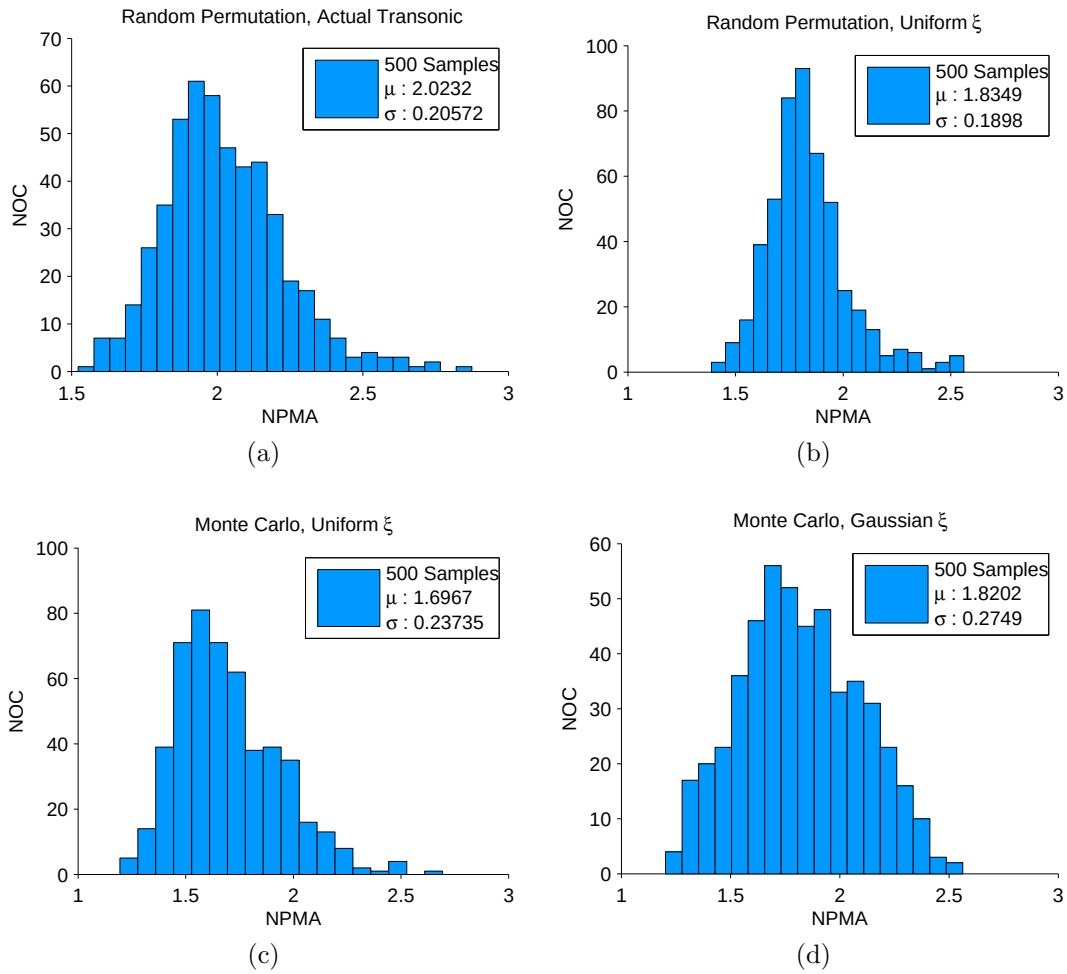

Figure 4.9: NPMA comparison for E.O. 2 and second family of modes excitation of Transonic rotor for 1000 simulations a) Transonic rotor random permutations b) Artificial rotor (Uniform ξ) random permutations c) Monte Carlo (Uniform ξ) d) Monte Carlo (Gaussian ξ)

created 18 bladed rotor from a known uniform distribution, case 2. Again, the statistical distribution for random permutations (case 2, Figure 4.9b) is close to that of the conventional Monte Carlo simulations (case 3, Figure 4.9c), thus suggesting that the random permutations is a good candidate to obtain the statistics of forced response for IBR. Here also the NPMA statistics for Monte Carlo simulations are dependent on the distribution of POD mistuning parameters.

For the case when the POD mistuning parameters are chosen from uniform distribution the KL distance for approximating the distribution obtained from Monte Carlo simulation to those obtained from random permutations is 0.1259. With this low values of KL distance we can again conclude that the distribution of forced response obtained from random permutation is similar to that from Monte Carlo simulations.

4.5. Computation Time

The simulations are performed on Lion–X clusters with Intel–Xeon 3.06 GHz, 8GB RAM at The Pennsylvania State University. Average computation time for a simulation for all the cases are given in Table 4.2. Various factors such as processor load and network traffic affect simulation time. From the Table 4.2, the huge difference in computation time required for Monte Carlo and random permutations is beneficial in obtaining faster forced response statistics.

Table 4.2: Time (in seconds) comparison for one sample of random permutations and Monte Carlo for forced response for various cases

		3DOF	*Academic* rotor	Transonic rotor
Preliminary data loading		0.4	0.21	0.12
Generate ANSYS FEM/model files			45	321
MMDA	Generate pre-processing data	0.05	23	425
	Load pre-processed data		3	80
	Eigenvalue analysis		4	150
	Total		30	655
Forced response		0.1	3	50
Monte Carlo		0.55	78.21	1026.12
Random Permutations		0.55	10.21	280.12

4.6. Summary

In the absence of a suitable method to approximate deviations in mass and stiffness matrices to estimate mistuned mode shape and frequencies, and hence forced

harmonic response statistics, the random permutations method can serve as a good, quick tool to compute these statistics with some confidence. The results from this chapter are summarized as follows.

1. From the study on *Academic* rotor, the NPMA statistics depends on the distribution of mistuning parameters.

2. Since additional FE analysis is not required for random permutations, computation of forced response statistics is faster for random permutations than Monte Carlo simulations.

3. As the number of sectors/parameters in the initial set for random permutations increases, the results from random permutations approach those of Monte Carlo simulations.

4. Even though the distribution of mistuning parameter is unknown for Transonic rotor, random permutations method still can be used to obtain the statistics of forced response. For artificially created rotors with uniform distribution of mistuning parameters, the statistics are compared and shown to have agreement between Monte Carlo simulations and random permutations.

Chapter 5
Forcing Function Estimation

Fluids (gas, air) flowing through the gas turbine in operating conditions have high velocities. The flow velocity profile across the bladed rotor is difficult to determine. Variation in flow velocity distribution on the surface of blades, turbulence, pressure fluctuation etc. can contribute to random forcing on blades. These random forcing can cause blades to vibrate at resonance at any of the natural frequency coincident with multiples of operating rotation speed of the bladed rotor. Also unsteady flow can increase the risk of flutter.

Various studies have been done to estimate these unsteady forcing function, involving experimental work like mounting sensors in the blades, to painting them [57, 58, 59, 60]. All these methods add extra components to bladed disk for forcing function measurement. With the technological advancement in non–intrusive measurements, the system response at resonance can be easily monitored for all the blades using Non–Intrusive Stress Measurement System (NSMS) data, as obtained in Choi [69]. MMDA with exact deviations in mass and stiffness matrices from ANSYS has been shown to estimate forced response accurately. A state estimator using MMDA ROM is proposed in this chapter to estimate the forcing function based on the system forced response, which is usually obtained in current health monitoring practices.

5.1. Dynamic Model

The dynamics of mistuned integrally bladed rotor (IBR) rotating at the angular speed Ω is described by

$$M\ddot{\mathbf{x}} + C\dot{\mathbf{x}} + K\mathbf{x} = B\mathbf{f}(t) \tag{5.1}$$

where M, K, C, $\mathbf{f}(t)$ and B are mass, stiffness, damping matrices, forcing vector and force distribution matrix respectively. $\mathbf{x}$ is the nodal DOF displacement vector. Choosing the basis matrix as used in MMDA, the ROM equation of motion becomes

$$M_r\ddot{\mathbf{y}} + C_r\dot{\mathbf{y}} + K_r\mathbf{y} = \mathbf{\Phi}^H B\mathbf{f}(t) \tag{5.2}$$

$$\mathbf{x}(t) = \mathbf{\Phi}\mathbf{y}(t) \tag{5.3}$$

where M_r, C_r, K_r and $\mathbf{\Phi}$ are explained in the Chapter 2. Let the forcing function $\mathbf{f}(t)$ across the IBR be given by,

$$\mathbf{f}(t) = \begin{bmatrix} \mathbf{f}_1^T(t) & \mathbf{f}_2^T(t) & \dots & \mathbf{f}_{N_b}^T(t) \end{bmatrix}^T \tag{5.4}$$

where $\mathbf{f}_s(t)$ is the forcing function column vector acting on sector # s of rotor with N_b number of sectors. Due to the bladed rotor rotation at angular frequency Ω, each blade will experience same forcing with a constant time lag, *i.e.*

$$\mathbf{f}_s(t) = \mathbf{f}_1(t + \tau_{s-1}) \tag{5.5}$$

$$\tau_s = \frac{2\pi(s-1)}{\Omega N_b} \quad p = 1, 2, \dots, N_b \tag{5.6}$$

It is assumed that certain elements of displacement vector $\mathbf{x}(t)$ are measured in steady state and represented in measurement vector $\mathbf{h}(t)$, given by

$$\mathbf{h}(t) = C_p\mathbf{x}(t) \tag{5.7}$$

where C_p is the observation matrix such that all but one elements in a row are zero, the element at index corresponding to the state being observed has value 1. Note that the velocities of the nodes can be also measured, the vector $\mathbf{h}(t)$ will be modified accordingly.

5.2. Forcing estimation

Let the system response $\mathbf{h}(t)$ be available online or its history is known. Since any steady forcing acting across the bladed rotor can always be decomposed into its Fourier components, thus $\mathbf{f}_1(t)$ can be assumed to be harmonic forcing given by

$$\mathbf{f}_1(t) = \mathbf{f}_0 e^{\iota\omega_f t} \tag{5.8}$$

where ω_f is the forcing frequency and $\mathbf{f}_0$ is a constant, unknown complex forcing vector, such that k^{th} element of $\mathbf{f}_0$ gives amplitude and phase of the forcing function on k^{th} nodal DOF of the sector # 1.

It can be observed that $\mathbf{f}_1(t)$ is a solution to the undamped harmonic oscillator equation

$$\ddot{\boldsymbol{\eta}}(t) + \omega_f^2 \boldsymbol{\eta}(t) = 0 \tag{5.9}$$

From equations (5.2), (5.4), (5.5) and (5.8) the equation of motion becomes

$$\ddot{\mathbf{y}} = -M_r^{-1} C_r \dot{\mathbf{y}} - M_r^{-1} K_r \mathbf{y} + M_r^{-1} \tilde{\boldsymbol{\Phi}}^H \boldsymbol{\eta} \tag{5.10}$$

where $\tilde{\boldsymbol{\Phi}}^H$ is a matrix and function of ω_f such that

$$\boldsymbol{\Phi}^H B \mathbf{f}(t) = \tilde{\boldsymbol{\Phi}}^H \boldsymbol{\eta} \tag{5.11}$$

Without any loss of generality, for $B = I$ the row vector of $\tilde{\boldsymbol{\Phi}}^H$ corresponding to

l^{th} POD feature and p^{th} nodal diameter is given by

$$\tilde{\mathbf{\Phi}}^H_{l,p} = \phi^H_{l,1,p} \sum_{s=1}^{N_b} e^{\iota \frac{2\pi}{N_b}(s-1)(p-\frac{\omega_f}{\Omega})} \tag{5.12}$$

where $\phi_{l,1,p}$ is the mode shape of sector # 1 for l^{th} POD feature and p^{th} nodal diameter. It can be shown that

$$\sum_{s=1}^{N_b} e^{\iota \frac{2\pi}{N_b}(s-1)(p-\frac{\omega_f}{\Omega})} = \begin{cases} N_b & \text{if } \frac{\omega_f}{\Omega} = p \\ 0 & \text{if } \frac{\omega_f}{\Omega} \neq p \text{ and integer} \end{cases} \tag{5.13}$$

When the frequency ratio $\frac{\omega_f}{\Omega}$ is not an integer then the summation is a complex number.

Define the state vector as

$$\mathbf{z} = \begin{bmatrix} \mathbf{y}^T & \dot{\mathbf{y}}^T & \boldsymbol{\eta}^T & \dot{\boldsymbol{\eta}}^T \end{bmatrix}^T \tag{5.14}$$

Using equations (5.9), (5.10) and (5.14) the state space model can be written as,

$$\dot{\mathbf{z}} = A\mathbf{z} \tag{5.15}$$

$$\mathbf{h} = E\mathbf{z} \tag{5.16}$$

where A, E and $\mathbf{h}$ are system matrix, measurement (output) matrix and measurement (output) vector respectively. Matrices A and E are given by

$$A = \begin{bmatrix} 0 & I_{N_r} & 0 & 0 \\ -M_r^{-1}K_r & -M_r^{-1}C_r & M_r^{-1}\tilde{\mathbf{\Phi}}^H & 0 \\ 0 & 0 & 0 & I_{N_n} \\ 0 & 0 & -\omega_f^2 I_{N_n} & 0 \end{bmatrix} \tag{5.17}$$

$$E = \begin{bmatrix} C_p\mathbf{\Phi} & 0 & 0 & 0 \end{bmatrix} \tag{5.18}$$

N_r, N_o and N_n are order of ROM, number of rows in C_p and number of elements in the forcing vector $\mathbf{f}_1(t)$ respectively.

In general, A and E are complex matrices. Then, real and imaginary components of states and measurement vectors in equation (5.15) and (5.16) are concatenated to obtain real state and measurement equations such that

$$\dot{\mathbf{z}}_a = A_a \mathbf{z}_a \tag{5.19}$$

$$\mathbf{h}_a = E_a \mathbf{z}_a \tag{5.20}$$

where

$$\mathbf{z}_a = \begin{bmatrix} \mathbf{z}_R \\ \mathbf{z}_I \end{bmatrix}; \mathbf{h}_a = \begin{bmatrix} \mathbf{h}_R \\ \mathbf{h}_I \end{bmatrix}; A_a = \begin{bmatrix} A_R & A_I \\ -A_I & A_R \end{bmatrix}; E_a = \begin{bmatrix} E_R & E_I \\ -E_I & E_R \end{bmatrix} \tag{5.21}$$

$$\mathbf{z} = \mathbf{z}_R + \iota \mathbf{z}_I; \mathbf{h} = \mathbf{h}_R + \iota \mathbf{h}_I; A = A_R + \iota A_I; E = E_R + \iota E_I \tag{5.22}$$

A state-estimator based on Kalman filter can be used to estimate states and thus forcing function. The estimator state equations are given by

$$\dot{\hat{\mathbf{z}}}_a = A_a \hat{\mathbf{z}}_a + L\left(\mathbf{h}_a - \hat{\mathbf{h}}_a\right) \tag{5.23}$$

$$\hat{\mathbf{h}}_a = E_a \hat{\mathbf{z}}_a \tag{5.24}$$

Here the observer gain matrix L is obtained by solving Filter Algebraic Riccati Equation (FARE) because of its robustness to yield a gain [70]. The FARE equation is given by

$$AX + XA^T - XE^T EX + Q = 0 \tag{5.25}$$

$$L = XE^T \tag{5.26}$$

where Q is the input noise covariance matrix, chosen to be an identity matrix of

appropriate dimensions.

It is assumed that measurements are taken for steady state response. The measurement output vector to be used in equation (5.23) is obtained by using Φ_a, mistuned rotor mode shapes, as the basis in equation (5.1). Thus, from equation (5.1), (5.4) and (5.8), the plant output in steady state is obtained as,

$$\mathbf{h} = C_o \boldsymbol{\eta} \tag{5.27}$$

$$C_o = C_p \Phi_a \left(-\omega_f^2 I_m + \iota \omega_f \Phi_a^H C \Phi_a + \Lambda_m\right)^{-1} \mathbf{g} \tag{5.28}$$

$$\mathbf{g} = \sum_{s=1}^{N_b} \Phi_a^{(s)^H} e^{\iota \frac{2\pi}{N_b} \frac{\omega_f}{\Omega}(s-1)} \tag{5.29}$$

where $\Phi_a^{(s)}$ is mode shape of s^{th} sector of the mistuned rotor. Λ_m is diagonal matrix of square of mistuned natural frequencies of m modes, the number of columns of Φ_a is also m.

5.2.1. 3DOF bladed rotor model

First the 3DOF bladed rotor model, described in the Chapter 4, is used to test the concept of force estimation. The design of filter for this model is a little different from method explained above. M_r, C_r, K_r and $\boldsymbol{\Phi}$ in equation (5.10) are real but $\tilde{\boldsymbol{\Phi}}$ is a complex matrix. This is due to the phase difference in forces acting between adjacent sectors. Few modification in the equation (5.10) are done to incorporate this difference, such that only real numbers are used in the model development. In this case the states will not be needed to split in real and imaginary components. The equation of motion for reduced order model is given by

$$\ddot{\mathbf{y}} = -M_r^{-1} C_r \dot{\mathbf{y}} - M_r^{-1} K_r \mathbf{y} + M_r^{-1} \mathbf{b}_1 \boldsymbol{\eta} + \frac{1}{\omega_f} M_r^{-1} \mathbf{b}_2 \dot{\boldsymbol{\eta}} \tag{5.30}$$

$$\tilde{\boldsymbol{\Phi}}^H = \mathbf{b}_1 + \iota \mathbf{b}_2 \tag{5.31}$$

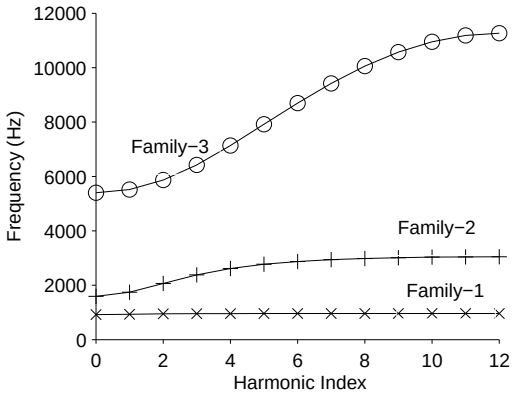

Figure 5.1: Nodal diameter map for 3DOF rotor model

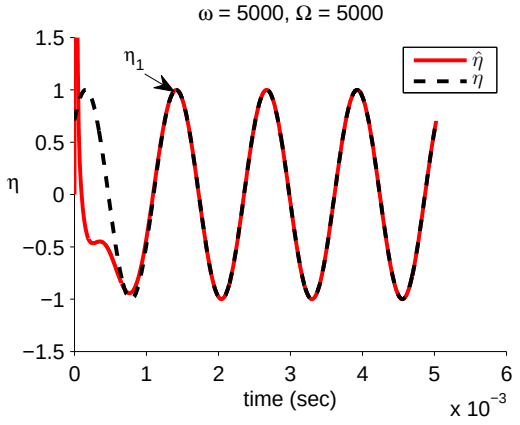

Figure 5.2: 3DOF rotor model force estimation convergence for tip excitation, displacement observed at tip and 1st family of modes used in ROM construction

Thus the system matrix A is given by

$$A = \begin{bmatrix} 0 & I_{N_r} & 0 & 0 \\ -M_r^{-1}K_r & -M_r^{-1}C_r & M_r^{-1}\mathbf{b}_1 & \frac{1}{\omega_f}M_r^{-1}\mathbf{b}_2 \\ 0 & 0 & 0 & I_{N_n} \\ 0 & 0 & -\omega_f^2 I_{N_n} & 0 \end{bmatrix} \tag{5.32}$$

Matrix E for observer remains same as given in equation (5.18). The displacement of observation nodes of plant is given by

$$\mathbf{h} = C_{oR}\boldsymbol{\eta} + \frac{1}{\omega_f}C_{oI}\dot{\boldsymbol{\eta}} \tag{5.33}$$

$$C_o = C_{oR} + \iota C_{oI} \tag{5.34}$$

where C_o is given by equation (5.28).

Figure 5.1 shows the nodal diameter map for the average rotor model with $N_b = 24$ sectors in the rotor. A mistuned rotor is created by adding random mistuning generated from a uniform distribution between $\pm 2.5\%$ of the mean value of mass # 1 and spring # 1 of each sector.

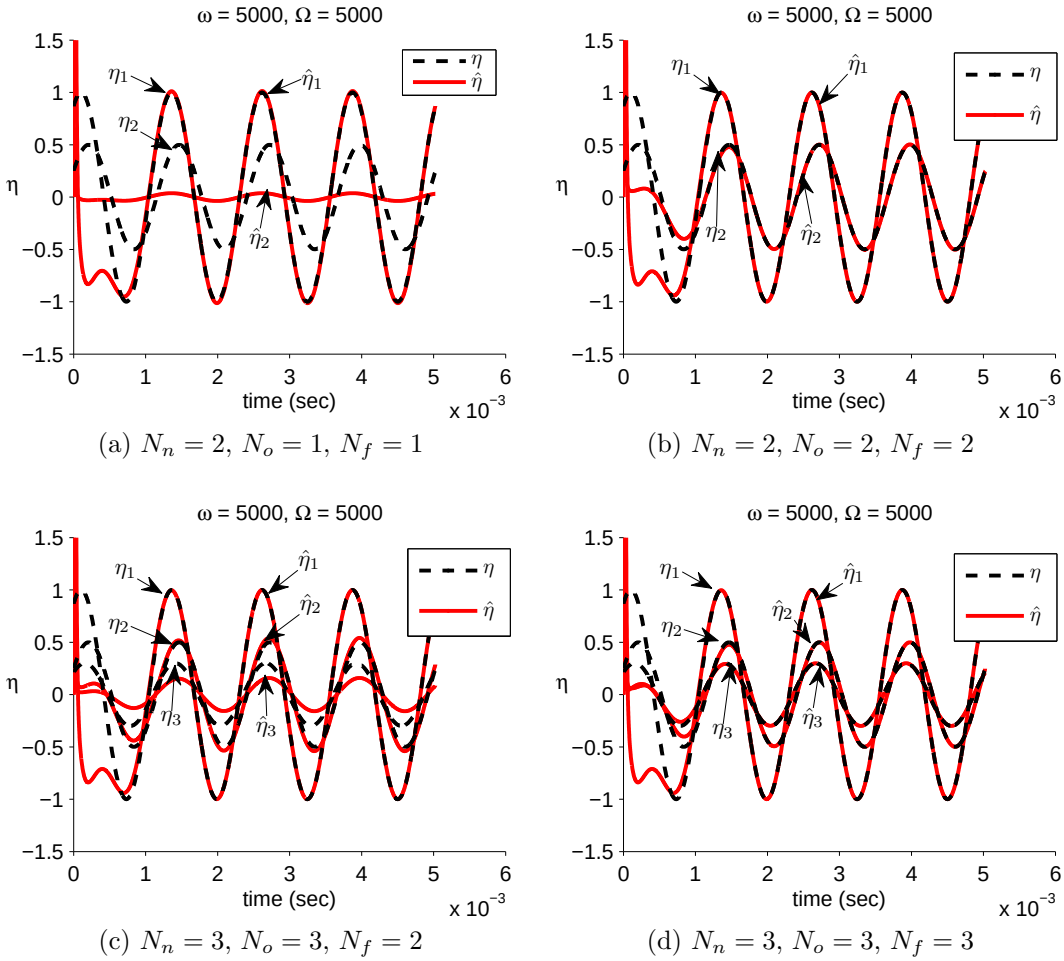

(a) $N_n = 2$, $N_o = 1$, $N_f = 1$ (b) $N_n = 2$, $N_o = 2$, $N_f = 2$

(c) $N_n = 3$, $N_o = 3$, $N_f = 2$ (d) $N_n = 3$, $N_o = 3$, $N_f = 3$

Figure 5.3: 3DOF rotor model force estimation convergence for numbers of force input (N_n), displacement measurements (N_o) and family of modes (N_f) used in ROM

The rotor frequency is $\Omega = 5000$ rad/s and the forcing is assumed to have 1$^{\text{st}}$ engine order excitation *i.e.* forcing frequency $\omega_f = \Omega$. Forcing is assumed to be of the form given in equation (5.8). The initial conditions of state estimator are chosen arbitrarily as $\hat{\mathbf{z}}_a(0) = \mathbf{0}$ for all the cases in this section. Different cases with varying number of force locations, observation points in the system and number of tuned modes used for reduced order model are studied.

Figure 5.2 shows quick convergence of estimated force towards actual force $\boldsymbol{\eta}$ value in time. In this case, only the tip of each sector is excited *i.e.* force of amplitude 1

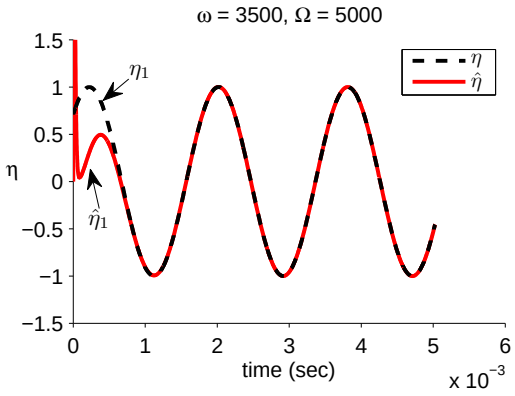

Figure 5.4: 3DOF rotor model force estimation convergence for asynchronous excitation with number of force input $N_n = 1$, displacement measurement $N_o = 1$ and family of modes $N_f = 1$ used in ROM

unit is applied only to mass # 1 of each sector. Only 1st family of tuned modes is used to create reduced order model. A state observer is created based on this ROM, with displacements of mass # 1 for each sector being observed.

In Figure 5.3a and 5.3b force is applied to whole blade of the rotor, *i.e.* force of amplitude 1 and 0.5 is applied to mass #1 and 2 respectively. In the first case, displacement of only mass #1 is observed and first family of tuned modes is used to create ROM. In the second case, displacements of both mass #1 and 2 are observed and the first two families of tuned modes are used to create ROM. The convergence of estimated force in the second case suggests that all the applied forces can be estimated accurately when sufficient numbers of outputs are used and the size of ROM is increased.

In Figure 5.3c and 5.3b force is applied to whole sector of the rotor, *i.e.* force of amplitude 1, 0.5 and 0.3 is applied to mass #1, 2 and 3 respectively. In the first case, displacements of all masses are observed and the first two families of tuned modes are used to create ROM. In the second case, displacements of all masses are observed and all three families of tuned modes are used to create ROM. Here, again it is observed from the second case that as the size of ROM is increased the state estimator's accuracy improves.

Figure 5.4 shows estimator force convergence for asynchronous excitation. The mass # 1 of each sector is excited with forcing frequency $\omega_f = 0.7\Omega$ and displacement of mass # 1 is measured. From plots it can be seen that estimated force converge to actual force values quickly. Thus, this approach is suitable for asynchronous excitation force estimation for 3DOF of rotor model. In next sections, this approach will be applied to more complex models such as *Academic* rotor and Transonic rotor.

5.2.2. *Academic* Rotor

The *Academic* rotor is described in section 4.3. The geometric mistuning in *Academic* rotor is comprised of two POD features. The reduced order model created for MMDA in previous chapters for *Academic* rotor is used again here. Here, matrices A and E are complex matrices thus the state estimator described in equation (5.23) and (5.24) is used for force estimation of an *Academic* rotor. This allows to obtain a real observer gain matrix for the filter.

The forcing frequency is kept same as the rotor frequency for 1^{st} engine order excitation. The rotor frequency is chosen to be same as the natural frequency of tuned rotor such that it excites first family of modes at first engine order. A force of magnitude 600 units with initial phase of 30 degree at $t = 0$ is applied only on one nodal location at the tip in the axial direction for all the cases. Initial conditions for estimator force and all other remaining states of estimator are 1000 units and zeros respectively.

Figure 5.5 shows force estimation convergence results for *Academic* rotor for various cases. The axial displacements of few nodes, other than the node where force is applied, are measured and used as an input to the estimator.

Comparison of the force convergence results for real and imaginary part of forces for all cases, from Figure 5.5a and 5.5c shows that the estimator forces quickly converge to applied forces values as the number of measurements are increased. The number of POD features is chosen to obtain the most accurate reduced order model.

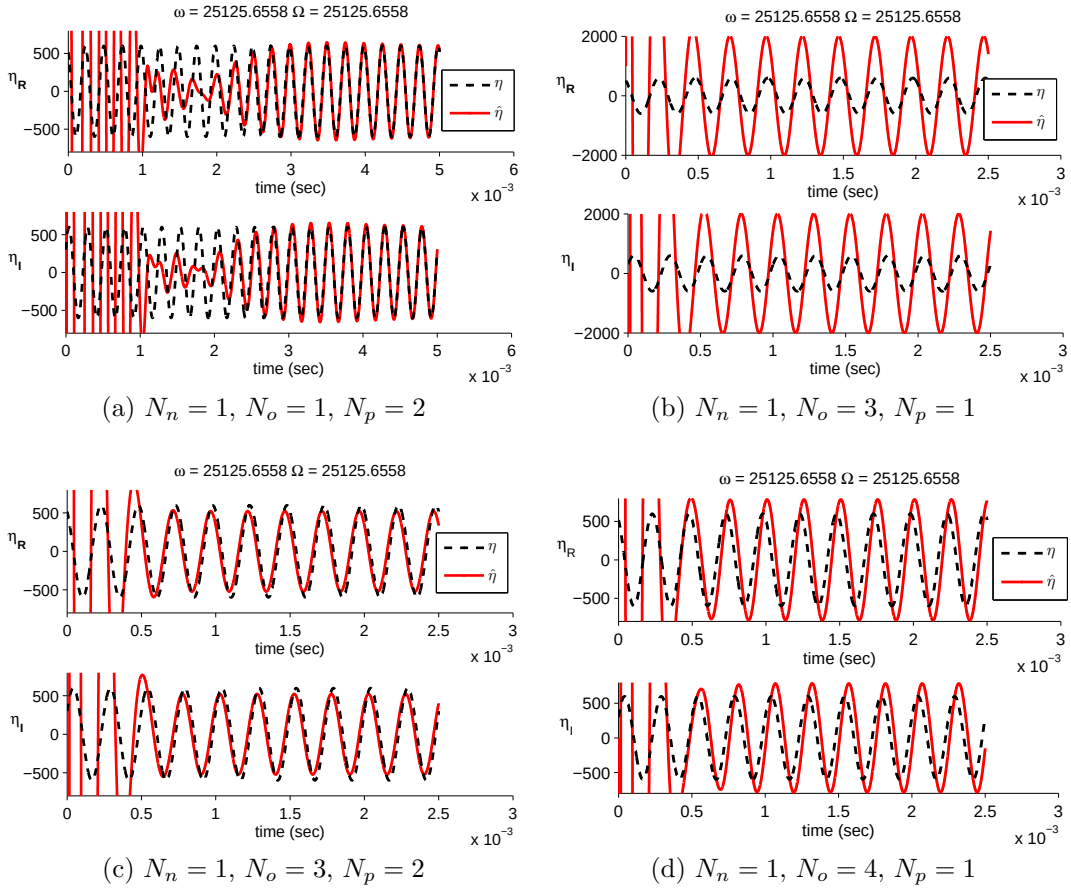

(a) $N_n = 1$, $N_o = 1$, $N_p = 2$

(b) $N_n = 1$, $N_o = 3$, $N_p = 1$

(c) $N_n = 1$, $N_o = 3$, $N_p = 2$

(d) $N_n = 1$, $N_o = 4$, $N_p = 1$

Figure 5.5: *Academic* rotor force estimation convergence for numbers of force input (N_n), displacement measurement (N_o), POD features (N_p) and ($N_f = 5$) families of modes used in ROM

From Figure 5.5b and 5.5d the estimator forces did not converge to applied forces even with increasing number of measurements because the reduced order model in these cases has low accuracy. The estimator forces for case such as $N_o = 8$ and $N_p = 1$ have been tested and found that they also do not converge to the values of applied forces. Thus, it can be concluded here that for a good estimation of applied forces the number of measurement points needs to be high and the ROM should be able to yield accurate results. It has been shown that the *Academic* rotor MMDA ROM results for mode shapes improved as the number of POD features are increased [44].

Figure 5.6 shows estimator force convergence for asynchronous excitation. One

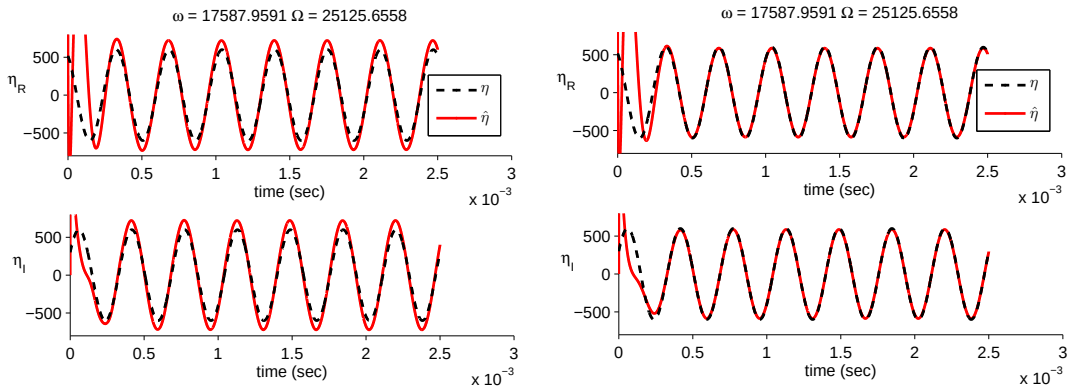

(a) $N_n = 1$, $N_o = 4$, $N_p = 2$ (b) $N_n = 1$, $N_o = 5$, $N_p = 2$

Figure 5.6: *Academic* rotor force estimation convergence for asynchronous case with numbers of force input (N_n), displacement measurement (N_o) and POD features (N_p) used in ROM

node at the tip of each sector is excited with forcing frequency $\omega_f = 0.7\Omega$ and displacements of neighboring nodes are measured. From plots it can be seen that estimated force converge to actual force values quickly. Also, as the number of measurement nodes are increased the accuracy of estimated force increases. Thus, this approach is suitable for asynchronous excitation force estimation for *Academic* rotor as well.

5.2.3. Transonic Rotor

Lastly, the state estimator is used for force estimation for a Transonic rotor. The Transonic rotor is described in section 2.1. The geometric mistuning in Transonic rotor is comprised of 17 POD features. The reduced order model created for MMDA in previous chapters for Transonic rotor is used again here.

Here also forcing frequency is kept same as the rotor frequency for 1^{st} engine order excitation. The rotor frequency is chosen to be same as the natural frequency of tuned rotor such that it excites the first family of modes at first engine order. A force of magnitude 500 units with initial phase of 30 degree at $t = 0$ is applied to only one nodal location at the tip in axial direction. Initial conditions for estimator force and all other remaining states of estimator are 1000 units and zeros respectively.

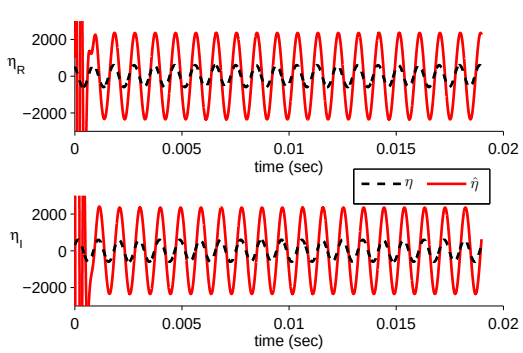

(a) $N_n = 1$, $N_o = 4$, $N_p = 17$

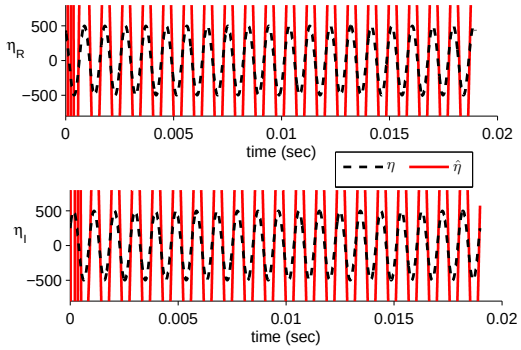

(b) $N_n = 1$, $N_o = 4$, $N_p = 15$

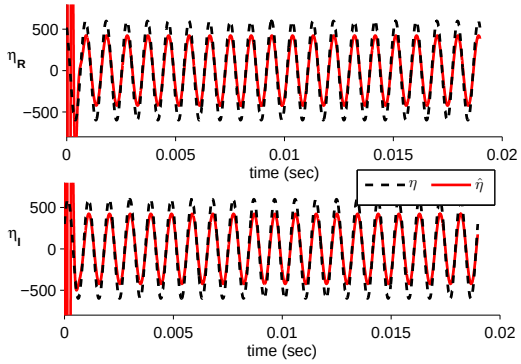

(c) $N_n = 1$, $N_o = 6$, $N_p = 17$

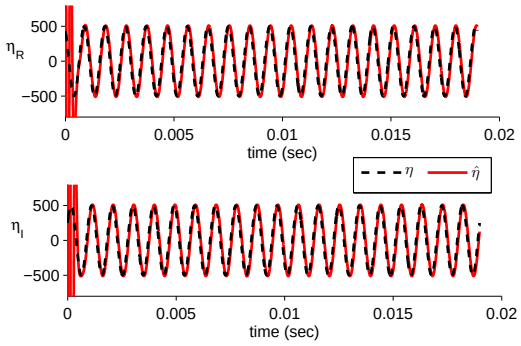

(d) $N_n = 1$, $N_o = 6$, $N_p = 15$

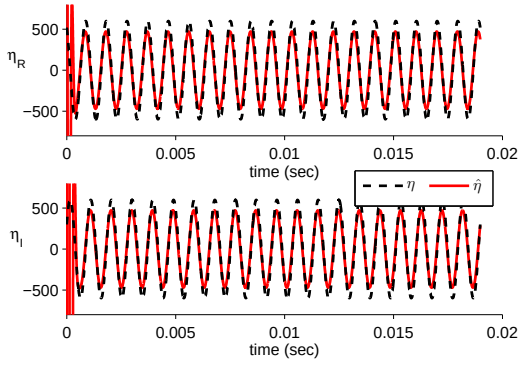

(e) $N_n = 1$, $N_o = 8$, $N_p = 17$

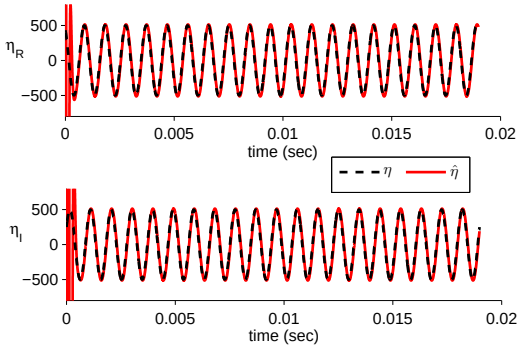

(f) $N_n = 1$, $N_o = 8$, $N_p = 15$

Figure 5.7: Transonic rotor force estimation convergence for numbers of force input (N_n), displacement measurement (N_o), POD features (N_p) and ($N_f = 5$) families of modes used in ROM

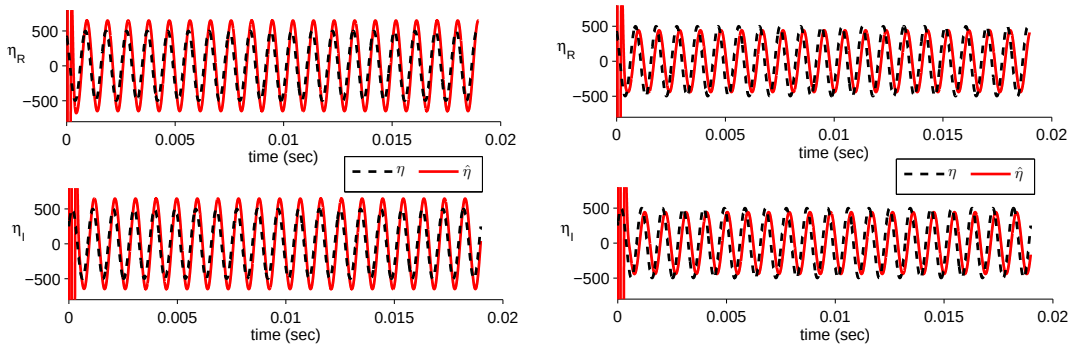

(g) $N_n = 1$, $N_o = 8$, $N_p = 12$ (h) $N_n = 1$, $N_o = 8$, $N_p = 9$

Figure 5.7: Transonic rotor force estimation convergence for numbers of force input (N_n), displacement measurement (N_o), POD features (N_p) and ($N_f = 5$) families of modes used in ROM

Figure 5.7 shows force estimation convergence results for various cases; real and imaginary part of forces are compared for Transonic rotor. The axial displacements of few nodes other than the node where force is applied are measured and used as an input to the estimator.

Figure 5.7a, 5.7c and 5.7e show the estimated force convergence for cases with 4, 6 and 8 nodal DOF's displacement, respectively measured for estimator with 17 PODs used in ROM. From Figure 5.7a the estimated force did not converge to applied force value but as the numbers of measurement nodal DOF are increased the accuracy of estimated force also increases.

Figure 5.7b, 5.7d and 5.7f show the estimated force convergence for 4, 6 and 8 nodal DOF's displacement measured respectively for estimator with 15 PODs used in ROM. Since only first family of modes are being excited in this case and the ROM with 15 POD features has been shown to capture this desired family of modes accurately (see Figure 2.6f), the force estimation convergence results are good for this case. Again, from Figure 5.7b the estimated force did not converge to applied force value for the case when number of measurement nodes is low but as number of measurement nodal DOF is increased the accuracy of estimated force also increases.

Figure 5.7g and 5.7h show results for the cases with 12 and 9 POD features used

in the basis to obtain ROM of lower order for force estimation. Even with this low order ROM the estimated force quickly converged to value close to actual force for the case with displacement of 8 nodal DOF being measured. Though this result is not as accurate as that from higher order ROM but it is surprisingly close to the actual value because these lower order ROM are accurate at estimating mode shapes of first family of modes. The force estimation convergence deteriorated as the numbers of measurement nodes are reduced. Increasing the number of measurement nodes does not improve the result, hence these results are not shown.

For asynchronous excitation of Transonic rotor the estimated force converged to wrong values and even after increasing number of nodes the results did not improve, hence these results are not shown.

From these results it can be seen that for a good estimation of applied forces the number of measurement points need to be higher and the ROM should be able to yield accurate results. For Transonic rotor MMDA ROM results for mode shapes improved as the numbers of POD features were increased, thus using better and accurate ROM for state estimator is beneficial.

5.3. Summary

Forcing function estimation can give useful information about the causes of such forcing. The use of Kalman filter and MMDA ROM for force estimation has been demonstrated for various cases. Following summarize the results from this chapter.

1. State estimator has been used to estimate harmonic forcing only from few measurements at each tip for 3DOF rotor model, *Academic* rotor and Transonic rotor.

2. It has been shown the state estimator based on MMDA ROM is successful in estimating the harmonic forces applied to the rotor.

3. The accuracy of the results improved with increasing the number of measurement points and size of ROM by increasing number of modes or number of POD features in the basis.

4. The time required for force estimate to converge is very small. This suggests that this method can also be used for real time force estimation.

Chapter 6
Conclusion and Future Research

Geometric mistuning in the bladed disk is inevitable. It causes simultaneous perturbations in mass and stiffness parameters, and changes natural frequencies and mode shapes of bladed disk from those of designed bladed disk. This gives rise to phenomenon such as mode localization, mode splitting and affect the forced response behaviour which can be detrimental to the bladed disk. In general, the assumption of cyclic symmetry becomes invalid for modal analysis. Thus, full 360° FEM analysis is required for accurate estimation of modal characteristics, but this kind of analysis is computationally intensive for industrial bladed disks that have very high FEM order. Modified Modal Domain Analysis (MMDA) was developed for reduced order modeling (ROM) for geometrically mistuned bladed disk. It had been shown to accurately estimate modal characteristics of geometrically mistuned Academic rotors.

This dissertation presents for the first time the study of MMDA as a faster and accurate reduced order modeling method for geometrically mistuned industrial scale bladed disks having very high FEM order. The efficacy and limitations of this method are discussed for such rotors. Methods for generating forced response statistics using MMDA via random permutation of blades are presented. The results are also compared with Monte Carlo simulations. Method for estimation of forced response using MMDA is also developed.

The first part of the dissertation focuses on the study of MMDA as a faster and accurate reduced order modeling method for geometrically mistuned industrial scale bladed rotor. MMDA ROM method is applied to a full scale industrial rotor (Transonic rotor) using exact estimation of mass and stiffness matrices from ANSYS

analysis and its results are comparable to those of ANSYS full scale rotor FEM analysis. Results such as mode shapes, natural frequencies and forced response are compared using metrics such as MAC, frequency deviations and NMA, respectively. Accuracy of MMDA results improves as the number of POD features in the basis increases. Even though higher index of POD features have lower contribution in blades' geometry perturbation, due to smaller singular values, they are much needed for accurate estimation of mistuned rotor frequencies and mode shapes. Also, as the number of families of modes in the basis increases, more mistuned modes' natural frequency and mode shape can be estimated accurately via MMDA. Results from other frequency mistuning approaches such as SNM and FMM are also compared, but only MMDA provides accurate results.

MMDA method with approximate deviations in mass and stiffness matrices via Taylor series expansion has potential for generating another faster approach for ROM. The method had been tested on *Academic* rotor with successful results. But from this study it has been found that the sensitivities generated via central difference approach did not result in accurate estimates of deviations in mass and stiffness matrices for Transonic rotor. The method has been further investigated and it is found that this approach is suitable for industrial scale bladed rotor with small geometric mistuning as compared to that of Transonic rotor. Sensitivities are then obtained using methods such as linear least squares approximation and interpolation of matrices on manifolds. Linear square approximation method has resulted in good agreement for MAC values for *Academic* rotor and the case of Transonic like rotor when sensitivities generated from training rotor are used to approximate mass and stiffness matrices of training rotor itself, but it performed poorly with other Transonic like test rotor. Thus, even though the approximated deviation in mass and stiffness matrices may have least square error for some set of rotors and but they may not be valid for other set of test rotors. These errors change system dynamics, thus ROM performs poorly. Interpolation of matrices on manifolds does result in accurate estimation of mass and

stiffness matrices on symmetric positive definite (SPD) manifold, thus ensuring SPD properties. The method has resulted in good estimates of mode shapes and natural frequencies for mistuned *Academic* rotor, but this method has not been successful for industrial scale bladed rotors because of its large computational resource requirement to generate mapping to–and–from manifold. Several areas for future research are possible:

1. Study of MMDA for industrial scale multistage rotors.
2. Development of MMDA for bladed disk with multiple rogue blades and test its accuracy for industrial scale bladed disks.
3. Development of reduced order model for industrial bladed rotor with geometric mistuning coupled with aerodynamic forces.
4. Development of method for faster computation of sensitivities for interpolation on manifold.
5. Develop mistuning identification methods for industrial scale bladed rotors.

The second part of dissertation focuses on generating forced harmonic response peak amplitude statistics and compare them with Monte Carlo simulations. In the absence of a suitable method to approximate deviations in mass and stiffness matrices to estimate mistuned mode shapes and frequencies, random permutations of blades are used to generate statistics of forced harmonic response (NPMA). The results are compared for 3 degree of freedom (DOF) rotor model, *Academic* rotor and industrial scale bladed rotors. From the study on 3DOF model and *Academic* rotor it is found that the NPMA statistics depends on the distribution of mistuning parameters. As the number of sectors/parameters in the initial set for random permutations increases, the results from random permutations approach those of Monte Carlo simulations. Even though the distribution of mistuning parameters is unknown for Transonic rotor, random permutations method still can be used to obtain the statistics of forced

response. For artificially created Transonic like rotors with uniform distribution of mistuning parameters, the statistics are compared and shown to have agreement between Monte Carlo simulations and random permutations. The random permutation method does not require additional finite element (FE) analysis, thus it can quickly generate forced response statistics as compared to Monte Carlo simulations and the method can serve as a good, quick tool to compute these statistics with some confidence. Several areas for future research are possible:

1. The statistics of forced response via random permutation is dependent on initial data set, thus a thorough study can be done for various cases of mistuning parameters or initial data set.

2. Develop a theoretical basis for similarity in results from random permutations and Monte Carlo simulations.

3. As the approximation of deviations in mass and stiffness matrices improves, verify the accuracy of the forced response statistics via Monte Carlo simulations with these approximation methods.

The third part of dissertation focuses on force estimation from measurement of few nodes on blades. Forcing function estimation can give useful information about the causes of such forcing. A state estimator has been developed based on MMDA ROM and Kalman filter for real time force estimation. This estimator is developed for cases where modeling parameters such as mass, stiffness matrices etc. can be real or complex numbers. It has been shown the state estimator based on MMDA ROM is successful in estimating the harmonic forces applied to the bladed rotor from only few measurements at each tip for 3DOF rotor model, *Academic* rotor and Transonic rotor. It has also been found that the accuracy of force estimation improves as the number of measurement points are increased. The accuracy of ROM is also an important factor, thus increasing number of modes or number of POD features in the basis improves force estimation. This method has been shown to be capable of estimating

force for both synchronous and asynchronous excitation for 3DOF rotor model and *Academic* rotor, whereas for Transonic rotor force has been accurately estimated only for synchronous excitation. The time required for force estimates to converge is very small, this suggests that this method can be used for offline as well as real time force estimation. Following areas for future research are possible:

1. Develop method to estimate force for asynchronous excitation for industrial scale bladed disks.

2. Study the effects of errors in damping parameters on forcing function estimation.

Appendix A
Modified Modal Domain Analysis (MMDA)

The MMDA technique was formulated by Sinha [40]. Its implementation details are given in Bhartiya [45].

The equation of free motion for an undamped mistuned bladed-disk assembly or a bladed rotor can be described by,

$$(M_t + \delta M)\ddot{\mathbf{x}} + (K_t + \delta K)\mathbf{x} = 0 \tag{A.1}$$

where M_t and K_t are mass and stiffness matrix respectively of the perfectly tuned bladed rotor with each blade having the average geometry. δM and δK are deviations in mass and stiffness matrices respectively due to mistuning. $\mathbf{x}$ is the displacement vector of nodal co-ordinate's degree of freedom (DOFs). The basis for ROM in MMDA is chosen as

$$\mathbf{x} = \mathbf{\Phi y} \tag{A.2}$$

where

$$\mathbf{\Phi} = \begin{bmatrix} \Phi_0 & \Phi_1 & \dots & \Phi_{N_p} \end{bmatrix} \tag{A.3}$$

Φ_0: N_f families of tuned modes of the system with blades having the mean geometry.

Φ_i: N_f families of tuned modes of the system with blades having perturbed geometry along l^{th} POD feature, $i = 1, 2 \dots N_p$

N_p: Number of POD features

N_f: Number of families of modes required in mistuned bladed rotor.

Substituting equation (A.2) into (A.1), and pre-multiplying by $\mathbf{\Phi}^H$, the reduced-order model is obtained as follows,

$$M_r\ddot{\mathbf{y}} + K_r\mathbf{y} = 0 \tag{A.4}$$

where

$$K_r = \mathbf{\Phi}^H K_t \mathbf{\Phi} + \mathbf{\Phi}^H \delta K \mathbf{\Phi} \tag{A.5}$$

$$M_r = \mathbf{\Phi}^H M_t \mathbf{\Phi} + \mathbf{\Phi}^H \delta M \mathbf{\Phi} \tag{A.6}$$

To obtain reduced-order mass and stiffness matrices, $\Phi_l^H K_t \Phi_r$, $\Phi_l^H \delta K \Phi_r$, $\Phi_l^H M_t \Phi_r$ and $\Phi_l^H \delta M \Phi_r$ are required to be calculated for $l, r = 0, 1, \ldots, N_p$. Using equation (A.3) the right hand side of equations (A.5) and (A.6) can be expressed as,

$$\mathbf{\Phi}^H K_t \mathbf{\Phi} = \begin{bmatrix} \Phi_0^H K_t \Phi_0 & & & \\ \Phi_1^H K_t \Phi_0 & \Phi_1^H K_t \Phi_1 & & \\ \vdots & \vdots & \ddots & \\ \Phi_{N_p}^H K_t \Phi_0 & \Phi_{N_p}^H K_t \Phi_1 & \cdots & \Phi_{N_p}^H K_t \Phi_{N_p} \end{bmatrix} \tag{A.7}$$

$$\mathbf{\Phi}^H M_t \mathbf{\Phi} = \begin{bmatrix} \Phi_0^H M_t \Phi_0 & & & \\ \Phi_1^H M_t \Phi_0 & \Phi_1^H M_t \Phi_1 & & \\ \vdots & \vdots & \ddots & \\ \Phi_{N_p}^H M_t \Phi_0 & \Phi_{N_p}^H M_t \Phi_1 & \cdots & \Phi_{N_p}^H M_t \Phi_{N_p} \end{bmatrix} \tag{A.8}$$

$$\mathbf{\Phi}^H \delta K \mathbf{\Phi} = \begin{bmatrix} \Phi_0^H \delta K \Phi_0 & & & \\ \Phi_1^H \delta K \Phi_0 & \Phi_1^H \delta K \Phi_1 & & \\ \vdots & \vdots & \ddots & \\ \Phi_{N_p}^H \delta K \Phi_0 & \Phi_{N_p}^H \delta K \Phi_1 & \cdots & \Phi_{N_p}^H \delta K \Phi_{N_p} \end{bmatrix} \tag{A.9}$$

$$\mathbf{\Phi}^H \delta M \mathbf{\Phi} = \begin{bmatrix} \Phi_0^H \delta M \Phi_0 & & & \\ \Phi_1^H \delta M \Phi_0 & \Phi_1^H \delta M \Phi_1 & & \\ \vdots & \vdots & \ddots & \\ \Phi_{N_p}^H \delta M \Phi_0 & \Phi_{N_p}^H \delta M \Phi_1 & \cdots & \Phi_{N_p}^H \delta M \Phi_{N_p} \end{bmatrix} \tag{A.10}$$

A.1. Computation of M_r and K_r via sector analysis

The computation of reduced-order stiffness and mass matrices, equations (A.5) and (A.6), are straightforward whenever the matrices K, M and $\mathbf{\Phi}$ are known for the full bladed disk. However, it is a common practice to use sector analysis for a perfectly tuned system. Therefore the reduced order matrices M_r and K_r are computed based on the sector analyses and described in Bhartiya [45]; *i.e.* without requiring any full rotor analyses. Only algorithms to compute $\Phi_l^H M_t \Phi_r$ and $\Phi_l^H \delta M \Phi_r$ are presented here. The procedures to compute $\Phi_l^H K_t \Phi_r$ and $\Phi_l^H \delta K \Phi_r$ are similar.

A.1.1. Reduced order tuned matrices

The set of tuned mode shapes due l^{th} POD feature is given as

$$\Phi_l = \begin{bmatrix} \varphi_{l,1,0} & \varphi_{l,1,1} & \cdots & \varphi_{l,1,N_s-1} \\ \varphi_{l,2,0} & \varphi_{l,2,1} & \cdots & \varphi_{l,2,N_s-1} \\ \vdots & \vdots & \ddots & \vdots \\ \varphi_{l,N_s,0} & \varphi_{l,N_s,1} & \cdots & \varphi_{l,N_s,N_s-1} \end{bmatrix} \tag{A.11}$$

where $\varphi_{l,s,p}$ represents the nodal displacements for sector # s and interblade phase angle $\dfrac{2\pi p}{N_s}$, and N_s is the number of sectors in the system. Note that

$$\varphi_{l,s,p} = e^{\iota(s-1)\psi_p} \varphi_{l,1,p} \tag{A.12}$$

$$\psi_p = \frac{2\pi p}{N_s} \tag{A.13}$$

where $\iota = \sqrt{-1}$. The tuned mass matrix of the full rotor is described as follows,

$$M_t = \begin{bmatrix} M_{t,1,1} & M_{t,1,2} & \cdots & M_{t,1,N_s} \\ M_{t,2,1} & M_{t,2,2} & \cdots & M_{t,2,N_s} \\ \vdots & \vdots & \ddots & \vdots \\ M_{t,N_s,1} & M_{t,N_s,2} & \cdots & M_{t,N_s,N_s} \end{bmatrix} \tag{A.14}$$

Note, M_t is a circulant matrix; *i.e.*, the second block row will be obtained by circular shifting the first block row by one column right, the third block row will be obtained by circular shifting the second block row by one column right, and so on. Mathematically $M_{t,l,r} = M_{t,1,1+(l-r \mod N_s)}$. Then,

$$\begin{aligned} M_t\Phi_r &= \begin{bmatrix} M_{t,1,1} & M_{t,1,2} & \cdots & M_{t,1,N_s} \\ M_{t,2,1} & M_{t,2,2} & \cdots & M_{t,2,N_s} \\ \vdots & \vdots & \ddots & \vdots \\ M_{t,N_s,1} & M_{t,N_s,2} & \cdots & M_{t,N_s,N_s} \end{bmatrix} \begin{bmatrix} \varphi_{r,1,0} & \varphi_{r,1,1} & \cdots & \varphi_{r,1,N_s-1} \\ \varphi_{r,2,0} & \varphi_{r,2,1} & \cdots & \varphi_{r,2,N_s-1} \\ \vdots & \vdots & \ddots & \vdots \\ \varphi_{r,N_s,0} & \varphi_{r,N_s,1} & \cdots & \varphi_{r,N_s,N_s-1} \end{bmatrix} \\ &= \begin{bmatrix} M^c_{t0}\varphi_{r,1,0} & M^c_{t1}\varphi_{r,1,1} & \cdots & M^c_{t(N_s-1)}\varphi_{r,1,N_s-1} \\ M^c_{t0}\varphi_{r,2,0} & M^c_{t1}\varphi_{r,2,2} & \cdots & M^c_{t(N_s-1)}\varphi_{r,2,N_s-1} \\ \vdots & \vdots & \ddots & \vdots \\ M^c_{t0}\varphi_{r,N_s,0} & M^c_{t1}\varphi_{r,N_s,2} & \cdots & M^c_{t(N_s-1)}\varphi_{r,N_s,N_s-1} \end{bmatrix} \end{aligned} \tag{A.15}$$

The $(s, p+1)$ block element of $M_t\Phi_r$ is written as $M^c_{tp}\varphi_{r,s,p}$. Where

$$M^c_{tp}\varphi_{r,s,p} = M_{t,s,1}\varphi_{r,1,p} + M_{t,s,2}\varphi_{r,2,p} + \ldots + M_{t,s,N_s}\varphi_{r,N_s,p} \tag{A.16}$$

$$\implies M^c_{tp} = M_{t,1,1} + e^{\iota\psi_p}M_{t,1,2} + \ldots + e^{\iota(N_s-1)\psi_p}M_{t,1,N_s} \tag{A.17}$$

Note that M^c_{tp} is the complex mass matrix for the interblade phase angle ψ_p. Pre-multiplying equation (A.15) by Φ^H_l which is the complex conjugate transpose of

Φ_l:

$$\Phi_l^H M_t \Phi_r = \begin{bmatrix} \varphi^H_{l,1,0} & \varphi^H_{l,2,0} & \cdots & \varphi^H_{l,N_s,0} \\ \varphi^H_{l,1,1} & \varphi^H_{l,2,1} & \cdots & \varphi^H_{l,N_s,1} \\ \vdots & \vdots & \ddots & \vdots \\ \varphi^H_{l,1,N_s-1} & \varphi^H_{l,2,N_s-1} & \cdots & \varphi^H_{l,N_s,N_s-1} \end{bmatrix} \times \cdots \\ \begin{bmatrix} M^c_{t0}\varphi_{r,1,0} & M^c_{t1}\varphi_{r,1,1} & \cdots & M^c_{t(N_s-1)}\varphi_{r,1,N_s-1} \\ M^c_{t0}\varphi_{r,2,0} & M^c_{t1}\varphi_{r,2,2} & \cdots & M^c_{t(N_s-1)}\varphi_{r,2,N_s-1} \\ \vdots & \vdots & \ddots & \vdots \\ M^c_{t0}\varphi_{r,N_s,0} & M^c_{t1}\varphi_{r,N_s,2} & \cdots & M^c_{t(N_s-1)}\varphi_{r,N_s,N_s-1} \end{bmatrix} \tag{A.18}$$

The $(q+1, p+1)$ element of $\Phi_l^H M_t \Phi_r$ is as follows:

$$\begin{aligned} &\varphi^H_{l,1,q} M^c_{tp} \varphi_{r,1,p} + \varphi^H_{l,2,q} M^c_{tp} \varphi_{r,2,p} + \ldots + \varphi^H_{l,N_s,q} M^c_{tp} \varphi_{r,N_s,p} \\ &= (1 + e^{\iota(\psi_p - \psi_q)} + \ldots + e^{\iota(N_s-1)(\psi_p-\psi_q)}) \varphi^H_{l,1,q} M^c_{tp} \varphi_{r,1,p} \\ &= \chi \varphi^H_{l,1,q} M^c_{tp} \varphi_{r,1,p} \end{aligned} \tag{A.19}$$

where

$$\chi = \frac{1 - e^{\iota N_s(\psi_p - \psi_q)}}{1 - e^{\iota(\psi_p - \psi_q)}} \tag{A.20}$$

A closer look at equation (A.20) shows that $e^{\iota N_s(\psi_p-\psi_q)} = e^{\iota 2\pi(p-q)}$. Therefore

$$\chi = \begin{cases} N_s & ; q = p \\ 0 & ; q \neq p \end{cases} \tag{A.21}$$

Hence the matrix $\Phi_l^H M_t \Phi_r$ is a block diagonal matrix.

M^c_{tp} and $\varphi_{l,1,q}$ are available from ANSYS cyclic symmetric analysis. It is then used to assemble the $\Phi_l^H M_t \Phi_r$ matrix.

A.1.2. Reduced order mistuned matrices

The perturbation in the mass matrix, δM, has the block diagonal form

$$\delta M = \begin{bmatrix} \delta M_1 & 0 & \cdots & 0 \\ 0 & \delta M_2 & \cdots & 0 \\ \vdots & \vdots & \ddots & \vdots \\ 0 & 0 & \cdots & \delta M_{N_s} \end{bmatrix} \tag{A.22}$$

where δM_s is the perturbation in the mass matrix of sector # s due to geometric mistuning. Therefore,

$$\Phi_l^H \delta M \Phi_r = \sum_{s=1}^{N_s} \Phi_l^H \delta M_s^b \Phi_r \tag{A.23}$$

where

$$\delta M_s^b = \begin{bmatrix} 0 & \cdots & 0 & \cdots & 0 \\ \vdots & \ddots & \vdots & \ddots & \vdots \\ 0 & \cdots & \delta M_s & \cdots & 0 \\ \vdots & \ddots & \vdots & \ddots & \vdots \\ 0 & \cdots & 0 & \cdots & 0 \end{bmatrix} \tag{A.24}$$

Now,

$$\Phi_l^H \delta M_s^b \Phi_r = \begin{bmatrix} \varphi_{l,1,0}^H & \varphi_{l,2,0}^H & \cdots & \varphi_{l,N_s,0}^H \\ \varphi_{l,1,1}^H & \varphi_{l,2,1}^H & \cdots & \varphi_{l,N_s,1}^H \\ \vdots & \vdots & \ddots & \vdots \\ \varphi_{l,1,N_s-1}^H & \varphi_{l,2,N_s-1}^H & \cdots & \varphi_{l,N_s,N_s-1}^H \end{bmatrix} \times \cdots$$

$$\begin{bmatrix} 0 & \cdots & 0 & \cdots & 0 \\ \vdots & \ddots & \vdots & \ddots & \vdots \\ \delta M_s \varphi_{r,s,0} & \cdots & \delta M_s \varphi_{r,s,p} & \cdots & \delta M_s \varphi_{r,s,N_s-1} \\ \vdots & \ddots & \vdots & \ddots & \vdots \\ 0 & \cdots & 0 & \cdots & 0 \end{bmatrix}$$

$$= \begin{bmatrix} \varphi_{l,s,0}^H \delta M_s \varphi_{r,s,0} & \varphi_{l,s,0}^H \delta M_s \varphi_{r,s,1} & \cdots & \varphi_{l,s,0}^H \delta M_s \varphi_{r,s,N_s-1} \\ \varphi_{l,s,1}^H \delta M_s \varphi_{r,s,0} & \varphi_{l,s,1}^H \delta M_s \varphi_{r,s,1} & \cdots & \varphi_{l,s,1}^H \delta M_s \varphi_{r,s,N_s-1} \\ \vdots & \vdots & \ddots & \vdots \\ \varphi_{l,s,N_s-1}^H \delta M_s \varphi_{r,s,0} & \varphi_{l,s,N_s-1}^H \delta M_s \varphi_{r,s,1} & \cdots & \varphi_{l,s,N_s-1}^H \delta M_s \varphi_{r,s,N_s-1} \end{bmatrix} \tag{A.25}$$

The $(q+1, p+1)$ element of $\Phi_l^H \delta M_s^b \Phi_r$ in equation (A.25) is as follows:

$$\varphi_{l,s,q}^H \delta M_s \varphi_{r,s,p} = e^{\iota(s-1)(\psi_p - \psi_q)} \varphi_{l,1,q}^H \delta M_s \varphi_{r,1,p} \tag{A.26}$$

From equations (A.19) and (A.26), $\mathbf{\Phi}^H M_t \mathbf{\Phi}$ and $\mathbf{\Phi}^H \delta M \mathbf{\Phi}$ can be assembled. Similarly $\mathbf{\Phi}^H K_t \mathbf{\Phi}$ and $\mathbf{\Phi}^H \delta K \mathbf{\Phi}$ can be assembled to solve the eigenvalue problem for reduced order model in equation (A.4).

Appendix B

Modified Modal Domain Analysis with Approximate Deviations in Mass and Stiffness Matrices

In this method, the mistuning in the mass (δM) and stiffness matrices (δK) is approximated via Taylor series expansion in terms of POD variables representing geometry variations of blades. The calculation of $\mathbf{\Phi}^H M \mathbf{\Phi}$ and $\mathbf{\Phi}^H K \mathbf{\Phi}$ in equations (A.5) and (A.6) gets modified with these estimated δM and δK. Details of the method are given in Bhartiya [45]. This chapter gives direction to compute these terms efficiently.

B.1. Mass and Stiffness Matrices Mistuning Approximation by Taylor Series expansion

Using Taylor series expansion, the perturbation mass/stiffness matrix of the actual sector can be expanded about the nominal sector matrix as:

$$\delta M_s = \sum_{p=1}^{N_p} \frac{\partial M_s^c}{\partial \xi_{s,p}} \xi_{s,p} + \sum_{p=1}^{N_p} \sum_{q=1}^{N_p} \frac{\partial^2 M_s^c}{\partial \xi_{s,p} \partial \xi_{s,q}} \frac{\xi_{s,p} \xi_{s,q}}{2} + \Theta\left(\partial \xi^3\right) \tag{B.1}$$

where

δM_s : Perturbation in mass matrix for sector $\#s$

M_s^c : Mass matrix of the mistuned sector from sector analysis.

M_t^c : Mass matrix of the nominal (tuned) sector from sector analysis.

$\xi_{s,p}$: Mistuning parameter associated with sector$\#s$ and POD $\#p$.

N_p : Number of POD features used to represent mistuning.

where $\delta M_l = M_l^c - M_t^c$. Since, M_t^c is the mass matrix of the nominal sector, it is independent of the mistuning parameter $\xi_{s,p}$, *i.e.* $\dfrac{\partial M_t^c}{\partial \xi_{s,p}} = 0$, equation (B.1) can be written as,

$$\delta M_s = \sum_{p=1}^{N_p} \frac{\partial \delta M_s}{\partial \xi_{s,p}} \xi_{s,p} + \sum_{p=1}^{N_p} \sum_{q=1}^{N_p} \frac{\partial^2 \delta M_s}{\partial \xi_{s,p} \partial \xi_{s,q}} \frac{\xi_{s,p} \xi_{s,q}}{2} + \Theta\big(\partial \xi^3\big) \tag{B.2}$$

Further, $\dfrac{\partial \delta M_s}{\partial \xi_{s,p}}$ & $\dfrac{\partial^2 \delta M_s}{\partial \xi_{s,p} \partial \xi_{s,q}}$ are independent of sector $\#s$ and can be written as $\dfrac{\partial \delta M}{\partial \xi_p}$ & $\dfrac{\partial^2 \delta M}{\partial \xi_p \partial \xi_q}$ respectively. As a result, equation (B.2) gets modified as

$$\delta M_s = \sum_{p=1}^{N_p} \frac{\partial \delta M}{\partial \xi_p} \xi_{s,p} + \sum_{p=1}^{N_p} \sum_{q=1}^{N_p} \frac{\partial^2 \delta M}{\partial \xi_p \partial \xi_q} \frac{\xi_{s,p} \xi_{s,q}}{2} + \Theta\big(\partial \xi^3\big) \tag{B.3}$$

B.1.1. Calculation of First and Second order partial derivative terms

From equation (B.3), N_p first order derivatives and $\dfrac{N_p(N_p+1)}{2}$ second order derivatives need to be calculated. These derivatives are independent of sector $\#s$, hence, subscript s in $\xi_{s,p}$ is not used. The derivatives can be computed using central difference approach.

First and Second order partial derivatives

Let only the k^{th} POD mistuning parameter be non-zero *i.e.* $\xi_k \neq 0$ and $\xi_p = 0$ for $p \neq k$. Thus,

$$\delta M(\xi_k) = \frac{\partial \delta M}{\partial \xi_k} \xi_k + \frac{\partial^2 \delta M}{\partial \xi_k^2} \frac{\xi_k^2}{2} \tag{B.4a}$$

$$\delta M(-\xi_k) = -\frac{\partial \delta M}{\partial \xi_k} \xi_k + \frac{\partial^2 \delta M}{\partial \xi_k^2} \frac{\xi_k^2}{2} \tag{B.4b}$$

where $\delta M(\xi_k)$ and $\delta M(-\xi_k)$ are the perturbation in mass matrix for mistuning parameter ξ_k and $-\xi_k$ respectively. Subtracting equation (B.4b) from (B.4a),

$$\frac{\partial \delta M}{\partial \xi_k} = \frac{\delta M(\xi_k) - \delta M(-\xi_k)}{2\xi_k} \tag{B.5}$$

And adding equations (B.4a) and (B.4b),

$$\frac{\partial^2 \delta M}{\partial \xi_k^2} = \frac{\delta M(\xi_k) + \delta M(-\xi_k)}{\xi_k^2} \tag{B.6}$$

Mixed second order partial derivatives

Let only the j^{th} and k^{th} POD mistuning parameter be non-zero *i.e.* $\xi_j, \xi_k \neq 0$ and $\xi_p = 0$ for $p \neq j, k$. Therefore,

$$\delta M(\xi_j, \xi_k) = \Big(\frac{\partial \delta M}{\partial \xi_j}\xi_j + \frac{\partial^2 \delta M}{\partial \xi_j^2}\frac{\xi_j^2}{2}\Big) + \Big(\frac{\partial \delta M}{\partial \xi_k}\xi_k + \frac{\partial^2 \delta M}{\partial \xi_k^2}\frac{\xi_k^2}{2}\Big) + \frac{\partial^2 \delta M}{\partial \xi_j \partial \xi_k}\xi_j\xi_k \tag{B.7}$$

$$\frac{\partial^2 \delta M}{\partial \xi_j \partial \xi_k} = \frac{\delta M(\xi_j, \xi_k) - \Big(\frac{\partial \delta M}{\partial \xi_j}\xi_j + \frac{\partial^2 \delta M}{\partial \xi_j^2}\frac{\xi_j^2}{2}\Big) - \Big(\frac{\partial \delta M}{\partial \xi_k}\xi_k + \frac{\partial^2 \delta M}{\partial \xi_k^2}\frac{\xi_k^2}{2}\Big)}{\xi_j\xi_k} \tag{B.8}$$

where the first and second order partial derivatives in equation (B.8) are calculated using equations (B.5) and (B.6).

B.1.2. Reduced order mistuning matrices

The expressions for $\mathbf{\Phi}^H \delta M \mathbf{\Phi}$ and δM are given in equations (A.10) and (A.22). From equations (A.23) and (A.25) we get,

$$\Phi_l^H \delta M \Phi_r = \sum_{s=1}^{N_s} \begin{bmatrix} \varphi_{l,s,0}^H \delta M_s \varphi_{r,s,0} & \varphi_{l,s,0}^H \delta M_s \varphi_{r,s,1} & \cdots & \varphi_{l,s,0}^H \delta M_s \varphi_{r,s,N_s-1} \\ \varphi_{l,s,1}^H \delta M_s \varphi_{r,s,0} & \varphi_{l,s,1}^H \delta M_s \varphi_{r,s,1} & \cdots & \varphi_{l,s,1}^H \delta M_s \varphi_{r,s,N_s-1} \\ \vdots & \vdots & \ddots & \vdots \\ \varphi_{l,s,N_s-1}^H \delta M_s \varphi_{r,s,0} & \varphi_{l,s,N_s-1}^H \delta M_s \varphi_{r,s,1} & \cdots & \varphi_{l,s,N_s-1}^H \delta M_s \varphi_{r,s,N_s-1} \end{bmatrix} \tag{B.9}$$

The $(q{+}1, p{+}1)$ element of $\Phi_l^H \delta M \Phi_r$ in equation (B.9) after Taylor series expansion of δM_s from equation (B.3) is as follows:

$$\begin{aligned} \sum_{s=1}^{N_s} \varphi_{l,s,q}^H \delta M_s \varphi_{r,s,p} &= \sum_{s=1}^{N_s} e^{-\iota \frac{2\pi}{N_s}(s-1)(q-p)} \varphi_{l,1,q}^H \delta M_s \varphi_{r,1,p} \\ &= \sum_{s=1}^{N_s} e^{-\iota \frac{2\pi}{N_s}(s-1)(q-p)} \varphi_{l,1,q}^H \Big(\sum_{j=1}^{N_p} \frac{\partial \delta M}{\partial \xi_j} \xi_{s,j} + \sum_{j=1}^{N_p} \sum_{k=1}^{N_p} \frac{\partial^2 \delta M}{\partial \xi_j \partial \xi_k} \frac{\xi_{s,j} \xi_{s,k}}{2} \Big) \varphi_{r,1,p} \\ &= \sum_{j=1}^{N_p} \varphi_{l,1,q}^H \frac{\partial \delta M}{\partial \xi_j} \varphi_{r,1,p} \sum_{s=1}^{n} e^{-\iota \frac{2\pi}{N_s}(s-1)(q-p)} \xi_{s,j} + \dots \\ &\quad \sum_{j=1}^{N_p} \sum_{k=1}^{N_p} \varphi_{l,1,q}^H \frac{1}{2} \frac{\partial^2 \delta M}{\partial \xi_j \partial \xi_k} \varphi_{r,1,p} \sum_{s=1}^{n} e^{-\iota \frac{2\pi}{N_s}(s-1)(q-p)} \xi_{s,j} \xi_{s,k} \end{aligned} \tag{B.10}$$

But

$$\overline{\xi}_j(t) = \sum_{s=1}^{N_s} e^{-\iota \frac{2\pi}{N_s}(s-1)(q-p)} \xi_{s,j} \qquad \text{and} \quad t = q - p \tag{B.11}$$

$$\overline{\xi_j \xi_k}(t) = \sum_{s=1}^{N_s} e^{-\iota \frac{2\pi}{N_s}(s-1)(q-p)} \xi_{s,j} \xi_{s,k} \tag{B.12}$$

where $\overline{\xi}_j(t)$ and $\overline{\xi_j \xi_k}(t)$ are the t^{th} Discrete Fourier Transform of ξ_j and $\xi_j \xi_k$ respec-

tively. Using the circular convolution property of Discrete Fourier Transform [71, 72], $\overline{\xi_j \xi_k}$ can be written as

$$\begin{aligned}\overline{\xi_j \xi_k}(t) &= \sum_{s=1}^{N_s} e^{-\iota \frac{2\pi}{N_s}(s-1)t} \xi_{s,j} \xi_{s,k} = \frac{1}{N_s} \sum_{m=0}^{N_s} \overline{\xi}_j(m) \overline{\xi}_k(t-m) \\ &= \frac{1}{N_s} \big\{ \overline{\xi}_j(0)\overline{\xi}_k(t) + \overline{\xi}_j(1)\overline{\xi}_k(t-1) + \cdots + \overline{\xi}_j(t)\overline{\xi}_k(0) + \cdots \\ &\quad \overline{\xi}_j(t+1)\overline{\xi}_k(-1) + \cdots + \overline{\xi}_j(N_s-1)\overline{\xi}_k(t-N_s+1) \big\}\end{aligned} \tag{B.13}$$

Using the periodicity property of Discrete Fourier transform [71] and combining equations (B.13) and (B.14), we get equation (B.15),

$$\overline{\xi}_j(-r) = \overline{\xi}_j(N_s - r) \tag{B.14}$$

$$\overline{\xi_j \xi_k}(t) = \frac{1}{N_s} Z_j^T P(t) Z_k \tag{B.15}$$

where

$$P(t) = \begin{bmatrix} 0 & \cdots & 1 & 0 & \cdots & 0 \\ & \iddots & & & & \\ 1 & 0 & \cdots & \cdots & \cdots & 0 \\ 0 & \cdots & 0 & 0 \cdots & & 1 \\ & & & & \iddots & \\ 0 & \cdots & 0 & 1 & 0 & \cdots \end{bmatrix} \quad \text{and} \quad Z_j = \begin{pmatrix} \overline{\xi}_j(0) \\ \overline{\xi}_j(1) \\ \vdots \\ \overline{\xi}_j(N_s-1) \end{pmatrix} \tag{B.16}$$

$P(t)$ is the permutation matrix used to reorder the rows of Z_j .The 1^{st} element of the $(t+1)^{\text{th}}$ row and 1^{st} element of the $(t+1)^{\text{th}}$ column of $P(t)$ is 1. Hence from

equation (B.10), the $(q+1, p+1)$ element of $\Phi_l^H \delta M \Phi_r$ can be written as:

$$\sum_{s=1}^{N_s} \varphi_{l,s,q}^H \delta M_s \varphi_{r,s,p} = \sum_{j=1}^{N_p} \varphi_{l,1,q}^H \frac{\partial \delta M}{\partial \xi_j} \varphi_{r,1,p} \bar{\xi}_j (q-p) + \sum_{j=1}^{N_p} \sum_{k=1}^{N_p} \varphi_{l,1,q}^H \frac{1}{2} \frac{\partial^2 \delta M}{\partial \xi_j \partial \xi_k} \varphi_{r,1,p} Z_j^T P(q-p) Z_k \tag{B.17}$$

Similarly $\Phi_l^H \delta K \Phi_r$ can be obtained.

Appendix C
Frequency Mistuning Approaches

C.1. Subset of Nominal Modes

Subset of Nominal modes (SNM) is a frequency mistuning approach based on the following idea; if the tuned (nominal) system has modes with closely spaced frequencies for a family of modes, then for small mistuning in the shape of blades, corresponding mistuned frequencies are also closely spaced [30]. Thus, these closely spaced tuned blade modes are used as the basis function for reduced order modeling to approximate mistuned blade mode shapes. SNM employs change in Young's modulus of a tuned blade to model mistuned blade. Following are the steps required for reduced order model based on SNM.

1. A mistuned blade is modeled by a tuned blade with Young's modulus altered from E_0 to E_m, so that the natural frequency of the modified tuned blade is same as mistuned blade natural frequency, as shown in Figure C.1.

$$E_m = E_0 \left(\frac{f_m}{f_t} \right)^2 \tag{C.1}$$

   f_t : natural frequency of the tuned blade clamped at the base with Young' modulus E_0.

   f_m : natural frequency of the mistuned blade clamped at the base with Young' modulus E_0.

2. The mistuned blades in the bladed rotor are then replaced by these modified blades.

3. The mass matrix (M) for the finite element model of mistuned bladed rotor is same as the mass matrix (M_t) of tuned bladed rotor. While, the stiffness matrix (K) due to modified blades is different, but easy to compute.

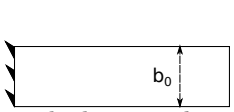

Thickness = b_0
Natural frequency = f_t
Young's modulus = E_0
(a) Tuned Blade

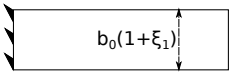

Thickness = $b_0(1+\xi_1)$
Natural frequency = f_m
Young's modulus = E_0
(b) Mistuned Blade

Thickness = b_0
Natural frequency = f_m
Young's modulus =
$E_m = E_0\left(\frac{f_m}{f_t}\right)^2$
(c) Blade for frequency mistuning

Figure C.1: Young's Modulus modification for SNM

The equation of motion for the frequency mistuned system can be written as,

$$M_t\ddot{\mathbf{x}} + K\mathbf{x} = 0 \tag{C.2}$$

In the SNM technique the family of modes of the nominal system is chosen as the basis vector for reduced order modeling.

$$\mathbf{x} = \Phi_0\mathbf{y} \tag{C.3}$$

where Φ_0 is the set of modes for the nominal tuned assembly. Substituting, equation (C.3) in (C.2) and pre-multiplying with Φ_0^H (conjugate transpose of Φ_0), the equation of motion is written as,

$$M_r^0\ddot{\mathbf{y}} + K_r^0\mathbf{y} = 0 \tag{C.4}$$

where

$$M_r^0 = \Phi_0^H M_t \Phi_0 \tag{C.5}$$

$$K_r^0 = \Phi_0^H K \Phi_0 \tag{C.6}$$

The eigenvalue problem associated with equation (C.4) can be solved to get the mode shapes and natural frequencies of the mistuned bladed disk assembly.

C.2. Fundamental Mistuning Model

Fundamental Mistuning Model (FMM) is basically an extension of SNM that takes advantage of the SNM formulation and simplified for the case when the nominal modes used in the representation are limited to a single family and have strain energy concentrated primarily in blades [33]. An example of where FMM is usually applicable is in representing mistuning in the "first bending" modes of bladed rotor. Following are the steps required in FMM formulation,

1. Determine the angular natural frequency (ω_t) of the blades with average geometry clamped at the base.

2. Determine the angular natural frequency ($\omega_m^{(s)}$) of the mistuned blades of sector # s clamped at the base.

Let M_t, K_t be tuned mass and stiffness matrices for the bladed rotor and δM, δK be the mistuning in mass and stiffness matrices due to mistuning. The equation of motion for mistuned bladed rotor is written as,

$$(M_t + \delta M)\ddot{\mathbf{x}} + (K_t + \delta K)\mathbf{x} = 0 \tag{C.7}$$

Choosing a family of tuned modes as basis vector for reduced order modeling,

$$\mathbf{x} = \Phi_0 \mathbf{y} \tag{C.8}$$

where $\Phi_0 = \begin{bmatrix} \phi_0 & \phi_1 & \dots & \phi_N \end{bmatrix}$ contains only a single family of tuned modes of N sector bladed rotor, and ϕ_m is the mode shape corresponding to m^{th} harmonic index of that family of modes. Substituting equation (C.8) in (C.7) and pre-muliplying the equation with Φ_0^H then, after an assumption of closeness of mistuned frequencies of blades in a family of modes, we get,

$$(\Lambda_t + 2\omega_{avg}^2 \bar{\Omega})\mathbf{y} = \omega_y^2 \mathbf{y} \tag{C.9}$$

where ω_y is the mistuned frequency of the rotor approximated using FMM. ω_{avg} is the average of the angular natural frequency of mistuned blades of all the sectors clamped at the base for that single family of modes, Λ_t is the modal stiffness matrix and $\bar{\Omega}$ is matrix containing Discrete Fourier Transform of blade frequency deviations.

$$\bar{\Omega} = \begin{bmatrix} \bar{\omega}_0 & \bar{\omega}_1 & \cdots & \bar{\omega}_{N-1} \\ \bar{\omega}_{N-1} & \bar{\omega}_0 & \cdots & \bar{\omega}_{N-2} \\ \vdots & \vdots & \ddots & \vdots \\ \bar{\omega}_1 & \bar{\omega}_2 & \cdots & \bar{\omega}_0 \end{bmatrix} \tag{C.10}$$

where

$$\bar{\omega}_k = \frac{1}{N} \sum_{s=0}^{N-1} e^{i2\pi sk/N} \Delta\omega_m^{(s)} \tag{C.11}$$

$$\Delta\omega_m^{(s)} = \omega_m^{(s)} - \omega_t \tag{C.12}$$

i.e. $\bar{\Omega}_{ij} = \bar{\omega}_{(j-i) \mod N}$, where N is the number of sectors in the rotor. Using equation (C.9), one can get approximated mistuned frequencies and mode shape of a family of modes for a mistuned rotor.

Appendix D
Karhunen-Loève expansion

Consider a random process $r(t,\theta)$, defined on a probability space (Θ,Σ,P) and indexed on a bounded domain D for $t \in D$. Let, the process has a mean $\bar{r}(t)$ and a finite variance $E\left[(r(t,\Theta)-\bar{r}(t))^2\right] < \infty, \forall t \in D$. Then the process can be expanded as [73],

$$r(t,\theta) = \bar{r}(t) + \sum_{n=0}^{\infty} \xi_n(\theta)\sqrt{\lambda_n}\psi_n(t) \tag{D.1}$$

The parameter $\xi_n(\theta)$ is a set of random variables satisfying $E(\xi_n(\theta)) = 0$ and $E[\xi_n(\theta)\xi_m(\theta)] = \delta_{nm}$, where δ_{nm} is Kronecker-delta function.

Furthermore, λ_n and $\psi_n(t)$ are eigenvalues and eigenfunctions of covariance function $C(t_1,t_2)$, such that:

$$\int_D C(t,u)\psi_n(t)dt = \lambda_n\psi_n(u) \tag{D.2}$$

$$\int_D \psi_n(t)\psi_m(t)dt = \delta_{nm} \tag{D.3}$$

Bibliography

[1] D. J. Ewins, "The effect of detuning upon the forced vibration of bladed disks," *Journal of Sound and Vibration*, vol. 9, no. 1, pp. 65–79, 1969.

[2] L. E. El-Bayoumy and A. V. Srinivasan, "Influence of mistuning on rotor-blade vibrations," *American Institute of Aeronautics and Astronautics*, vol. 13, no. 4, pp. 460–464, 1975.

[3] D. L. Thomas, "Dynamics of rotationally periodic structures," *International Journal for Numerical Methods in Engineering*, vol. 14, no. 1, pp. 81–102, 1979.

[4] A. Sinha, "Calculating the statistics of forced response of a mistuned bladed disk assembly," *AIAA Journal*, vol. 24, no. 11, pp. 1797–1801, 1986.

[5] R. C. F. Dye and T. A. Henry, "Vibration amplitudes of compressor blades resulting from scatter in blade natural frequencies," *Journal of Engineering for Gas Turbines and Power*, vol. 91, no. 3, pp. 182–187, 1969.

[6] S. Tobias and R. Arnold, "The influence of dynamical imperfections on the vibration of rotating disks," in *Proceedings of the Institution of Mechanical Engineers*, vol. 171, pp. 669–690, SAGE Publications, 1957.

[7] D. Whitehead, "Effect of mistuning on the vibration of turbo–machine blades induced by wakes," *Journal of Mechanical Engineering Science*, vol. 8, no. 1, pp. 15–21, 1966.

[8] D. J. Ewins, "Vibration characteristics of bladed disc assemblies," *Journal of Mechanical Engineering Science*, vol. 15, no. 3, pp. 165–186, 1973.

[9] R. E. Kielb and K. R. V. Kaza, "Effects of structural coupling on mistuned cascade flutter and response," *Journal of Engineering for Gas Turbines and Power*, vol. 106, no. 1, pp. 17–24, 1984.

[10] O. O. Bendiksen, "Flutter of mistuned turbomachinery rotors," *Journal of Engineering for Gas Turbines and Power*, vol. 106, no. 1, pp. 25–33, 1984.

[11] G. Sogliero and A. V. Srinivasan, "Fatigue life estimates of mistuned blades via a stochastic approach," *AIAA Journal*, vol. 18, no. 3, pp. 318–323, 1980.

[12] W.-H. Huang, "Vibration of some structures with periodic random parameters," *AIAA Journal*, vol. 20, no. 7, pp. 1001–1008, 1982.

[13] J. H. Griffin and T. M. Hoosac, "Model development and statistical investigation of turbine blade mistuning," *Journal of Vibration, Acoustics, Stress, and Reliability in Design*, vol. 106, no. 2, pp. 204–210, 1984.

[14] A. Sinha and S. Chen, "A higher order technique to compute the statistics of forced response of a mistuned bladed disk assembly," *Journal of Sound and Vibrations*, vol. 130, no. 2, pp. 207–221, 1989.

[15] S.-T. Wei and C. Pierre, "Localization phenomena in mistuned assemblies with cyclic symmetry, part i: Free vibrations," *Journal of Vibration, Acoustics, Stress and Reliability in Design*, vol. 110, no. 4, pp. 429–438, 1988.

[16] S.-T. Wei and C. Pierre, "Localization phenomena in mistuned assemblies with cyclic symmetry, part ii: Free vibrations," *Journal of Vibration, Acoustics, Stress and Reliability in Design*, vol. 110, no. 4, pp. 439–449, 1988.

[17] S.-T. Wei and C. Pierre, "A statistical analysis of the effects of mistuning on the forced response of cyclic assemblies," *American Institute of Aeronautics and Astronautics*, vol. 28, no. 5, pp. 861–868, 1989.

[18] C. C. Lin and M. P. Mignolet, "Effects of damping and damping mistuning on the forced vibrations response of bladed disks," *Journal of Sound and Vibrations*, vol. 193, no. 2, pp. 525–543, 1996.

[19] J. Griffin, "Friction damping of resonant stresses in gas turbine engine airfoils," *Journal of Engineering for Gas Turbine and Power*, vol. 102, no. 2, pp. 329–333, 1980.

[20] A. Sinha and J. H. Griffin, "Friction damping of flutter in gas turbine engine airfoils," *Journal of Aircraft*, vol. 20, no. 4, pp. 372–376, 1983.

[21] D. J. Ewins, "The effects of blade mistuning on vibration response - a survey," *IFToMM 4th International Conference on Rotordynamics*, 1991. Prague, Czechoslovakia.

[22] A. V. Srinivasan, "Flutter and resonant vibration characteristics of engine blades," *Journal of Engineering for Gas Turbines and Power*, vol. 119, no. 4, pp. 742–775, 1997.

[23] J. C. Slater, G. R. Minkiewicz, and A. J. Blair, "Forced response of bladed disk assemblies-a survey," *Shock and Vibration Digest*, vol. 31, no. 1, pp. 17–24, 1999.

[24] R. R. Craig, JR and M. C. Bampton, "Coupling of substructures for dynamic analyses," *AIAA Journal*, vol. 6, no. 7, pp. 1313–1319, 1968.

[25] P. Seshu, "Substructuring and component mode synthesis," *Shock and Vibration*, vol. 4, no. 3, pp. 199–210, 1997.

[26] R. R. Craig, "Substructure methods in vibration," *Journal of Vibration and Acoustics*, vol. 117, no. B, pp. 207–213, 1995.

[27] M. P. Castanier, G. Ottarsson, and C. Pierre, "A reduced order modeling technique for mistuned bladed disks," *Journal of Vibration and Acoustics*, vol. 119, no. 3, pp. 439–447, 1997.

[28] M. J. Kruse and C. Pierre, "Dynamic response of an industrial turbomachinery rotor," in *Proceedings of the 32nd AIAA/ASME/SAE/ASEE Joint Propulsion Conference and Exhibit*, (Lake Buena Vista, Florida), 1996.

[29] M. T. Yang and J. H. Griffin, "A reduced-order approach for the vibration of mistuned bladed disk assemblies," *Journal of Engineering for Gas Turbines and Power*, vol. 119, no. 1, pp. 161–167, 1997.

[30] M. T. Yang and J. H. Griffin, "A reduced-order model of mistuning using a subset of nominal system modes," *Journal of Engineering for Gas Turbines and Power*, vol. 123, no. 4, pp. 893–900, 2001.

[31] R. Bladh, M. P. Castanier, and C. Pierre, "Component-mode-based reduced order modeling techniques for mistuned bladed disks part ii: Application," *Journal of Engineering for Gas Turbines and Power*, vol. 123, no. 1, pp. 100–108, 2001.

[32] R. Bladh, M. P. Castanier, and C. Pierre, "Component-mode-based reduced order modeling techniques for mistuned bladed disks part i: Theoretical model," *Journal of Engineering for Gas Turbines and Power*, vol. 123, no. 1, pp. 89–99, 2001.

[33] D. M. Feiner and J. H. Griffin, "A fundamental model of mistuning for a single family of modes," *Journal of Turbomachinery*, vol. 124, no. 4, pp. 597–605, 2002.

[34] S.-H. Lim, R. Bladh, M. P. Castanier, and C. Pierre, "Compact, generalized component mode mistuning representation for modeling bladed disk vibration," *AIAA Journal*, vol. 45, no. 9, pp. 2285–2298, 2007.

[35] D. Amsallem, J. Cortial, K. Carlberg, and C. Farhat, "A method for interpolating on manifolds structural dynamics reduced-order models," *International Journal for Numerical Methods in Engineering*, vol. 80, no. 9, pp. 1241–1258, 2009.

[36] E. P. Petrov, K. Y. Sanliturk, and D. J. Ewins, "A new method for dynamic analysis of mistuned bladed disks based on the exact relationship between tuned and mistuned systems," *Journal of Engineering for Gas Turbines and Power*, vol. 124, no. 3, pp. 586–597, 2002.

[37] J. M. Brown, *Reduced Order Modeling Methods for Turbomachinery Design*. PhD thesis, Wright State University, Dayton, Ohio, 2008.

[38] J. A. Beck, "Stochastic mistuning simulation of integrally bladed rotors using nominal and non-nominal component mode synthesis," Master's thesis, Wright State University, Dayton, Ohio, 2010.

[39] R. Bladh, M. P. Castanier, and C. Pierre, "Dynamic response predictions for a mistuned industrial turbomachinery rotor using reduced-order modeling," *Journal of Engineering for Gas Turbines and Power*, vol. 124, pp. 311–324, 2002.

[40] A. Sinha, "Reduced–order model of a bladed rotor with geometric mistuning," *Journal of Turbomachinery*, vol. 131, no. 3, p. 031007, 2009.

[41] Y. Bhartiya and A. Sinha, "Reduced order model of a bladed rotor with geometricmistuning: comparison between modified modal domain analysis and frequency mistuning approach," in *ASME 2011 Turbo Expo: Turbine Technical Conference and Exposition*, pp. 981–992, American Society of Mechanical Engineers, June 2011.

[42] Y. Bhartiya and A. Sinha, "Reduced order modeling of a bladed rotor with geometric mistuning via estimated deviations in mass and stiffness matrices," *Journal of Engineering for Gas Turbines and Power*, vol. 135, no. 5, p. 052501, 2013.

[43] Y. Bhartiya and A. Sinha, "Reduced order modeling of a bladed rotor with geometric mistuning: Alternative bases and extremely large mistuning," *International Journal of Gas Turbine, Propulsion and Power Systems*, vol. 5, no. 1, 2013.

[44] A. Sinha and Y. Bhartiya, "Modeling geometric mistuning of a bladed rotor: Modified modal domain analysis," in *IUTAM Symposium on Emerging Trends in Rotor Dynamics, K. Gupta (ed.)*, pp. 177–184, IUTAM Book Series, Springer, March 2011.

[45] Y. Bhartiya, *Single and Multi-Stage Bladed Rotors With Geometric Mistuning: Reduced Order Modeling and Mistuning Identification*. PhD thesis, Pennsylvania State University, July 2011.

[46] M. P. Mignolet, A. J. Rivas-Guerra, and J. P. Delor, "Identification of mistuning characteristics of bladed disks from free response data – part i," *Journal of Engineering for Gas Turbines and Power*, vol. 123, no. 2, pp. 395–403, 1999.

[47] A. J. Rivas-Guerra, M. P. Mignolet, , and J. P. Delor, "Identification of mistuning characteristics of bladed disks from free response data - part ii," *Journal of Engineering for Gas Turbines and Power*, vol. 123, no. 2, pp. 404–411, 1999.

[48] S.-H. Lim, M. P. Castanier, and C. Pierre, "Mistuning identification and reduced-order model updating for bladed disks on a component mode mistuning technique," in *Proceedings of the 9th National Turbine Engine High Cycle Fatigue Conference*, 2004.

[49] D. M. Feiner and J. H. Griffin, "Mistuning identification of bladed disks using a fundamental mistuning model - part 1: Theory," *Journal of Turbomachinery*, vol. 126, no. 1, pp. 150–158, 2004.

[50] D. M. Feiner and J. H. Griffin, "Mistuning identification of bladed disks using a fundamental mistuning model - part 2: Application," *Journal of Turbomachinery*, vol. 126, no. 1, pp. 159–165, 2004.

[51] D. M. Feiner and J. H. Griffin, "Identification of damping variations in mistuned bladed disks," in *10th National Turbine Engine High Cycle Fatigue Conference*, 2005.

[52] H. Hattori, "Application of fmm for mistuning analysis of radial inflow turbine," in *International Gas Turbine Conference*, 2011.

[53] Y. Bhartiya and A. Sinha, "Geometric mistuning identification of integrally bladed rotors using modified modal domain analysis," *ASME 2012 International Design Engineering Technical Conferences and Computers and Information in Engineering Conference*, 2012.

[54] M. Mercadal, A. von Flotow, and P. Tappert, "Damage identification by nsms blade resonance tracking in mistuned rotors," in *Aerospace Conference IEEE proceedings*, vol. 7, pp. 7–3277, IEEE, 2001.

[55] W. F. Obrien, Jr, W. T. Cousins, and M. R. Sexton, "Unsteady pressure measurements and data analysis techniques in axial-flow compressors," in *Proceedings of the Joint Fluids Engineering Gas Turbine Conference and Products Show*, vol. 1, pp. 195–201, March 1980.

[56] B. Lakshminarayana, "Techniques for aerodynamic and turbulence measurements in turbomachinery rotors," *Journal of Engineering for Gas Turbines and Power*, vol. 103, no. 2, pp. 374–392, 1981.

[57] T. Liu, S. Torgerson, J. Sullivan, R. Johnston, and S. Fleeter, "Transonic rotor blade pressure measurement using fluorescent paints," *Journal of Propulsion and Power*, vol. 18, no. 2, pp. 491–493, 2002.

[58] R. J. Miller, R. W. Moss, R. W. Ainsworth, and N. W. Harvey, "Wake, shock, and potential field interactions in a 1.5 stage turbine – part i: Vane-vane interaction and discussion of results," *Journal of Turbomachinery*, vol. 125, no. 1, pp. 33–39, 2003.

[59] R. J. Miller, R. W. Moss, R. W. Ainsworth, and N. W. Harvey, "Wake, shock, and potential field interactions in a 1.5 stage turbine – part ii: Vane-vane interaction and discussion of results," *Journal of Turbomachinery*, vol. 125, no. 1, pp. 40–47, 2003.

[60] A. Kammerer and R. S. Abhari, "Blade forcing function and aerodynamic work measurements in a high speed centrifugal compressor with inlet distortion," *Journal of Engineering for Gas Turbines and Power*, vol. 132, no. 9, p. 092504, 2010.

[61] C. Wu, "Arbitrary surface flank milling of fan, compressor, and impeller blades," *Journal of Engineering for Gas Turbines and Power*, vol. 117, no. 3, pp. 534–539, 1995.

[62] A. Sinha, B. Hall, B. Cassenti, and G. Hilbert, "Vibratory parameters of blades from coordinate measurement machine data," *Journal of Turbomachinery*, vol. 130, no. 1, p. 011013, 2008.

[63] A. Lange, K. Vogeler, V. Gümmer, H. Schrapp, and C. Clemen, "Introduction of a parameter based model for considering measured geometric uncertainties in numerical simulation," in *ASME Turbo Expo 2009: Power for Land, Sea, and Air*, (Orlando, Florida), pp. 1113–1123, American Society of Mechanical Engineers, June 2009.

[64] Y. S. Choi, D. A. Gottfried, and S. Fleeter, "Resonant response of mistuned bladed disk including aerodynamic damping effects," *Journal of Propulsion and Power*, vol. 26, no. 1, pp. 16–24, 2010.

[65] R. J. Allemang, "The modal assurance criterion (mac): Twenty years of use and abuse," *Journal of Sound and Vibrations*, vol. 37, no. 8, pp. 14–23, 2003.

[66] B. N. Datta, *Numerical Linear Algebra and Applications*. Brooks Cole Publishing Company, 1995.

[67] G. S. Óttarsson, *Dynamic Modeling and Vibration Analysis of Mistuned Bladed Disks*. PhD thesis, University of Michigan, Ann Arbor, 1994.

[68] T. M. Cover and J. A. Thomas, *Elements of information theory*. Delhi: Wiley India, 2006.

[69] Y. S. Choi, N. Key, and S. Fleeter, "Vane clocking effects on the resonant response of an embedded rotor," *Journal of Propulsion and Power*, vol. 27, no. 1, pp. 71–77, 2011.

[70] A. Sinha, *Linear Systems: Optimal and Robust Control*. CRC Press, 2007.

[71] A. V. Oppenheim and R. W. Schafer, *Digital Signal Processing*. Englewood Cliffs, New Jersey: Prentice – Hall, Inc., 1975.

[72] S. K. Mitra, *Digital Signal Processing*. Burr Ridge, Illinois: McGraw–Hill Higher Education, 3 ed., 2006.

[73] R. G. Ghanem and P. D. Spanos, *Stochastic Finite Elements: A Spectral Approach*. New York: Springer, 1991.

Vita

Vinod Vishwakarma

Vinod Vishwakarma was born in a village Dhaukalganj, Varanasi, Uttar Pradesh, India on Dec 14, 1987 to Ramlalli and Satyanarayan Vishwakarma. He completed his schooling upto senior secondary level from New Look H.S. School, Indore, Madhya Pradesh. He received his baccalaureate degree with honors in Mechanical Engineering from the Indian Institute of Technology, Kharagpur, India in the year 2009. Thereafter he worked with National Thermal Power Corporation Ltd., India during 2009–2010. He joined The Pennsylvania State University, University Park, USA for Ph. D. in Mechanical Engineering in January, 2011. He worked with Dr. Alok Sinha for his Ph.D. in the area of reduced order modeling of geometrically mistuned bladed rotors. His research interests include control systems, structural dynamics, statistical analysis, analyses of vibratory systems and design.

He is a student member of the American Society of Mechanical Engineers (ASME).

Refereed Journal Publications

1. Vinod Vishwakarma and Alok Sinha, "Estimation of forcing function for a geometrically mistuned bladed rotor via modified modal domain analysis", *In progress.*

2. Vinod Vishwakarma and Alok Sinha, "Forced Response Statistics of a Bladed Rotor with Geometric Mistuning", Submitted to AIAA Journal.

3. Vinod Vishwakarma, Alok Sinha, Yasharth Bhartiya and Jeffery Brown, "Modified Modal Domain Analysis of a Bladed Rotor Using Coordinate Measurement Machine Data on Geometric Mistuning", Accepted for publication in ASME Journal of Engineering for Gas Turbines and Power.

Peer Reviewed Conferences Publications

1. Vinod Vishwakarma and Alok Sinha, "Forced response statistics of a bladed rotor with geometric mistuning", AIAA-2014-0495, 55th AIAA/ASMe/ASCE/AHS/SC Structures, Structural Dynamics, and Materials Conference, AIAA SciTech (2014).

2. Vinod Vishwakarma, Alok Sinha, Yasharth Bhartiya and Jeffery Brown, "Modified modal domain analysis of a bladed rotor using coordinate measurement machine data on geometric mistuning", GT2013-94393, Proceedings of ASME Turbo Expo: Turbine Technical Conference and Exposition, San Antonio, Texas, USA, June 3 - 7, (2013).